Università Politecnica delle Marche
Scuola di Dottorato di Ricerca in Scienze dell'Ingegneria
Curriculum in Ingegneria Industriale

In-line quality control for Zero Defect Manufacturing: design, development and uncertainty analysis of vision-based instruments for dimensional measurements at different scales

Ph.D. Dissertation of:

Alessia Baleani

Alessia Baleani

Advisor:

Prof. Nicola Paone

Prof. Steve Vanlanduit

Curriculum supervisor:

Prof. Giovanni di Nicola

XXXV edition - new series

Università Politecnica delle Marche
Dipartimento di Ingegneria Industriale e Scienze Matematiche (DIISM)
Via Brecce Bianche — 60131 - Ancona, Italy

Acknowledgements

This thesis would not have been possible without the support of my main supervisor, Prof. Nicola Paone, who gave me this opportunity and has provided me with guidance throughout my PhD. I would also like to thank my co-supervisor Prof. Steve Vanlanduit for his help during my stay at InViLab at the Universiteit Antwerpen.

I would like to thank the Regione Marche for providing the funds for my PhD through the POR Marche FSE 2014/2020 Project "Dottorato Innovativo - Borse di studio per dottorato di ricerca per l'innovazione del sistema regionale, Edizione Anno Accademico 2019/2020" for the scholarship for the project "Sistemi di misura "smart" per controllo qualità in linea di produzione."

The aim of this industrial PhD project was to promote the involvement of local factories and companies and to produce research in line with the needs of the industrial environment. Hence, I would like to also acknowledge the contribution of Zannini s.p.a. and Z4tec s.r.l. which provided part of the instrumentation and their expertise in measurements for quality control.

Last but not least, this PhD would not have been successful without the help from Jona Gladines, Luca Violini and Professors Paolo Chiariotti and Paolo Castellini, which supported me throughout this experience. Moreover, a special thanks goes to my fellow PhDs Alessandro, Nicola and Lorenzo, which in the last three years have spent many hours explaining things to me.

Abstract (EN)

The purpose of this industrial PhD project financed through a scholarship from the Regione Marche was to develop research with potential impact on an industrial sector, to promote the involvement of local factories and companies in research and innovation performed jointly with the university and to produce research in line with the needs of the industrial environment, not only at regional level.
Hence, through collaborating with a local turning factory (Zannini SpA) and a small high-tech company focused on introducing mechatronic innovation in the turning sector (Z4Tec srl), and also thanks to an international collaboration with the University of Antwerp, we designed and developed new instruments for in-line quality control, based on non-contact technologies, specifically electro-optical technologies. While also bringing attention to the importance of taking uncertainty into consideration, since it is pivotal in data-based decision making which are at the base of a Zero Defect Manufacturing strategy. This means that poor quality of measurements can prejudice the quality of the data. In particular, this work presents two measurement instruments that were designed and developed for the purpose of in-line quality control and the uncertainty of each of the two instruments was evaluated and analyzed in comparison with instruments already present on the market. In the last part of this work, the uncertainty of a hand-held laser-line triangulation profilometer is estimated.

Hence, the research conducted in this thesis can be organized in two main objectives: the development of new vision-based dimensional measurement systems to be implemented in production line and the uncertainty analysis of these measurement instruments. For the first objective we focused on two types of dimensional measurements imposed by the manufacturing industry: macroscopic (measuring dimensions in mm) and microscopic (measuring roughness in μm). For macroscopic measurements the target was the in-production dimensional quality control of turned parts through telecentric optical profilometry. The sample to be inspected was placed between illuminator and objective in order to obtain the projection of the shadow of the sample over a white background. Dimensional measurements were then performed by means of image processing over the image obtained. We discussed the mechanical arrangements targeted to optimize images acquired as well as the main issues that eventual mechanical misalignments of components might introduce in the quality of images. For microscopic measurements we designed a backlit vision-based surface roughness measurement system with a focus on smart behaviors such as determining the optimal imaging conditions using the modulation transfer function and the use of an electrically tunable lens. A turned sample (a cylinder) is placed in front of a camera and it is backlit

by a collimated source of light; such optical configuration provides the image of the edge of the sample. A set of turned steel samples with different surface roughness was used to test the sensitivity of the measurement system.
For the second objective, the measurement uncertainty evaluation techniques used in this work were a Type A statistical uncertainty analysis and a Gage R&R analysis.
In the case of the telecentric profilometer, the analysis was performed in comparison with other on-the-market devices with a Type A analysis and a Gage R&R analysis. The measurement uncertainty of the profilometer proved to be sufficient to obtain results within the tolerance interval required. For the backlit vision system, the comparison of the results was made with other state-of-the-art instruments, with a Type A analysis. The comparison showed that the performance of the backlit instrument depends on the values of surface roughness considered; while at larger values of roughness the offset increases, the results are compatible with the ones of the reference instrument (stylus-based) at lower values of roughness. Lastly, the repeatability and reproducibility of a laser-line triangulation profilometer were assessed, through a Gage R&R study. Each measuring point was inspected by three different operators and the data set has been, at first, processed by a Type A uncertainty analysis. Then, a Gage R&R study helped investigate repeatability, reproducibility and the system variability. This analysis showed that the presented laser-line triangulation system has an acceptable uncertainty.

Abstract (NL)

Het doel van dit doctoraat was het ontwerpen en ontwikkelen van nieuwe instrumenten voor kwaliteitscontrole in de productielijn, gebaseerd op contactloze technologieën, in het bijzonder op elektro-optische technologieën. Verder is aandacht besteed aan het belang van het meewegen van meetonzekerheid, aangezien dit essentieel is voor het nemen van beslissingen op basis van de gegevens die de basis vormen van Zero Defect Manufacturing-strategieën. De slechte kwaliteit van de metingen kan de kwaliteit van de gegevens beïnvloeden. Dit werk stelt twee meetinstrumenten voor die zijn ontworpen en ontwikkeld met als doel kwaliteitscontrole uit te voeren in de productielijn. De meetonzekerheid van elk instrument is geanalyseerd in vergelijking met andere instrumenten op de markt. In het laatste deel van dit werk werd de onzekerheid van een triangulatielaserprofiler geëvalueerd. Het onderzoek in dit proefschrift is georganiseerd in twee hoofddoelstellingen: de ontwikkeling van nieuwe op visie gebaseerde dimensionale meetsystemen die in de productielijn kunnen worden geïmplementeerd en de onzekerheidsanalyse van deze meetinstrumenten. Voor de eerste doelstelling hebben we ons gericht op twee soorten maatmetingen opgelegd door de maakindustrie: macroscopisch (afmetingen in mm) en microscopisch (afmetingen in µm). Voor macroscopische metingen was het doel online controle van de dimensionale kwaliteit van gedraaide onderdelen door middel van telecentrische optische profilometrie. Het te inspecteren proefstuk werd tussen de lichtbon en het objectief geplaatst om de projectie van de schaduw van het proefstuk te verkrijgen. De metingen werden uitgevoerd door grafische analyse van het beeld. We analyseerden de mechanische regelingen gericht op het optimaliseren van de verkregen beelden en de problemen die een mechanische foutieve uitlijning van de componenten zou kunnen veroorzaken in de kwaliteit van de beelden. Voor de microscopische metingen hebben we een meetsysteem voor oppervlakteruwheid ontworpen op basis van back-illuminated vision, met als doel de optimale beeldcondities te bepalen met behulp van de modulatieoverdrachtsfunctie en het gebruik van een elektrisch afstelbare lens. Een gedraaid werkstuk (cilinder) wordt voor een camera geplaatst en wordt van achteren verlicht door een gecollimeerde lichtbron; deze optische configuratie geeft het beeld van de rand van het werkstuk. Om de gevoeligheid van het meetsysteem te testen, is gebruik gemaakt van een reeks gedraaide werkstukken met verschillende oppervlakteruwheden. Voor de tweede doelstelling waren de meetonzekerheidsevaluatietechnieken die in dit werk werden gebruikt een type A statistische onzekerheidsanalyse en een Gage R&R-analyse. In het geval van de Telecentric Profilometer werd de analyse uitgevoerd in vergelijking met andere apparaten op de markt met een Type A-analyse en Gage R&R. De

meetonzekerheid van de profilometer bleek voldoende om resultaten binnen het vereiste tolerantiebereik te verkrijgen. Voor het back-illuminated vision-systeem werden de resultaten vergeleken met andere state-of-the-art instrumenten, met een Type A-analyse. De vergelijking toonde aan dat de prestaties van het instrument met achtergrondverlichting afhangen van de beschouwde oppervlakteruwheidswaarden; terwijl bij hogere ruwheidswaarden de offset toeneemt, zijn de resultaten bij lagere ruwheidswaarden compatibel met die van het referentie-instrument (naald). Ten slotte werden de herhaalbaarheid en reproduceerbaarheid van een laserlijntriangulatieprofiler geëvalueerd door middel van een Gage R&R-onderzoek. Elk meetpunt werd geïnspecteerd door drie operators en de dataset werd verwerkt met een onzekerheidsanalyse van type A. Vervolgens hielp een Gage R&R-studie de herhaalbaarheid, reproduceerbaarheid en variabiliteit van het systeem te onderzoeken. Deze analyse toonde een aanvaardbare onzekerheid aan.

Contents

List of Figures

List of Tables

Chapter 1.

Introduction

Quality control is a process that takes place to make sure that the quality of the product is maintained. In this context, quality means conformity to specifications. This is also to identify defective or unsafe products in order to discard them and prevent sending defective products to the customer which could hold the producer responsible for any issue. Ideally, the variables at fault of having caused the defective products should be identified and corrected.
This approach is the basis on which the evolving trend of Zero Defect Manufacturing (ZDM) is based. In fact the goal of ZDM is to obtain a sustainable and effective production eliminating production scraps, not only through detecting and correcting defective products but also thanks to defect prediction and prevention [1].

1.1. Quality control in Industry 4.0 and meaning of Zero Defect Manufacturing

Quality control is based on testing the production and check if it is within the specifications for the final product. Quality testing is completed in each step of a manufacturing process, from testing raw materials, pulling samples from the production line, to the finished product [2]. Testing at the various stages of manufacturing helps identify where a production problem is occurring and the remedial steps it requires to prevent it in the future.
In the 1960s the idea of a ZDM production was introduced. A few decades later, with the arrival of Industry 4.0, the development of new enabling technologies, like in-line data gathering and digital twins, allowed ZDM to move forward [3]. Hence, this idea has promoted the development of a quality first approach and then of a "first-time-right" strategy.
Today, this means that the quality control of the finished product has moved from the end of the production line to being distributed along the complete production line itself. This is mandatory in order to develop a strategy that involves the prediction and correction of defects by exploiting early detection of defects and trends, also through sharing of data between processes which allow to deal with streams of variations [4].
The European research landscape has been focusing on these topics for quite some time now, first with the Horizon 2020 programme (H2020), now with the Horizon Europe program which covers the period from 2021 to 2027. The pillars of Horizon Europe tackle climate change, the UN's Sustainable Development Goals and the competitiveness and growth of Europe [5]. Within this framework, the subject of sustainable production and Factories of the Future is widely spread. Through the years, many projects about ZDM have been developed and some of them have been funded through the European Commission. In Figure 1 the evolution of several ZDM

projects is shown and it is illustrated how the timeline will continue in the near future, given the fact that this is still a topic of interest.

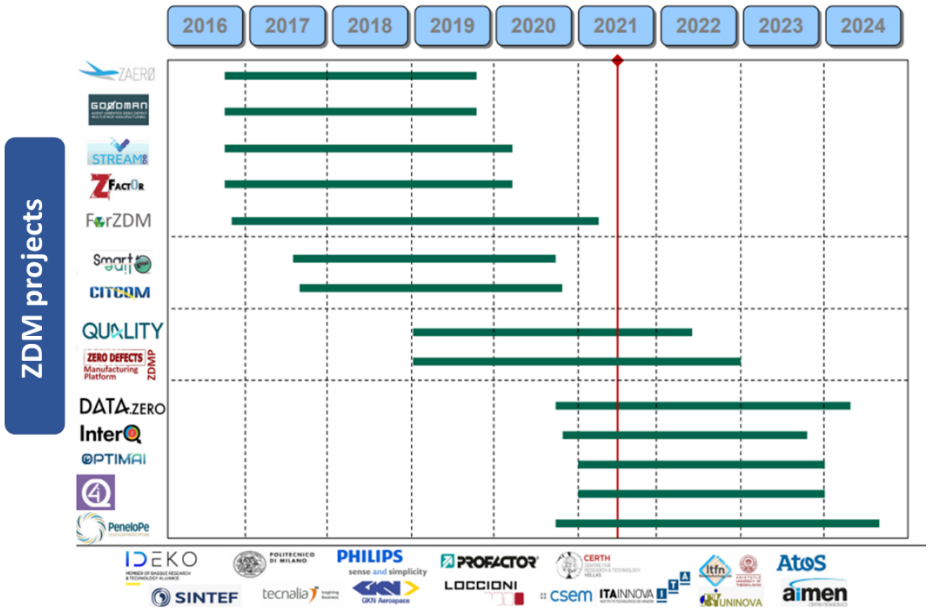

Figure 1. *Evolution of ZDM projects and current timeline of ZDM projects. Image from ZDM projects cluster web-meeting of July 2021[6].*

In the next paragraph we will give an overview of some examples of ZDM contributions and some projects funded by the European Union.

Cristalli et al. in 2011 [7] designed a distributed manufacturing control system based on multi-agent principles, self-learning and self-adaptation. They focused on modelling the production process and promoted interaction between manufacturing and the distributed control system, using the information gathered at the quality and process levels of a washing machine production line. They were able to improve the quality of products and the efficiency of the production and to obtain a cost reduction within production.

Arsuaga Berrueta et al. in 2012 [8] developed a system for quality control of large parts obtained through boring. When concerning these parts, e.g. gears for wind mills, defects in the final product mean a high production cost and time loss. Hence, they developed a model of the cutting process and the performed in-line monitoring with telemetry hardware integrated in the boring head. The force and the vibration measurements they performed were correct, making it feasible to monitor in-line forces with the device they proposed.

Wang in 2013 [9] demonstrated how Data Mining approaches can help reach the goal of ZDM. They are used to gather useful information from huge manufacturing datasets. They extracted models and patterns which they used for fault diagnosis and failure prognosis and to help managers make better decisions.

Montironi et al. in 2014 [10] developed an adaptive strategy to place a camera automatically during vision-based robotized quality control. This was tested for on-

line quality control. They used a FFT algorithm for obstacle detection which proved robust to changes in environmental conditions. The use of a robot made the system more flexible and the use of only one camera proved to be an advantage in terms of reduced system complexity.
Stroppa et al. in 2015 [11] presented an on-line quality control system as an agent within a multi-agent system conceived for control of a production line. To improve reliability and confidence level of the diagnosis they used self-optimizing behaviors. They showed that a self-optimizing robot vision system is effective to improve the confidence level of quality inspections and the quality of the manufactured goods.
Queiroz and Leitão in 2016 [12] introduced an agent-based data analysis approach to control industrial processes endowing agents with data analysis capabilities and cooperation strategies which allow them to improve their analysis capability thanks to shared knowledge. They showed a promising perspective while pointing out some remaining issues, for example, the dynamic nature of the industrial environments.
Chiariotti et al. in 2018 [13] designed a test station for high accuracy dimensional measurements for tests by the line. The test station was provided of self-compensating behaviors which optimize the metrological performance of the system, avoiding e.g. temperature disturbances and eccentricity. Once these behaviors were implemented, the performance of the instrument went from being compromised, for example by temperature changes, to being within the target accuracy.
Caccamo et al. in 2021 [14] addressed the complexities in implementing a cyber-physical production system for ZDM in dynamic, low-volume contexts that have a low level of digitalization. Some of the advantages they expect are to ensure data security, the compatibility with legacy systems and a greater architectural flexibility.
Eger et al. in 2022 [15] showed an approach to model part variations in multi-stage productions and propose a strategy of downstream compensation to eliminate superimposed defects. They demonstrated its functionality and it will be used in the future for compensating faulty production of parts.
Campbell et al. in 2020 [16] presented the European Manufacturing Platform for Zero-Defects build in the frame of the H2020 project entitled “Zero Defect Manufacturing Platform” (ZDMP). It combines state-of-the-art technological approaches with an innovative integration concept, it would allow the platform to be integrated in the whole plant, to be modified based on the needs of the production process, and to be interconnected to multiple different systems and devices.

Moreover, under the Horizon Europe programme the following projects have been funded [17] [18].
Open Platform For Realizing Zero Defects In Cyber Physical Manufacturing (OPENZDM) is aimed at challenging the manufacturing state-of-art and delivering high-quality products while minimizing waste and energy consumption. This will be achieved through an open platform integrating ICT solutions and innovative non-destructive testing.
Zero-defect manufacturing for green transition in Europe (ENGINE) is developed to increase industry competitiveness, reduce manufacturing waste and improve employee well-being by developing a first-time-right and zero-defect metal product

design and manufacturing system, then demonstrate it on marine engine supply-chain.
AI Powered human-centred Robot Interactions for Smart Manufacturing (AI-PRISM) is an industrial-end-user driven project. It will provide human-centred AI-based solutions for manufacturing scenarios with tasks where speed and versatility are essential and difficult to automate. The result will be a semi-automated and collaborative manufacturing in flexible production processes.
Towards tURbine Blade production with zero waste (TURBO), similarly to Arsuaga Berrueta et al. [8], focuses on turbine blade quality control since manufacturing methods have not changed significantly since the 1970s, with little or no in-line control, leading to high defect, repair and scrap rates. TURBO will reduce defects and improve repair strategies using non-destructive technologies and digital twins.
Non-Destructive Inspection Services for Digitally Enhanced Zero Waste Manufacturing (ZDZW) has the main goal of reducing defects and the waste generated in manufacturing processes. ZDZW addresses defects and waste reduction in three key areas: monitoring and control improvement for process quality assurance, increasing first-time-right rates; digitally enhanced Rework & Repair procedures for part recovery and scrap reduction; and continuous sustainability evaluation to ensure the efficient use of materials and components.
Automated Maskless Laser Lithography Platform for First Time Right Mixed Scale Patterning (OPTIMAL) will integrate different laser lithography technologies, quality monitoring systems and processes in one platform for the development of structures. It will increase the process efficiency, reduce energy consumption and material waste, decrease costs and lead time.
DAT4.Zero aims to approach the challenge of ZDM by combining all manufacturing data into one location, enabling much greater levels of analysis. This will allow more complete predictions to be made that can enable better compensation methods for defect reduction.
As demonstrated by the recent and on-going projects reviewed above, a shift in quality approach is mandatory, since the new strategies in development need data collected directly from the process and the product in order to obtain a close integration of process and quality control and to achieve testing on 100% of production [19],[7]. Given this, in many industrial realities, measurements for quality monitoring are still based on a statistical approach, where a random sample is picked from the production line and checked for defects. This is particularly true in batch production, where no individual part tracking is implemented. It would be best to have a more holistic approach to data gathering, so that data would be more readily available for analysis.

1.2. How to perform quality control

Right now, in manufacturing industries, measurements performed at the production level involve two main approaches, measurements are carried out either by human operators or by means of an automated process. Below we will discuss both approaches.

1.2.1. Measurements performed by human operators

Measurements performed in-line by human operators usually involve the use of hand-held instruments. Measurements that require a human operator to pick a sample for a periodical check involve the use either of bench tools which might be located by the production line or of measurement instruments placed in the controlled environment of a quality control lab. In fact, many instruments need a specific range of temperatures and a clean environment which would not be guaranteed by the production line.

When considering the future development of manufacturing industries, understanding that human operators have a fundamental role, even in factories with a high level of automation is pivotal. In fact, for a variety of technical reasons and at the same time to keep occupational levels at an ethically and legally acceptable level, humans are in charge of complex operations, including measurements [20]. Hence, there are recent studies [21] modelling the role of humans with the goal of integrating human-machine interaction in the perspective of a Social Human-in-the-Loop Cyber-Physical Production System.

This also refers to the concept of 'Operator 4.0', understood as a "*smart and skilled operator who performs not only cooperative work with robots but also work aided by machines as and if needed by means of human cyber-physical systems, advanced human-machine interaction technologies and adaptive automation towards achieving human-automation symbiosis work systems*" [22]. Romero et al. introduce this idea in their research and show a set of key enabling technologies, which involve a physical or a cognitive interaction, and explain how technologies can transform operators in 'smarter operators'.

Pacaux-Lemoine et al. in 2022 [23] presented a review of studies and results from current manufacturing processes which highlight ways to design manufacturing systems for Industry 4.0 that are intelligent but also take into consideration human involvement. This review shows how there is an ongoing interest in the role of human in Industry 4.0. This interest is shared also by the European Commission, which in 2020 was already exploring the concept of an Industry 5.0 where the wellbeing of the industry worker is at the center of the production process [24].

The idea is to aim for operator inclusiveness without hindering the objectives of production. In fact, when operators are involved, there is an added contribution to the uncertainty of the measurement: this is schematized in a simple way in Figure 2. The result of every measurement process has an uncertainty component due to the uncertainty of the instrument itself; when you include the operator in the measurement process there is another uncertainty component which contributes to the uncertainty of the result. It goes without saying that the uncertainty of the instrument is already a big influence on the measurement result and it cannot be eliminated completely, because of this, the uncertainty due to the operator needs to be reduced to the minimum level. In this sense, technology can be used to improve the knowledge and capabilities of operators. If this is the case, questions like ergonomics, human dexterousness, operator training but also human-machine interface design need to be taken into consideration and analyzed.

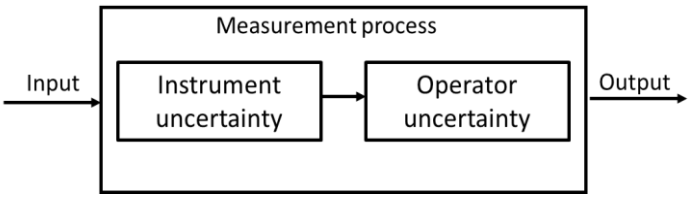

Figure 2. *Uncertainty of a measurement process that involves the participation of a human operator.*

1.2.2. Measurements performed automatically

The other component in quality control inspections is the use of automated machines, which require only the supervision or the assistance of human operators. The evolving digitalization of the production process has meant that the trend for automatization of processes has been growing progressively.
Automated quality control is able to reduce mistakes in the workflow, in fact, replacing manual proof reading can eliminate inefficiencies and improve performance, speeding up the time-to-market [25]. This approach has some advantages which include [26]:

- speeding up the time-to-market by eliminating inefficiencies and improving production performance;
- automatic detection of errors;
- identifying the processes which are prone to error;
- safety: robots and machine can take over unsafe tasks in dangerous locations;
- lower operating costs.

What automated processes are not able to do is reproduce the ability, experience, and critical judgement of human operators. Automatic processes are not flexible, they can be changed through programming which might require a lot of effort; on the other hand, a human operator is more easily reconfigurable. Hence production line quality control usually integrates both aspects, taking advantage of automatization to relieve operators of alienating and repetitive tasks.
These systems are not substituting workers, they give employees the chance to focus on more valuable tasks, like equipment maintenance and programming. Manufacturers who implement these techniques often see an improvement in employee satisfaction, an increase in productivity, and an enhancement in product quality.

There are three main types of automation: fixed, programmable and flexible [27]:

- Fixed automation systems: for manufacture of a single product and have a fixed automation system. They make it difficult to switch production methods;

- Programmable automation systems: they can be programmed to complete the desired task and can be easily reprogrammed but it requires downtime between batches;
- Flexible automation systems: similar to the programmable ones but are conceived to work with a limited production downtime, to achieve this, they have a limited number of variations to choose from.

At the manufacturing level, the use of automation in production and in quality control is widespread. The lack of literature on these topics is also a demonstration of this. In fact, these are topics more related to the application field, within which this PhD thesis finds its context.
Depending on the process, measurement automation can look different: the following short summary is intended not as an extensive review of methods, but only as a list of examples of state-of-the-art automated processes present in a typical industry involved in manufacturing. The information reported here has been collected through different websites of manufacturers and resellers of this type of technology.
A common way of automating the measurement process is to use a sensor placed on the production line which measures each sample that comes through on the conveyor belt (Figure 3, 4 and 5) or it might consist in a robotic arm which picks samples and places them in front of sensors and depending on the measurement outcome it places them in the OK or NOT OK piles (Figure 6).

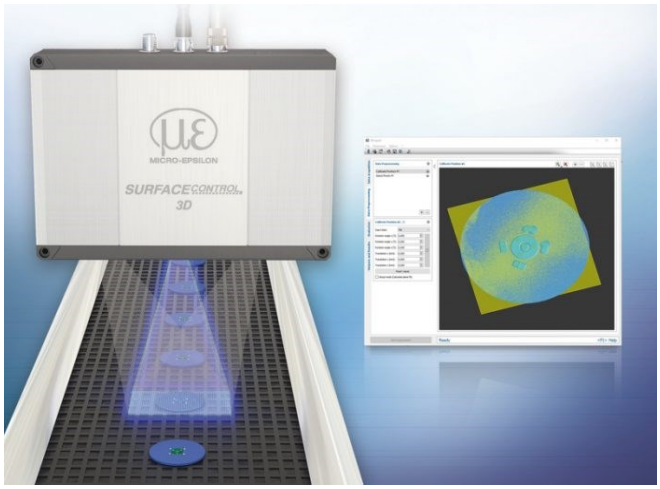

Figure 3. *Example of a snapshot sensor integrated in the production line: it allows automated inspection of geometry and shape. Photo by Micro-Epsilon Messtechnik GmbH & Co. KG [28].*

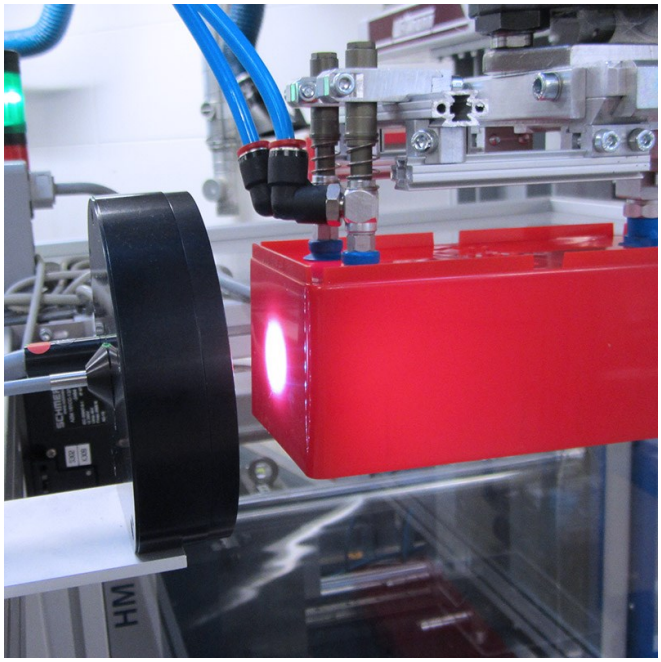

Figure 4. *In-line inspection of 100% of products straight from the mold with colorCONTROL ACS inline color measurement system from Micro-Epsilon [29].*

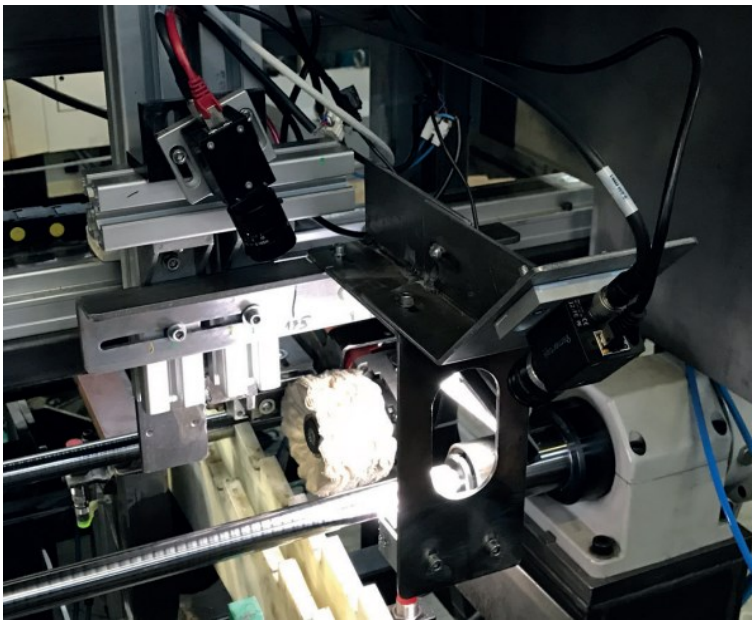

Figure 5. *Metal surfaces quality inspection system by Nirox: it detects cosmetic defects, corner damages, stains, dents and residues [30].*

Figure 6. *Collaborative optical inspection cell, photo by Z4tec. Example of robotic arm performing pick and place measurements [31].*

Another strategy for automated quality control is to have robotic arms hold and move sensors to perform measurements: they can move sensors automatically (Figure 7 (Left)) or they can be used in a collaborative way by holding the sensor, relieving the operator of the weight of the tool, hence allowing long inspections without any fatigue (Figure 7 (Right)). This might also be integrated directly on the conveyor belt and have multiple robots perform measurements at the same time (Figure 8).

Figure 7. *(Left)Example of a robotic arm holding a sensor for quality inspections. Photo by Creaform [32]; (Right) Photo of Ace arm by Kreon [33].*

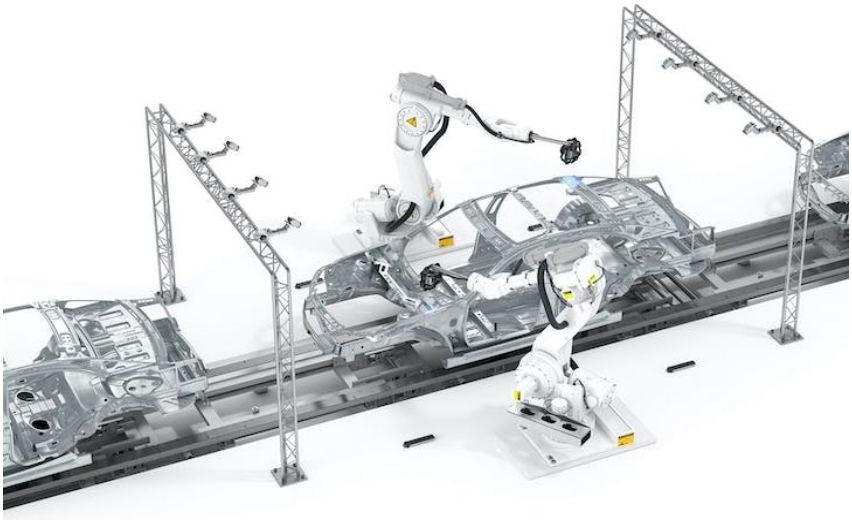

Figure 8. *Example of robotic arms performing measurements directly on the conveyor belt. Photo by Zeiss AICell trace [34].*

1.3. Dimensional quality control in industrial processes

Quality control differs greatly depending on the type of industry and the requirements the final product has to guarantee. For example, in electronics quality testing involves measuring the flow of electricity, while in food manufacturing, quality control tests chemical and microbiological characteristics.
In automobile manufacturing, quality control focuses on parts meeting specifications and tolerances. It ensures mechanical parts operate smoothly, efficiently, safely, and as designed. These kinds of tests mainly fall into the category of dimensional measurements.
Dimensional measurements are measurements which quantify the size and shape of the measurand, and they are critically important for interchangeability and trade. This kind of measurements are also fundamental in guarantying that products perform as intended [35].

1.3.1. Machining processes: turning

In the manufacturing industry that produces metal parts, turning is one of the most relevant production processes, in fact cylindrical parts are present in all kinds of finished products. It is a process that requires a high velocity and precision, especially for high-precision mechanical parts. When producing parts in batches, usually the operators are in charge of performing dimensional measurements in metrological laboratories. Dimensions and surface quality are the characteristics they check to determine compliance to specifications of the finished product [36]:

- Dimensions: turned pieces have a cylindrical shape due to their production techniques, hence the most common dimensions to be

measured are lengths and diameters. Every sample has numerous measurements to be checked and there are thousands of samples to be measured. Hence, some of the goals are to have a short inspection time, the possibility to simultaneously measure several dimensions on different sides of the part and the suitability for automated charge and discharge of parts.

- Surface quality: is assessed by quantifying the surface roughness of samples to ensure that it stays within specifications. This is especially important whenever the samples in question are going to be used for moving or rotating parts. In fact, a larger surface roughness is one of the main influences on properties of the workpieces, such as appearance, reliability and function [37]. This depends on the production process and on tool wear: tool geometry, a damaged tool or the choice of the cutting parameters can cause a larger surface roughness. To counter this effect, the tool is replaced regularly, and the surface roughness is periodically checked.

1.3.2. Assembly operations

Assembly operations refer to the process of putting together individual parts to create a final product. It usually involves manual, or automated, techniques to fasten or join different components, depending on the size or weight of the components and the required level of precision. The goal is to create an end product that satisfies specific quality standards. Common examples of products obtained through assembly are: electronics, vehicles (from cars to airplanes), furniture and appliances.
Amongst these, car body assembly is a typical production process which involves fairly complex operations, because of this many tasks are done by operators. They assemble manually the parts and continuously check their geometric alignment by measuring gap and flush. The gap is the tangent distance between the two parts, while the flush is the relative orthogonal displacement, as can be seen in Figure 9.

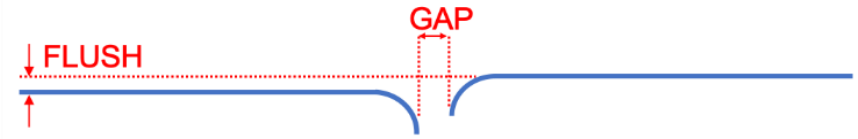

Figure 9. *Definition of gap and flush.*

Gap and flush are crucial aspects of car body manufacturing, because they contribute to the positive perception of the car both from an aesthetic and functional point of view and are fundamental in assessing the quality of the production [38]. Not only this, but they are important parameters that are checked whenever two parts need to be aligned and alignment is a fundamental part of any assembly operation.
Traditionally, gap and flush measurements were executed manually with feeler gauges, calipers and dial gauges; nowadays, since mechanical devices often struggle with the complex surfaces of modern vehicles, optical systems are being developed

to perform them in a non-contact way, in order to reduce damage (e.g. scratches) and to increase the quality of the measurement.
Gap and flush are also very important in other manufacturing processes, for example in appliance manufacturing and in furniture assembly.

In Chapter 2, we will introduce the research objectives of this PhD work.

Chapter 2.

Research Objectives

The purpose of this PhD project is to design and develop new instruments for in-line quality control, based on non-contact technologies, specifically electro-optical technologies. While also bringing attention to the importance of taking uncertainty into consideration, since it is pivotal in data-based decision making, as demonstrated by the many standards regulating conformity checks. This means that poor quality of measurements can prejudice the quality of the data.
In particular, this work presents two vision-based measurement instruments that were designed and developed for the purpose of in-line quality control and the uncertainty of each of the two instruments was evaluated and analyzed in comparison with instruments already present on the market. In the last part of this work, the uncertainty analysis of a hand-held laser triangulation profilometer is estimated.
Hence, the research conducted in this thesis can be organized in two main objectives, as follows.

Objective 1:
Design and development of vision-based dimensional measurement systems for quality control which could be integrated in-line.

Considering that the manufacturing industry imposes dimensional checks both macroscopic (dimensions [mm]) and microscopic (surface roughness [µm]), in this PhD project these two separate but complementary topics were addressed.

Objective 1.1:
Macroscopic measurements [millimeters]: the target was the in-production dimensional quality control of turned parts through telecentric optical profilometry.

For the first part of this thesis (Chapter 4), we will address a study conducted in collaboration with Zannini s.p.a., which is a turning factory of highly precise mechanical components, and with Z4tec s.r.l. which is a tech provider for Zannini. We developed a measurement instrument, based on telecentric optical profilometry, to control the quality of turned parts. The key specifications of the device were: suitability to charge and discharge parts automatically, short inspection time and possibility to simultaneously measure several dimensions on different sides of the part.
The sample to be inspected was placed between illuminator and objective in order to

obtain the projection of the shadow of the sample over a white background and the field of view was of 35 mm by 30 mm, see Figure 10. Dimensional measurements were then performed by means of graphical analysis over the image obtained, and the results obtained were in the millimeter range, with a spatial resolution of 25.5 μm.

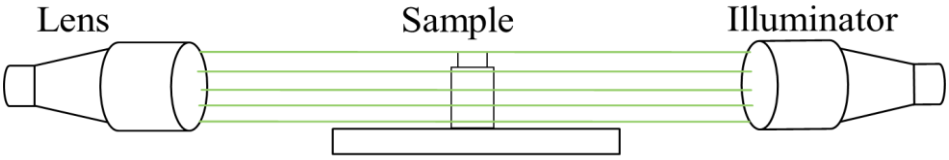

Figure 10. *Scheme of the optical profilometer developed for dimensional measurements.*

For this instrument, the goal was to obtain a performance-cost compromise. The instruments that are usually available on the market present a series of performances and abilities which are not always needed, resulting in a higher cost. Moreover, a fully customizable software also results in a lower intervention time and cost since it can be edited by internal personnel.

Objective 1.2:
Microscopic measurements (micrometers): the target was the in-line surface roughness measurement of turned parts through a backlighting system.

For the second part of this thesis (Chapter 5), we will address a backlit vision-based surface roughness measurement system with a focus on determining the optimal imaging conditions through the use of the Modulation Transfer Function (MTF) and the use of an Electrically Tunable Lens (ETL) which is a lens with a shape that can be controlled electronically in order to find the exact focus point. This component makes it a smart system that can be controlled with a feedforward type of control. The setup will be described in depth in Chapter 5, here a scheme of how it works is presented in Figure 11: the system is thought to take images during turning and process them to determine surface roughness; a turned sample (a cylinder) is placed in front of a camera, its axis is orthogonal to the camera axis, the camera axis is aligned tangent to the cylinder and it is backlit by a collimated source of light; such optical configuration is typical of telecentric vision or backlit vision and it provides the image of the edge of the sample.

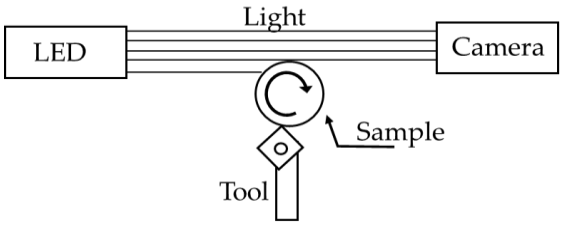

Figure 11. *Simplified scheme of the conceived backlit vision-based measurement instrument where a cylindric bar is turned between a camera and a light source and surface roughness is measured in-line during production.*

The images will show a close-up view of the edge of the sample where the wavy profile generated by the turning process is visible, in a field of view of approximately 1.5 mm by 1.8 mm. This will allow to make measurements in the range of micrometers, with a spatial resolution between 0.6 µm and 0.7 µm.
The system is thought to take images during turning and process them to determine surface roughness. the system would open the possibility to have a short inspection time and a completely non-contact measurement, which would fit appropriately the requirements of ZDM, i.e. in-line quality control of 100% of production on moving/rotating parts. Such instruments are not commercially available and this is the main reason for focusing on this design.

Objective 2:
Uncertainty analysis of the measurement instruments

Quality control in ZDM requires the samples produced to be checked for conformity assessment, this implies a lot of measurements which have a measurement uncertainty that needs to be considered.
Each chapter of this thesis will contain a section dedicated to the analysis of the measurement uncertainty of the measurement system considered.
Techniques to evaluate measurement uncertainty are described in the Guide to the expression of Uncertainty in Measurement (GUM) in ISO IEC GUIDE 98-3 [39] and will be further explained in Chapter 3.
The techniques used in this work were a Type A statistical uncertainty analysis and a Gage R&R analysis to evaluate the repeatability and reproducibility among different instruments measuring the same value.
The instruments that were considered are listed in the objectives below.

Objective 2.1:
Uncertainty analysis of a telecentric profilometer

In Chapter 4 there will be a section where the performance of the instrument is evaluated with both a Type A statistical uncertainty analysis and a Gage R&R.
The analysis was performed on measurements of lengths and diameters collected both with the telecentric profilometer and other instruments commonly used in the company to check the compliance to the technical drawings of the parts produced.
Two measurement campaigns were carried out respectively to:

- Estimate the metrological performance of each instrument: trueness and repeatability (i.e. bias and precision);

- Evaluate the combination of the variability due to the instruments (reproducibility) and the variability due to the pieces, and their relative weight on the results.

Each time, the mean value and two times the standard deviation were calculated and the mean values were compared to the results obtained with the reference instrument, which was identified by measuring certified gauge pieces, different for diameters and lengths.

Objective 2.2:
Uncertainty analysis of a vision-based surface roughness measurement system

In Chapter 5, the performance of the backlit surface roughness measurement system was analyzed through a Type A statistical uncertainty analysis. Given the limited number of samples available, we used the range as an estimate of the scatter of data instead of the standard deviation.
The results were compared to other state-of-the-art measurement instruments, both contact and non-contact. We based the performance comparison on a reference instrument.
The conclusions drawn from this analysis were different depending on the magnitude of surface roughness considered.

Objective 2.3:
Uncertainty analysis of a laser-line triangulation profilometer

In Chapter 6, the repeatability and reproducibility of a laser-line triangulation profilometer were assessed.

The instrument is a portable device that measures gap and flush in car body assembly; it integrates: a distance sensor, a laser-line projector and a camera creating a triangulation system. A laser beam is projected orthogonally both at the surface and at the gap between two adjacent car parts and a picture of the projection is taken, then, based on the laser profile, gap and flush are measured. A scheme of the functioning of the device is shown in Figure 12.

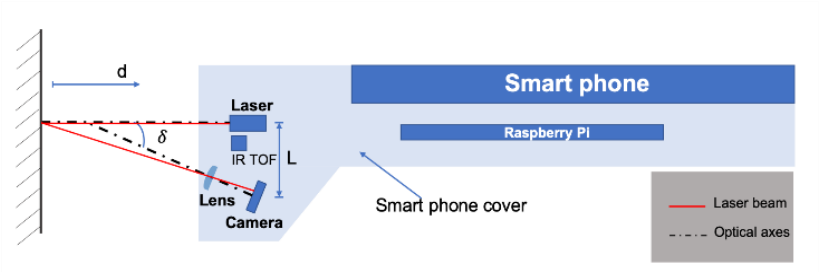

Figure 12. *Scheme of the triangulation system, where d is the distance from the target, δ is the fixed angle between the laser beam and the optical axis of the camera and L is the fixed distance between the laser and the camera.*

The uncertainty associated to the instrument and to the measurement chain is assessed with a Type A performance analysis and a Gage R&R study: different investigation points are identified on the body of a car and, in order to evaluate reproducibility, a series of measurements is taken by different human operators.

Chapter 3.

State of The Art

In this chapter, the state of the art of each topic discussed in this thesis will be reviewed. The first section will be about measurement uncertainty definitions and standards. Then different measurement techniques for dimensional measurements will be discussed, both for macroscale dimensions and for microscale features.
Lastly, a brief explanation will be given of the Modulation Transfer Function, which was used in multiple occasions for assessing the optical resolution of the instruments, in particular the lateral resolution which is closely related to measurement uncertainty in dimensional measurements.

3.1. Measurement uncertainty in conformity checks

Uncertainty is a complex concept and is expressed and described differently, depending on the field of application.
When talking about measurement uncertainty, its main components are described by standards at national and international level (EN, ISO, UNI etc.). In this section the following main standards regarding measurement uncertainty and measurement uncertainty in conformity checks will be discussed:

- UNI ISO 5725 – 1: 2004 Accuracy (trueness and precision) of measurement methods and results. Part 1: General principles and definitions [40].
- ISO 5725 – 2: 2019 Accuracy (trueness and precision) of measurement methods and results. Part 2: Basic method for the determination of repeatability and reproducibility of a standard measurement method [41].
- UNI ISO 3534 – 2: 2006 Statistics – Vocabulary and symbols – Part 2: Applied statistics [42].
- ISO IEC GUIDE 98– 3 Uncertainty of measurement. Part 3: Guide to the expression of uncertainty in measurement (GUM: 1995) [39].
- ISO 14253 – 1: 2017 Geometrical product specifications (GPS) – Inspection by measurement of workpieces and measuring equipment. Part 1: Decision rules for verifying conformity or nonconformity with specifications [43].
- ISO 14253 – 5: 2015 Geometrical product specifications (GPS) – Inspection by measurement of workpieces and measuring equipment. Part 5: Uncertainty in verification testing of indicating measuring instruments [44].
- JCGM 106: 2012 Evaluation of measurement data: Role of measurement uncertainty in conformity assessment [45].

- JCGM: 2006 International Vocabulary of Metrology – Basic and General Concepts and Associated Terms (VIM) 3rd Edition [46].

3.1.1. What is measurement uncertainty?

When reporting the result of a measurement of a physical quantity, a quantitative indication of the quality of the result is required so that it can be used to assess its reliability and its level of confidence. Without such an indication, measurement results cannot be compared, nor amongst themselves, nor with reference values.
The use of error and error analysis has been common practice for a long time, while the concept of uncertainty as a quantifiable attribute is relatively new in measurement science or metrology and engineering. Now it is understood that even if all of the known or suspected components of error have been evaluated and appropriately corrected, there still remains an uncertainty about the correctness of the result. Therefore, there is the need of a shared and accepted procedure for evaluating and expressing uncertainty.
In this section, to answer the question "What is measurement uncertainty?" the different components that are part of uncertainty are described, then we will focus on the terms accuracy and precision. In the last part, a method for Measurement System Analysis, based on reproducibility and repeatability is explained.

Components of measurement uncertainty

The uncertainty of measurement is associated with the result of a measurement, and it characterizes the dispersion of the values that could be attributed to the measurand. Depending on how the components of uncertainty are estimated, the evaluation methods can be grouped in two categories [39]:

- Type A evaluation: components evaluated through statistical analysis of a series of observations;
- Type B evaluation: components evaluated through other methods which do not include statistical analysis.

Below are described some of the main terms involved in measurement uncertainty:

- Measurand: *a particular quantity subject to measurement* [46].

The result of a measurement is only an approximation or estimate of the value of the measurand and thus is complete only when accompanied by a statement of the uncertainty of that estimate.

- Combined standard uncertainty: *standard uncertainty of the result of a measurement when that result is obtained from the values of a number of other quantities, equal to the positive square root of a sum of terms, the terms being the variances or covariances of these other quantities weighted according to how the measurement result varies with changes in these quantities* [39].

- Coverage factor: *numerical factor used as a multiplier of the combined standard uncertainty in order to obtain an expanded uncertainty* [39], often a coverage factor of 2 is used;
- Expanded uncertainty: *quantity defining an interval about the result of a measurement that may be expected to encompass a large fraction of the distribution of values that could reasonably be attributed to the measurand* [39], for example if the coverage factor is 2, then the confidence with which one could expect the results to be within the interval would be 95%.

Accuracy and precision

A common way to express the measurement uncertainty of an instrument is also in terms of accuracy and precision. To this regard, a very interesting and recent paper was proposed by Shirmohammadi, Mari and Petri in 2021 [47]. They explain how and why accuracy and precision are commonly misrepresented and misunderstood, pointing out the fact the general confusion that these terms bring along.

In UNI ISO 5725-1: 2004, *accuracy* is defined as *the closeness of agreement between a test result and the accepted reference value* [40]. As an example of the nonunivocity of this term and of its difficult interpretation, we provided other texts in which accuracy is defined. For example, in the 3rd edition of the VIM of 2006 [46], two approaches for the definition are presented: a "classical approach" which refers to the traditional way of defyning these terms, and an "uncertainty approach", which is a reviewed approach. The terms used in both approaches designate two different concepts and in such cases two different definitions are needed:

- "Classical approach" for accuracy: *closeness of agreement between a measured quantity value and a true quantity value of the measurand* [46].
- "Uncertainty approach" for accuracy: *closeness of agreement between measured quantity values that are being attributed to the measurand* [46].

In 2021 the Bureau International des Poids et Mesures [48] published a draft of the 4th edition of the VIM which is yet to be finalized, where they give the definition of accuracy as: *closeness of agreement between a measured value and a reference value of a measurand*, followed by generalizing notes which make this definition less clear, such as:

- "*NOTE 2 Accuracy is customarily thought of as pertaining to either:*
  1) a measurement procedure. In this case accuracy is generally known and reported quantitatively, sometimes in terms of bias and standard deviation.
  2) a measuring instrument or a measuring system. In this case accuracy is generally known and reported quantitatively, sometimes in terms of an accuracy class;

3) a single measured value or a set of measured values. In either of these cases accuracy cannot be known because the reference value in this case is a true value of the measurand. While accuracy and measurement uncertainty are not the same, sometimes accuracy is reported in terms of measurement uncertainty and sometimes measurement uncertainty is reported in terms of accuracy."

- *"NOTE 3 Accuracy can be interpreted as the combination of measurement trueness and measurement precision. However, the term "measurement accuracy" should not be used for measurement trueness and the term "measurement precision" should not be used for measurement accuracy."*

After saying that accuracy is not a quantity with a numerical value, in Note 2.1 is said that is reported quantitively as bias and standard deviation, which are not terms that describe accuracy. In Note 2.3 they admit that often the terms accuracy and measurement uncertainty are used interchangeably even if they are not the same. Similarly, in Note 3 they show the confusion around the terms accuracy, trueness and precision.
The nonunivocity of these terms and the confusion around them is certainly an inconvenience for the ones that must work every day with these standards, for example for performing conformity checks. Instead of giving clear directions, these definitions leave room for the workers to make their own interpretations.

This section will give a short and hopefully clear summary on how these terms should be used to describe measurement uncertainty, based on the paper already mentioned [47]. Figure 13 shows the representation proposed by [47] of the terms that will be discussed.

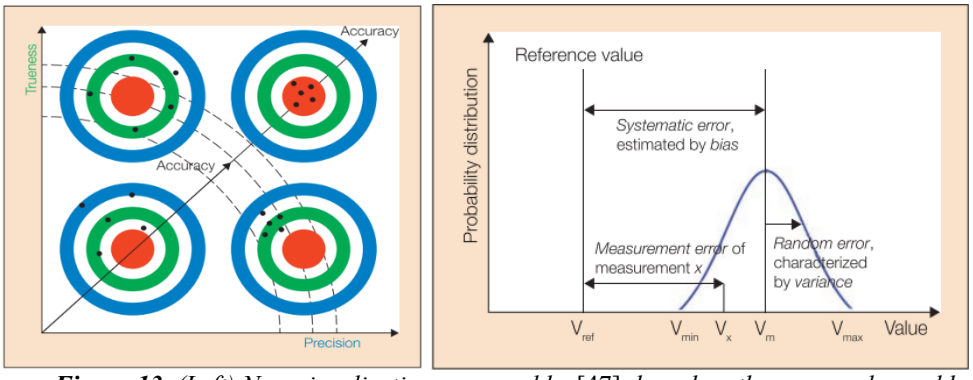

Figure 13. *(Left) New visualization proposed by* [47]*, based on the commonly used bulls-eye representation of accuracy and precision. (Right) Visualization of the influence of error on the distribution of measured values proposed by* [47].

First, it is important to say that accuracy and precision are terms that can be referred to either measuring instruments or measurement results.

We would like to stress that the final users of these standards and definitions are operators and technicians working in a production line or in a laboratory for quality control. They are interested in the uncertainty of the measurement results, these are the numbers their decisions are based on, so it is of the utmost importance that these definitions and concepts are expressed clearly in order to help, and not hinder, this decisional process.
For example in UNI ISO 5725-1: 2004, *accuracy* is defined as *the closeness of agreement between a test result and the accepted reference value* [40]*;* but, in the case of measurement results the reference value in unknowable because it would be the true value of the measurand, which cannot be measured or known. So, in this case, accuracy is not the term that should be used.

When a reference value is known (when considering measuring instruments, a reference value could be obtained from a measurement standard), the measurement error consists of two components: systematic error and random error.
Systematic error, which is also known as *bias* is the *component of measurement error that in replicate measurements remains constant or varies in a predictable manner* [46].
Random error, which is often referred to as *noise* is the *component of measurement error that in replicate measurements varies in an unpredictable manner* [46].
Similarly to how measurement error has two components (systematic and random error), accuracy consists of trueness and precision of the instrument. And since measurement error affects the accuracy of the instrument, trueness is affected by systematic errors and precision is affected by random errors. This is also visually explained in Figure 14.

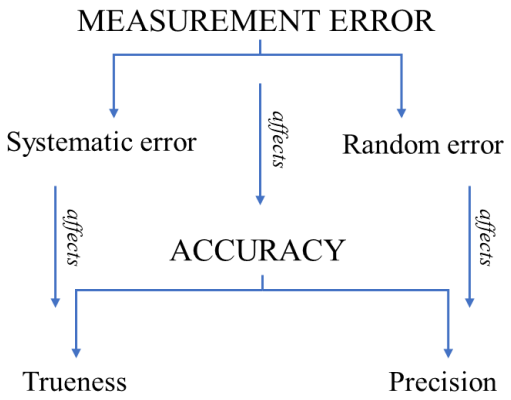

Figure 14. *Scheme of the relationship between the terms related to accuracy and precision.*

In these terms, *trueness* indicates the ability of an instrument to avoid systematic errors and it is defined as the *closeness of agreement between the average value obtained from a large series of test results and an accepted reference value* [40].
Precision on the other hand, is the ability of an instrument to avoid random errors and is defined as the *closeness of agreement between independent test results obtained under stipulated conditions* [40].

We can talk of *precision under repeatability conditions (Repeatability) and precision under reproducibility conditions (Reproducibility)* whenever these conditions respect the standards for repeatability and reproducibility (see next section).
Lastly, it is important to remember that accuracy should be part of the characterization of a measurement instrument but not of measurement results, since evaluating accuracy requires a reference value to be known, which is impossible for measurement results. About this, a summary of the availability of the reference value is presented in Figure 15.

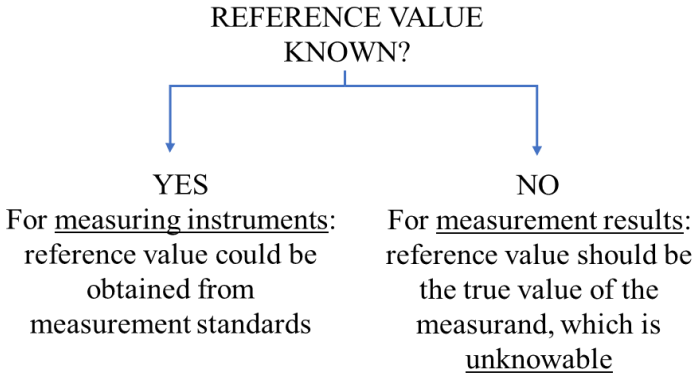

Figure 15. *Availability of the reference value for measuring instruments or measurement results.*

As already mentioned, one should remember that in the manufacturing industry, especially in quality control, we are interested in measurement results of unknown measurands, because these are the data on which conformity checks are based on (section 3.1.3).
We hope and suggest a revision and harmonization of the definitions and of the standards that refer to them, in order to have a convergence of terms and ideas, without the risk of misunderstanding. This would prove effective in the actual contexts in which these standards need to be interpreted, clearly understood and put to use. In-line quality control, to which this thesis largely refers, is a typical industrial context which would profit from such an harmonization.

Measurement System Analysis (Gage R&R)

Measurement System Analysis (MSA) is a tool for assessing the variation present in each type of inspection, measurement and test equipment. In other words, it evaluates the quality of measurement system [49].
Gage R&R studies are a type of MSA, where R&R stands for Repeatability & Reproducibility, and are often used to assess the variation in data caused by the measurement process [50] and they are part of the class of ANOVA (ANalysis Of Variance) analyses. In a typical study, multiple parts are measured multiple times by multiple operators, to estimate repeatability and reproducibility. The variation in measurement given by a particular operator on a particular part is called the repeatability variation of the gauge. Variation which can be attributed to differences

between the operators is called reproducibility variation of the measurement system [51].

Repeatability is defined in ISO 3534 – 2 as the *precision under repeatability conditions* which are *observation conditions where independent measurement results are obtained with the same method on identical measurement items in the same test or measuring facility by the same operator using the same equipment within short intervals of time* [42]. More simply, it quantifies the variation we see in measurements taken by the same person, on the same part, with the same instrument. *Reproducibility* is defined in ISO 3534 – 2 as the *precision under reproducibility conditions* which are *observation conditions where independent measurement results are obtained with the same method on identical measurement items in different measurement facilities with different operators using different equipment* [42]. In other words, it quantifies the variation we see in measurements taken by different people on the same part, using the same instrument.

Gage R&R is very important whenever there is a change in workers, a new instrument is used or the process has been changed significantly, in fact it determines the variability of the measurement system compared to the total variability. The measurement system variability is the sum of the variability components given by repeatability and reproducibility.

The studies presented in this work should not be confused with interlaboratory studies where repeatability standard deviation and reproducibility standard deviation are estimated based on a design in which each laboratory conducts a number of independent measurements on the same sample under repeatability conditions. Indications on the statistical analysis of such experiments are given in ISO 5725 – 2: 2019 [41]. In our case, even if the sample was the same, the instruments used to measure it were different.

3.1.2. What to consider when performing measurements

The result of a measurement after correction for systematic effects is still only an estimate of the value of the measurand because of the uncertainty arising from random effects and from imperfect correction of the result for systematic effects.

In practice, there are many possible sources of uncertainty in a measurement. It is obvious that the quality of data depends entirely on the uncertainty of measurement and on the reliability of the data. Hence, it is important to keep all contributing factors in mind [39]:

- incomplete or imperfect definition of the measurand, for example a part may be assumed to be perfectly straight, when in fact it may not be straight;
- effects of environmental conditions on the measurement or imperfect measurement of environmental conditions: the shop-floor environment is often characterized by seasonal or daily temperature fluctuations, a lack of cleanliness or the presence of significant vibrations, just to mention a few;

- personal bias in reading analogue instruments: human operators need appropriate training before performing measurements, moreover human error is always possible;
- finite instrument resolution or discrimination threshold: an uncertainty intrinsic to the measurement instrument, an example of this will be discussed in Section 3.2.2 and Section 5.3.2;
- inexact values of measurement standards and reference materials, such as a worn gauge block used for calibration of the instrument;
- approximations and assumptions incorporated in the measurement method and procedure, for example when using measurement algorithms and mathematical models;
- variations of the measurand under observation due to non-stationarity of measurement conditions, for example a higher temperature causes metal samples to dilate.

3.1.3. Standards regarding conformity checks

Measurements are used to make important decisions ranging from accepting or rejecting product, for example in in-line quality control, to deciding modifications to the product, for example during its laboratory testing at prototype level. However, because all measurements have an associated uncertainty, there is inherent risk that incorrect decisions will be made [50]. There is a lot of interest in having instrument with smaller measuring uncertainties, alas these are usually more expensive. But it is also expensive to re-engineer a product after it proved difficult to measure [52].
In manufacturing and quality control processes, Geometric Dimensioning and Tolerancing is one of the main parts [53]. And there are standards which provide guidance about reducing the size of the acceptance band to allow the uncertainty of the measuring instrument, reducing also the risk of making incorrect decisions.
This section will review some of the standards involved in regulating conformity checks.

Tolerance interval

The Joint Committee for Guides in Metrology (JCGM) [45] uses the term *tolerance limits* (T_L = lower limit, T_U = upper limit) and defines the tolerance interval to be the range of acceptable values between the limits. The Test Uncertainty Ratio (TUR) has been used as an indicator of a measurement's suitability to make an accept or reject decision and is defined as [50]:

$$TUR = \frac{\pm Tolerance\ Limit}{\pm\ Measurement\ uncertainty\ (95\%\ confidence)} \tag{3.1}$$

To ensure the adequacy of a measurement to make a particular accept/reject decision, a TUR of at least 4 (referred to as "meeting a 4:1 ratio") is often used. Sometimes for more conservative work, a TUR of at least 10 is required. The use of a TUR assumes that all measurement biases have been removed and the measurements

involved follow a normal distribution. The TUR will not account for the increased risk, if there are significant biases that cannot be removed.

By defining an acceptance interval of permissible measured values of a measurand (A_L = lower limit, A_U = upper limit), the risks of incorrect accept/reject decisions associated with measurement uncertainty can be balanced. An example of acceptance interval, and its corresponding tolerance interval is shown in Figure 16.

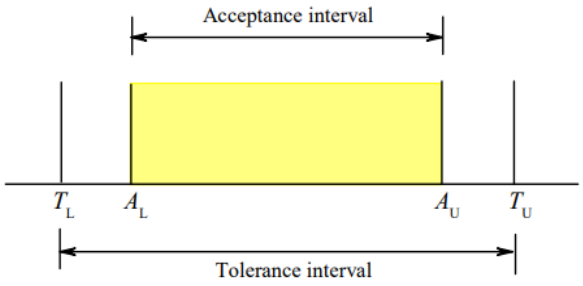

***Figure 16**. The true values of a measurand will lie in a tolerance interval (from T_L to T_U), the object measured will be conform if the measurand lies within the acceptance interval (from A_L to A_U)* [45].

A false reject, or false positive, occurs when a system rejects a valid part, while a false accept, or false negative, is when the system accepts a part which is not within tolerance. Both of these instances should be avoided in order to minimize waste, in the first case, and avoiding delivering faulty parts to the customer, in the second case. Moreover, wrong accept/reject decisions imply an extra cost for the company, for example in the automotive industry, precision parts need to be perfectly within tolerance. In case the customer, during their non-conformity checks, finds one part out of tolerance, they will ask for a complete re-check of the production lot. It goes without saying that this would imply extra costs that the supplier has to cover.

The graph in Figure 17 is a schematization of the Cost of Quality (COQ): it is a measure of all the costs related to achieving quality and the costs due to quality issues [54]. Specifically, the cost of conformance is described by the resources necessary to achieve the quality required and its increase is associated with a decrease of marginal utility, i.e. the higher the quality of the final product, the higher is the cost required. The cost of non-conformance is determined by the resources needed for fixing failures and taking corrective actions and it is indirectly proportional to the quality of the finished product.

To optimize the total costs, the optimal balance between the costs of conformance and the costs of non-conformance has to be determined. This corresponds to the lowest point on the curve of COQ.

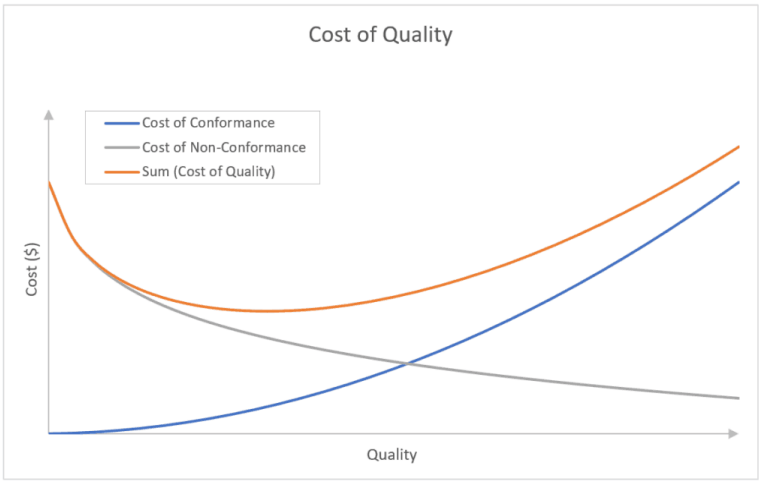

Figure 17. *Chart showing the cost of conformance and non-conformance. The sum of the two curves is the cost of quality. Image from* [54].

The guidelines for conformity and non-conformity checks are further explained in ISO 14253-1:2017, where is clearly stated that "*the estimated measurement uncertainty is to be taken into account when verifying conformity or nonconformity with specification. The problem arises when a measured value falls close to the upper or lower specification limit. In this case, verification of conformity or nonconformity with specifications is not possible: the measurement uncertainty induces a probability that a true value of the characteristic is out of specification even if the measured valued falls inside the specification zone, or is in specification even if the measured value falls outside*."

Other than stating that the measurement uncertainty is an important part of the measurement, it also establishes the rules for verifying conformity or nonconformity with a given tolerance, including when the measured value falls close to the specification limits. For example, the figure below illustrates the difference between specifications when no uncertainty is involved and when the uncertainty imposes limitations.

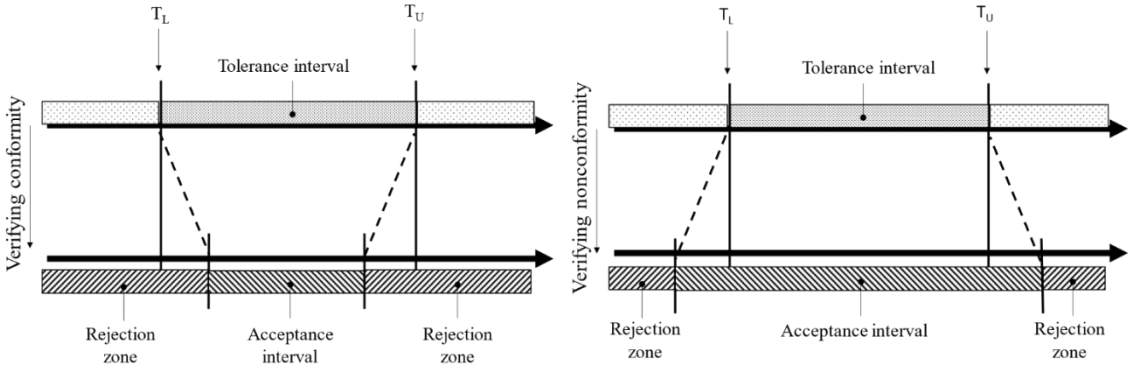

Figure 18. *Measurement uncertainty reduces the zone where to check conformity (Left) or nonconformity (Right).*

Similarly, in standard ISO 14253-5:2015, the uncertainty of indicating measuring instruments is discussed. An indicating instrument is a type of instrument that gives as a result the measuring quantity at a particular instant and it is part of the secondary instruments' class, which require calibration before use [55].
Standard ISO 14253-5 states that measurement uncertainty of indicating measuring instruments is not conceptually straightforward and to test it there are many possible measuring tasks and environmental conditions. In principle, all of these possible scenarios should be tested, but since it is impossible and not economically viable, a test protocol is needed and is often agreed upon by both supplier and customer.
Moreover, in section 7.2 of ISO 14253-5 it is highlighted that indicating measuring instruments introduce errors which affect the uncertainty of the measurement results of, for example, the characteristics of a workpiece. Therefore, they have to be accounted for in the measurement uncertainty associated with the workpiece measurement.

3.2. Measurement systems for dimensional measurements for macroscopic and microscopic measurements

The topic of dimensional measurement is extremely wide, since it includes all measurements which quantify the geometry, size and shape of the measurand, and it would be impossible analyzing all of the different possible types of measurements of dimensions. In this work we focus on two main industrial processes which occupy a relevant share of the production industry in multiple different sectors:

- Assembly of adjacent parts;
- Machining of metal parts through turning.

Assembly operations refer to the process of putting together individual parts to create a final product and are a widespread process which is used in all sectors which make final products through the manufacturing of individual parts. It usually involves manual, or automated, techniques to fasten or join different components; a subgroup of this category of operations is the assembly of adjacent parts. A fundamental part of this process involves the alignment of these parts. For example, in vehicle manufacturing: from cars, during the alignment of the car door and the frame; to airplanes, during alignment of adjacent panels. Or in appliance manufacturing, for example during alignment of washing machine door and chassis.
In the manufacturing industry that produces metal parts, turning is one of the most relevant production processes, in fact cylindrical parts are present in all kinds of finished products, regardless of their application.
Given the spread use of these two industrial processes, there are many measurement aspects that one can focus on. In this work we narrowed the measurements down to two main categories:

- For the assembly of adjacent parts, we focused on gap and flush measurements, which are characteristics commonly checked in several assembly process. The method used for this evaluation was a laser-line triangulation system;
- For the turning of metal parts, we focused on the most important geometrical characteristics of cylindrical products, which are lengths, diameters and surface finish. The methods used for this evaluation were backlit vision-based measurement systems.

The state-of-the-art of dimensional measurements is constantly evolving with the development of new technologies and techniques. Currently, the most advanced dimensional measurements are being carried out using non-contact methods such as optical or laser-based systems, structured light scanning or computed tomography scanning. Among the advantages they provide there are high accuracy and high measurement speed.
Other techniques that are still widely used include touch-probe measurements, contact measurements, and confocal microscopy. These methods have the advantage

of being relatively low-cost and easy to use, but they may not provide the same level of accuracy as the latest non-contact systems.

3.2.1. Macroscale: technologies for inspections of dimensional measurements

This section focuses on laser-line triangulation systems and backlighting systems for dimensional measurements. These are the two main recent and promising technologies for in-line applications used in the industrial context.

1. Laser-line triangulation systems for gap and flush measurements

Dimensional inspection of gaps between adjacent parts and panels is one of the most difficult tasks of assembly and often performed by operators by means of manual tools like feeler gauges, calipers and dial gauges (Figure 19).

Figure 19. *Examples of manual measurements of gap and flush: (Top) a caliper* [56] *and feeler gauge* [57]. *(Bottom) feeler gauges used on car body* [58] [59].

The most common measurements they have to check are those regarding gap and flush. The gap is the tangent distance between the two parts, while the flush is the relative orthogonal displacement, as can be seen in Figure 20.

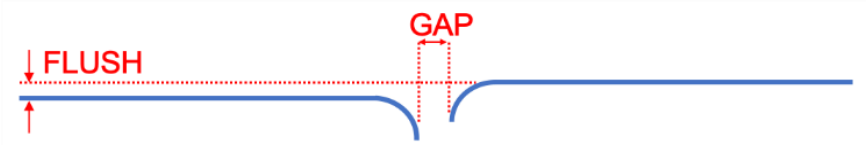

Figure 20. *Definition of gap and flush.*

Since these instruments are contact devices and the feedback they provide is visual, there are often disadvantages which include:

- Physical contact: it can damage the parts;
- Interaction force: it can increase the gap even further;
- Measurement results depend on the relative position between the system and the surface;
- Low resolution: it is limited by the physical dimension of the probe and it causes a higher measurement uncertainty;
- Time consuming: properly aligning he instruments requires manual skills and precision;
- No collection of data: the data is lost after the inspection because data is not recorded. This is particularly relevant in the context of Industry 4.0, where one of the main goals is to collect and integrate data coming from different stages of production.

Nowadays, since mechanical devices often struggle with the complex surfaces of modern vehicles, optical systems are being developed to perform them in a non-contact way, in order to reduce damage (e.g. scratches) and to increase the quality of the measurement.
Optical inspection systems have significant advantages:

- High speed of measurement;
- High accuracy;
- No risk of damages;
- Measurements can be stored in databases automatically.

Laser triangulation principle

In laser triangulation the object to be measured is illuminated by a laser line projector. The image is recorded by a camera positioned at a known angle to the laser emitter. The laser line is deflected based on the geometry of the object and this is recorded by the camera. This generates a profile and the shape of the object can be estimated through the height information obtained using the deviation of the points from the undeformed laser line [60] [61].
Figure 21 (Left) presents a scheme of the triangulation principle: the laser line is projected on features of the target at different positions (h_1 - h_3), light is scattered by diffuse reflection and imaged on the camera sensor. Light will strike the sensor in different locations *d'* which are dependent on the vertical offset (*d*) between the target and the laser. The distance *d* will produce a proportional change in position *d'* at the sensor [62]:

$$d = \frac{ad' \sin\beta}{b \sin\theta - d' \sin(\theta+\beta)} \tag{3.2}$$

where a and b are the segments shown in Figure 21 (Right), θ is the angle between the axis of the laser and the optical axis of the camera, and β is the angle between the camera sensor and the optical axis of the camera.

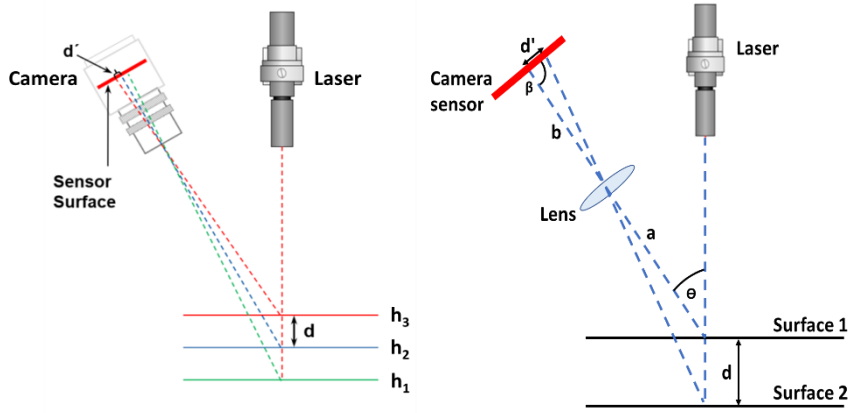

Figure 21. *Laser light diffused from different distances (h_1 – h_3) strikes the sensor in different locations (d'). Images from* [62], [63].

Some of the downsides connected to this technique are listed below:

- Shadowing: depending on the shape of the surface, the laser line can be blocked by elements of the object itself (see Figure 22) so that height information on the shadowed structures cannot be detected.

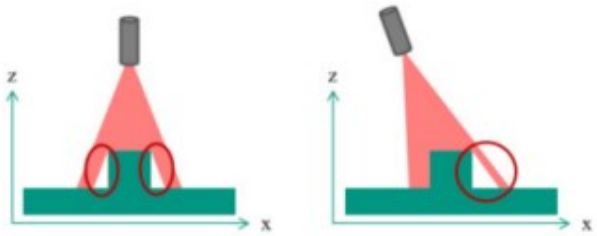

Figure 22. *Effects of shadowing* [64].

- Physical size of the sensor: a change in the vertical distance d can result in a displacement d' on the sensor, which might exceed its physical size (d' would fall outside of the camera sensor);
- Limited pixel resolution: like all camera-based systems, the pixel resolution of the sensor is a limiting factor, especially when the measurement range is increased. This relationship has to be kept in mind when designing the system. Sub-pixel accuracy can be reached by proper image processing.

Along this line of research, Kosmopoulos and Varvarigou [65] developed an automated system that uses computer vision, based on stereo cameras and infrared LED lamps.
Kumar et al. in 2006 [61], presented a triangulation based range sensor for profile measurements independent from optical surface properties. They also explain a least square method for obtaining depth information.
Garcia et al. in 2002 [66], developed a flatness measurement system which used non-linear optical triangulation. They introduced a different and innovative geometry in the disposition of the optic elements, this increased the measurement range without hindering its accuracy.
Castellini et al. in 2007 [67], designed a folded optical system with two laser line projectors and a CMOS camera, operating over a Region of Interest. The scanner was used for real time on-line detection of the shape of wood panels on a transport belt.
Pham et al. in 2021 [68], presented a portable smartphone-based laser measurement system to measure gap and flush. A 3D printed structure is used to hold together the smartphone and the laser-line projector.
Slossberg et al. in 2016 [69], demonstrated the possibility to obtain a good quality 3D reconstruction by using a mobile device. They used a smartphone and a laser pointer, and thanks to the line location, the phone position, and the 3D orientation they were able to reconstruct point clouds of the objects.
Pribanić et al. in 2016 [70], integrated with a smartphone a structured light 3D scanner which uses an infrared projector. The system was used to scan human faces.
Barbosa et al. in 2014 [71], evaluated the variability of measurements obtained with manual instruments and laser instruments to measure gaps and steps. They used a reproducibility and repeatability gage study to perform the assessment and the results demonstrated the advantages of laser devices.
Kholkhujaev et al. in 2022 [72], proposed and metrologically characterized an optical measurement system based on machine vision for gap and flushness measures. They used an ultraviolet laser and mounted the sensor on a robotic arm and performed measurements on a real vehicle body. The metrological characterization was performed through a Gauge R&R study.

Many industrial suppliers also develop and implement this kind of technology to manufacture measurement instruments. Micro-Epsilon uses laser triangulation sensors for displacement, distance and position measurements [73]. They are used in measurement and monitoring tasks in factory automation, production, robotics and vehicle assembly.
Their sensors have a high measuring rate and accuracy, making them suitable for measurements in continuous operations, see Figure 23.

Figure 23*. OptoNCDT laser sensors: (Left) sensors for flatness measurement of IC pins. (Right) OptoNCDTBL blue laser sensor for vibration measurements on an engine. Photos by Micro-Epsilon* [73].

Kreon developed both laser line triangulation sensors and robotic arms (see Figure 24) able to aid the operator in supporting the instrument and relieving them of the weight. Thus, enabling longer and faster inspections.

Figure 24. *Blue laser technology developed by KREON* [74]. *Photo of Ace arm with Skyline sensor integrated, by KREON* [33].

LMI Technologies produces red- and blue-based laser models for 3D line profiling [75], they are designed for the inspection of difficult targets in high-speed in-line applications, for example for measurements of small electronic parts but also for measurements on car body parts (see Figure 25).

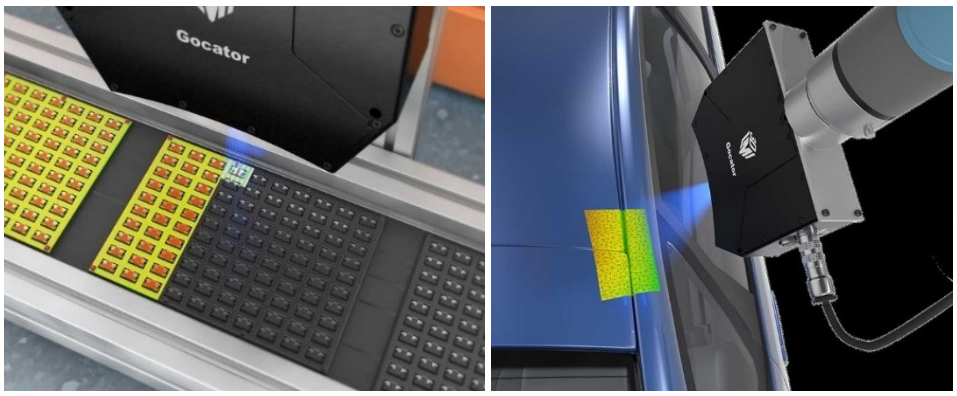

Figure 25. *LMI Gocator sensors for measurements of electronic parts (Left) and for car body parts (Right). Photos by* [76].

QFP developed a precision non-contact measurement tool which projects a red or violet laser blade on the part to be measured and uses different measuring heads, Figure 26 [77].

Figure 26*. GapGun Pro 2 by QFP* [77].

Wenglor is a company that develops smart sensors and image processing technologies which can be used in automated industry [78]. Among their products they have 2D/3D profile sensors, which project a laser line on the object to be detected.

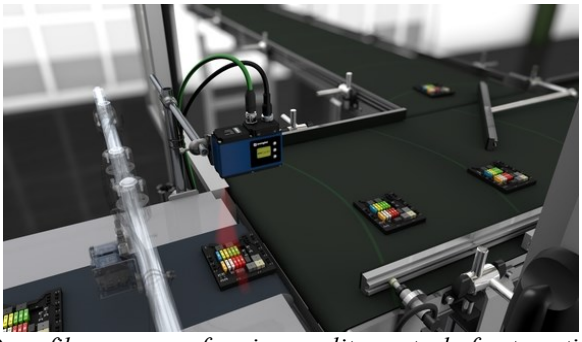

Figure 27. *2D/3D profile sensor performing quality control of automotive fuses. Image by* [78].

Keyence is another main manufacturer of vision-based measurement systems, and they include in their portfolio also the production of 2D triangulation methods. Such as the one showed in Figure 15: it involves a laser beam, which is expanded into a laser line, shined on the surface of an object and then reflected on the camera sensor.

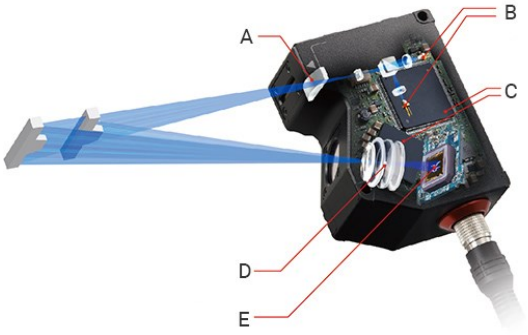

Figure 28. *Triangulation sensor by Keyence: A) Cylindrical lens, B) Laser, C) Processor, D) 2D Ernostar Lens, E) Camera sensor. Image from* [79].

The laser-line triangulation sensor used in this work to study the variation in measurement introduced by the operator was developed in 2018 within the framework of the GO0D MAN (aGent Oriented Zero Defect Multi-stage mANufacturing) European project and presented by Minnetti et al. in 2020 [80]. The scope of the project was to develop a device with the following characteristics: portability, sensing capabilities, wireless connectivity to a network, computational power, a human-machine interface and the possibility to implement smart behaviors. All of which were integrated in a smartphone. This device was patented in 2019 [81].

Details of the measurement instrument will be explained more in depth in Chapter 6 and the reader is encouraged to read [80] if further interested.

In this thesis, we were interested in the measurement uncertainty of non-contact instruments such as the ones described above. Hence, we used this laser-line triangulation sensor to perform measurements of gap & flush, in order to evaluate its measurement uncertainty, particularly the influence of the operator on the total variance.

2. Backlighting vision systems for dimensional measurements

Contact instruments for dimensional measurement are those that require physical contact with the object being measured. Some common examples of contact instruments, which are used daily for quality control checks, include:

1. Micrometers: handheld precision instrument used for measuring small dimensions and thicknesses;

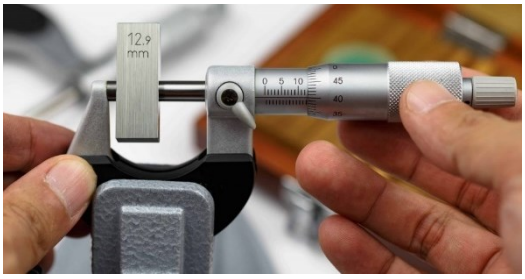

Figure 29. *Manual micrometer. Photo by* [82].

2. Calipers: used to measure linear dimensions, such as length and width, as well as internal and external diameters. It requires some handling skills but it is more versatile than the micrometer, even if less accurate;

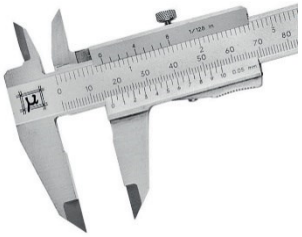

Figure 30. *Vernier caliper with round shaft from Rupac. Image from* [56]**.**

3. Dial indicators: used to measure small displacements and deviations from a reference surface, often used in machining and manufacturing.

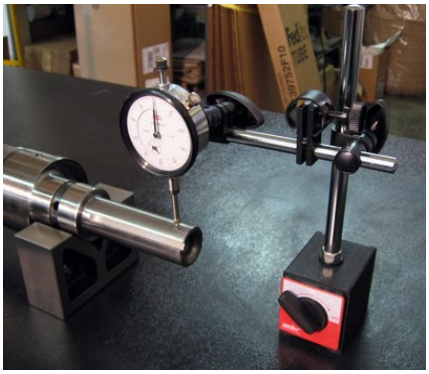

Figure 31. *Dial indicator performing a measurement* [83].

4. Coordinate measuring machines (CMMs): complex measurement equipment that use touch-probes to measure the position of points on the object being measured, often used for high-precision measurements of complex parts, through automated or semi-automated procedures.

Figure 32. *Coordinate Measuring Machine with different types of probes. Photo by* [84].

Contact instruments are often less expensive than non-contact ones and are relatively simple to use, making them a popular choice for many industrial and manufacturing applications. However, they are limited by the need for physical contact, which can result in damage to delicate or sensitive parts, and they may not provide the same level of accuracy as the latest non-contact systems.
These are the reasons why the modern measurement industry is moving towards non-contact measurement systems. Among these, instruments which rely on backlighting are increasingly more common. What is the measurement uncertainty of these instruments? This is one of the focuses of this PhD work and it will be explicitly covered in Chapters 4, 5 and 6.

Telecentric profilometry is a non-contact, optical measurement technique that is used to measure surface profiles, roughness, and other physical properties of materials. An object is illuminated through backlighting with a collimated light source and observed with a telecentric lens, this will provide the viewer with an image that highlights the outline of the object on the camera sensor (black object on white or grey background). This concept is schematized in Figure 33.

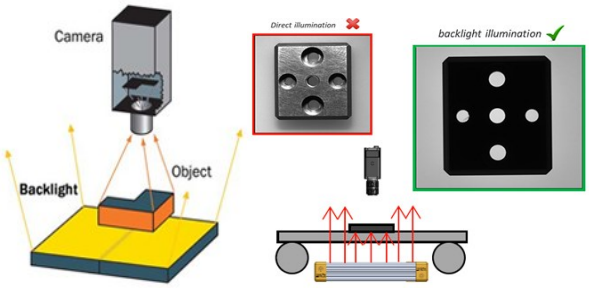

Figure 33. *(Left) Backlighting principle schematized by US Auto Corp* [85]. *(Right) Examples of images obtained with direct illumination and backlight illumination by Effilux* [86].

Such images allow to measure the outer geometry of the object and also the features of passing holes. By choosing the right components of the vision system, one is able to obtain really high-quality images that would be even suitable for quality control of dimensions with small tolerance interval.
The main components responsible for quality image are:

- Type of illumination: depending on the source of light, the light rays can be deflected by the object creating a distortion on the image;
- Type of objective: a standard lens will show an image whose dimensions change depending on the distance between the camera and the object; a special lens, like a telecentric lens, will not be influenced by the distance of the object;
- Sensor size of the camera: it is the dimension of the image sensor and is directly related to the spatial resolution, which is the number of pixels present on the sensor. A high resolution means that the size of the pixels is small, hence more pixels can fit on the sensor area, consequently the details that can be detected are smaller.

The type of illumination and type of objective will influence the sharpness of the outline of the object, while the resolution of the camera will of course influence the resolution of the measurement system.
Backlighting illumination can be of two main types:

- Diffused: light is provided by a LED panel, it might be uniform but it is not collimated, hence the outgoing light rays are not parallel to the camera axis;

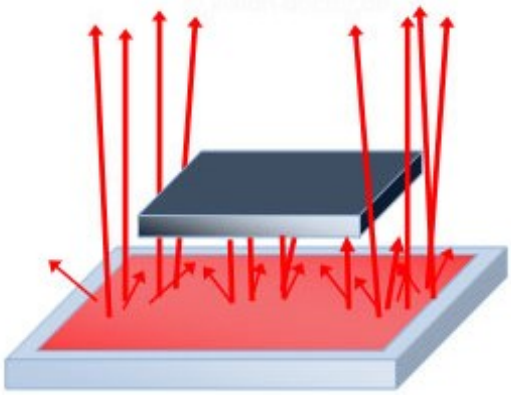

Figure 34. *Principle of backlight illumination with diffused light* [87].

- Collimated: light is provided by a collimated source, usually a telecentric illuminator; light rays are parallel to the axis of the camera;

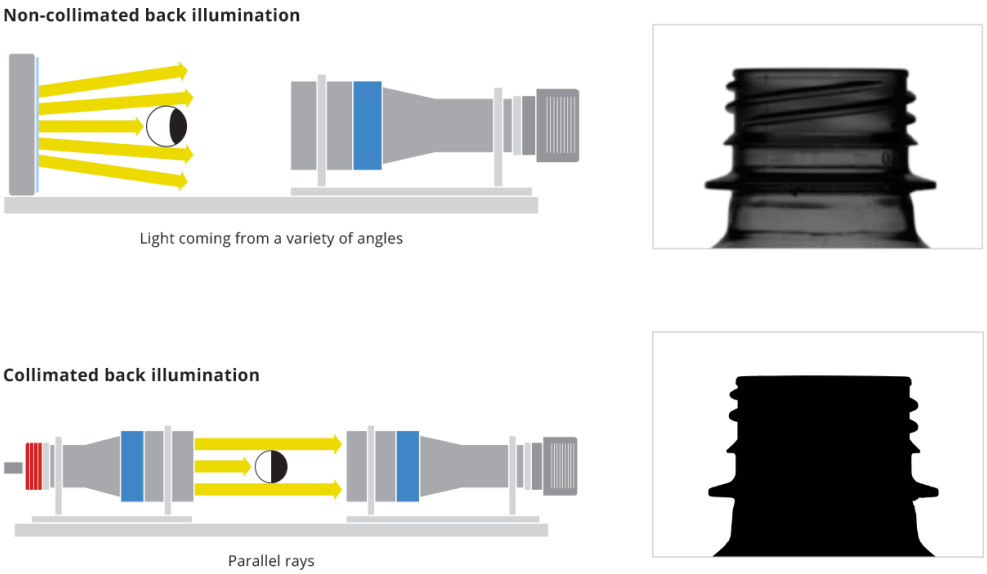

Figure 35*. Examples of images of the same object obtained through diffused an collimated backlighting* [81].

Another important aspect to obtain high-quality images that can allow measurements with small tolerances is the type of lens placed in front of a camera. The types of objectives can be multiple, for the purpose of this work, we will review only standard lenses and telecentric lenses:

- Standard lenses: they will provide an image of the object that will have a different magnification depending on the object-to-lens distance. An example is shown in Figure 36 [88].

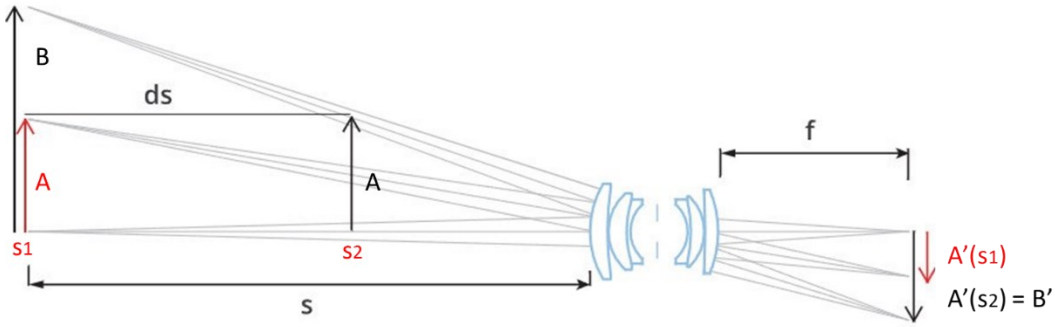

Figure 36. *The same object (A) can appear as having different sizes depending on the distance (s) from the lens: A'(s_1) ≠ A'(s_2). On the other hand, objects of different sizes (A and B) can appear as being equal if they are placed at the same viewing angle: A'(s_2) = B'.*

- Telecentric lenses: they provide an image whose size is not dependent on the distance to the lens, if within the working range of the objective and they eliminate perspective effects. This is possible because the objective collects only the light rays which are parallel to the camera axis. This is exemplified in Figure 37 [88].

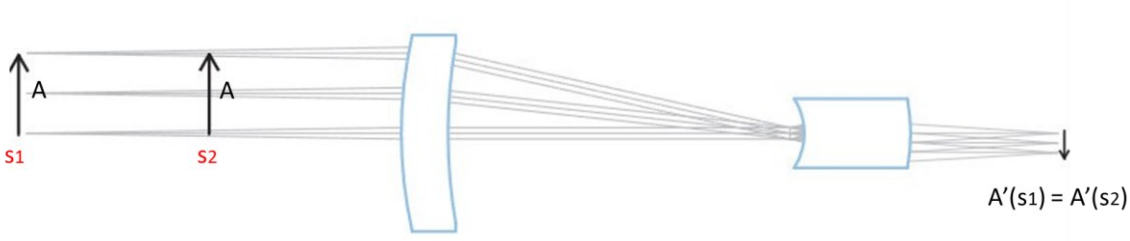

Figure 37. *The same object (A) at different distances (s_1 and s_2) appear as the same size on the image plane: A'(s_1) = A'(s_2).*

To get an idea of just how different the same objects can appear if viewed with a standard lens or with a telecentric lens, let's look at Figure 38 [88].

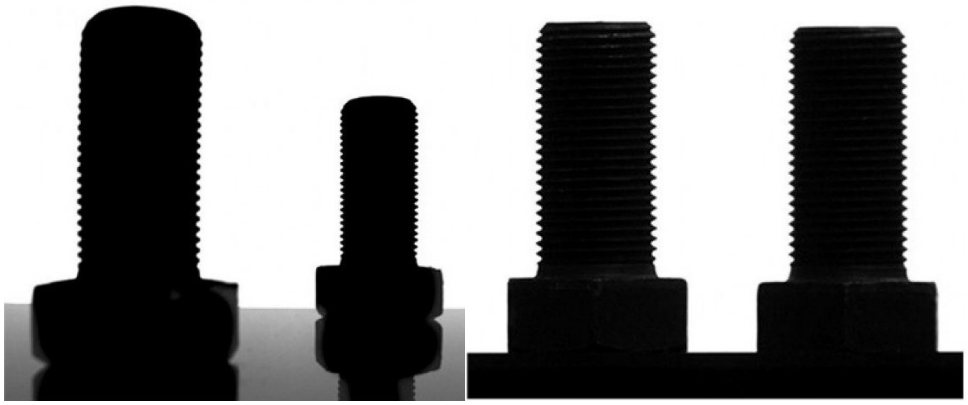

Figure 38. *(Left) Proportional effect of standard lenses: two identical screws, placed at different distances appear as having different sizes. (Right) Telecentric view: the same two screws, placed at different distances, appear identical.*

Measuring instruments commonly used in industrial settings make use of this technology, some examples are presented below.
Delta Visione is a company that provides solutions for marking systems, traceability systems, sorting machines and machine vision systems. Among their products they also make use of telecentric optics, in particular the one showed in Figure 39 is part of an automatic sorting machine for quality control.

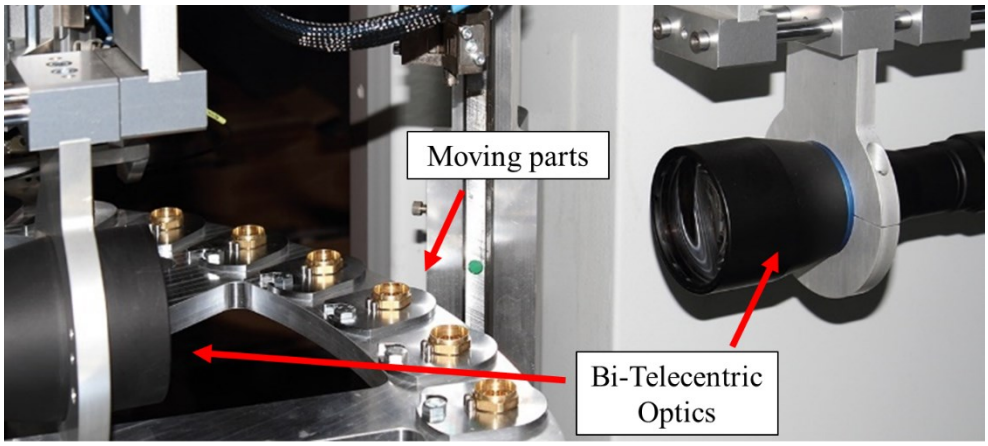

Figure 39. *Detail of the DV-RDSM for sorting by Delta Visione [89]. Visual controls are made with high-resolution cameras and bi-telecentric optics on moving parts.*

VICIVISION designs and produces optical measurement systems and automation systems, in their optical systems they include backlighting illumination on a rotating cylindrical part (Figure 40): the part is placed on a rotating mount and is illuminated from one side, while the camera placed on the opposite side records the images.

***Figure 40**. M609 Techno by VICIVISION: optical measurement system for cylindric elements* [90]

Marposs produces high-tech devices used in production line, among which 2D optical gauging solutions [91]. In Figure 41 is presented a system for quality control on small-size shafts and fasteners, based on 2D optical technology: similarly to the system shown in Figure 40, the part is moved by a rotating mount and a blue light casts the profile of the part onto the camera sensor placed on the opposite side.

***Figure 41.** Optoflash S100 by Marposs. Used for 2D optical measurements of rotating parts.*

Keyence [92] is a supplier of sensors, measuring systems, laser markers, microscopes and machine vision systems. Among them there are included high-speed 2D optical micrometers such as shown in Figure 42. A part is placed in the range of view of the telecentric lenses and based on the measurements performed on the image collected the light turns red or green depending on the conformity with specifications.

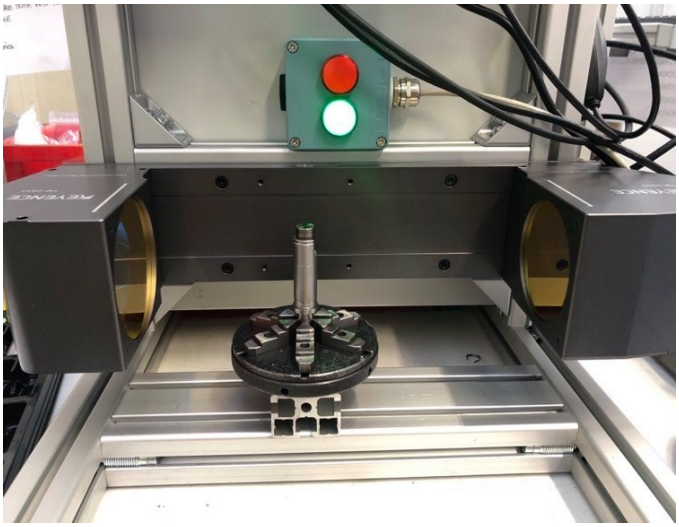

Figure 42. *Sensor head TM-065 by Keyence. The system includes telecentric lenses, the part is placed between them and the measurements are performed on the resulting image.*

As already mentioned in Chapter 2, Objective 1.1, the goal for the OASIS was to obtain a compromise between performance and cost. The reason for this is to be found in the specific needs of an industrial environment. For example, the instruments that are usually available on the market present a series of performances and abilities which are not always needed, resulting in a higher cost. Moreover, the design and software are not usually customizable. The turning factory that commissioned this instrument was specifically interested in the possibility to fully customize the design, based on the measurement target, and to customize the software. An accessible software means that possible bugs can be fixed by internal personnel, cutting both intervention time and costs.

3.2.2. Microscale: technologies for surface roughness measurements

Definition of surface roughness

The definitions and parameters for determining surface texture are described in ISO 4287: 1999 Geometrical Product Specifications (GPS). Surface texture: Profile method – Terms, definitions and surface texture parameters [93]. Among these parameters, in this work we focused on measuring the average surface roughness, R_a, which is calculated as the *arithmetic mean of the absolute ordinate values within a sampling length,* and expressed as:

$$R_a = \frac{1}{n}\sum_{i=1}^{n}|Z_i| \quad (3.3)$$

Where n is the number of data points (i.e. the sampling length) and Z_i is the ordinate value of the i^{th} point from the mean line, see also Figure 43.

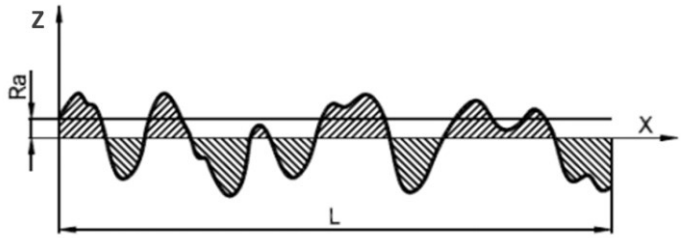

Figure 43. *Definition of average surface roughness: L is the length of the profile, Z(x) is the height absolute value from the reference mean line X. Image from* [94].

The specifics on how to choose parameters are described in ISO 4288: 1996 Geometrical Product Specifications (GPS). Surface texture: Profile method – Rules and procedures for the assessment of surface texture [95].
For example, the areas to be inspected are specified, depending on if the surface appears homogeneous or not. Surface defects should not be considered during inspection of surface texture. Measurements should be carried out on the surface where critical values are expected, this decision will be based on a visual examination.

Measurement methods for surface roughness

The state-of-art measurements of surface roughness are carried out using contact measurements systems and can be implemented only off the production line. Therefore, such measurements are used in the context of statistical process control and batch production. Indeed, surface roughness measurements can be divided in two main categories: contact techniques and non-contact ones. The first usually involve the use of a stylus with a diamond tip which is scanned along a straight line over the surface and acquires the deviation in the form of a 1-dimensional surface profile, see Figures 44 and 45 [96].

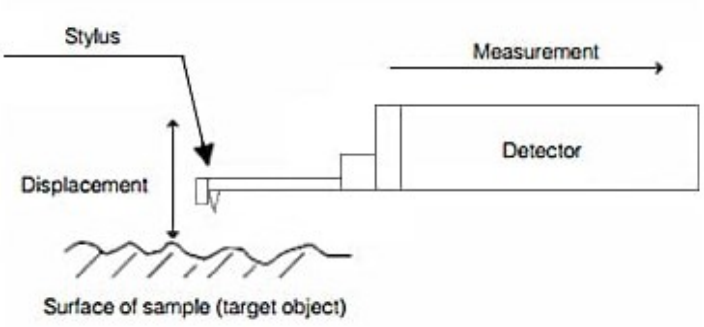

Figure 44. *Description of the working principle of a contact-type surface roughness measuring system. Image from* [97].

Figure 45. *Laboratory surface roughness tester by Mitutoyo.*

This method, even though is still commonly used, has some limitations:

- Workers have to randomly select a sample from the production line to test it with the stylus;
- The stylus inspects only a relatively small area, which does not represent the whole surface;
- The sample could be scratched by the stylus and its local mechanical properties be compromised, in fact the stylus tip is pressed against the surface with such a force that allows it to remain in contact with the surface under measurement during the transducer movement [98];
- The stylus tip radius represents a resolution limit of the instrument, since the finite size of the stylus tip results in some loss of information [99];
- Overall, it is a method usable only off-line and not suitable to test 100% of production for large lot sizes.

Non-contact measurements are a topic of interest and different techniques have been explored to perform roughness measurements, among which there are:

- Shearing interferometry: a microscopy technique used to obtain images of samples with small height deviations, it consists in overlapping two images of an object which are shifted laterally relatively to each other [100];

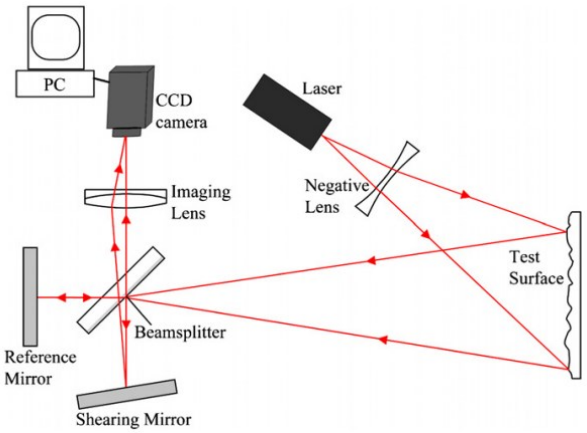

Figure 46. *Functioning principle of a shearography system based on a Michelson shearing interferometer. Image from* [101].

- Atomic Force Microscopy (AFM): is based on the atomic scale repulsive or attractive forces on a sprung cantilever. There are three types of operation of an AFM: contact, tapping and non-contact mode. In the non-contact mode, a diode laser is focused on the cantilever tip and as the tip scans the surface the laser beam is deflected onto a photodiode. Hence the light beam also changes position. Its resolution is limited to tens of micrometers and a roughness measurement with AFM requires multiple scans at different locations of a sample surface. To apply this technique sample cleanliness must be ensured to avoid artefacts and AFM is sensitive to the surrounding environment [102], [103];

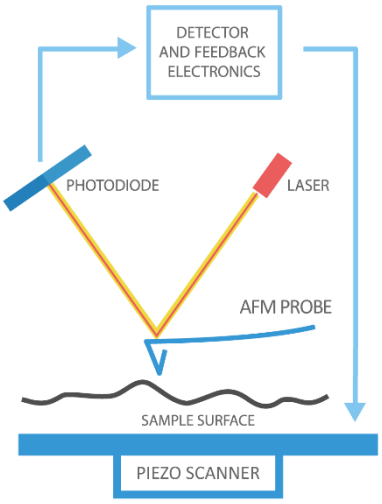

Figure 47. *Functioning principle of the AFM. Image by* [104].

- Scatterometry: the phase changes of light reflected from the surface are detected and used to extract information about the shape of the surface. Measuring surface roughness through scatterometry requires careful modeling and re-constructing of signals, moreover samples must be perfectly flat and with roughness lower than 5 nm [103] [105]; literature reports also some attempts to apply scatterometry for in-line measurements [106] [107];

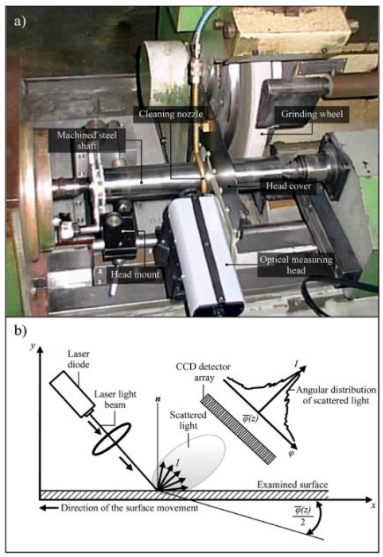

Figure 48. *In-process inspection of a steel shaft used during the grinding process. Image from* [106].

- Laser speckle photography: the contrast of the speckle image is used to trace back to surface roughness. It is needed a translation of the surface or the detector to have an intensity of the speckle field high enough for the calculation. This real time technique has a range of measurement limited to less than 1 μm [108];

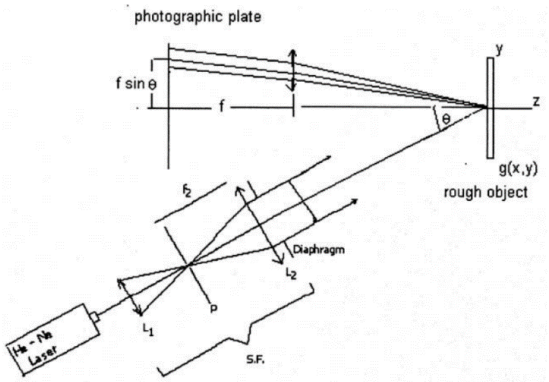

Figure 49. *Optical arrangement used for recording speckle patterns. Image from* [108].

- Digital holography: based on optical interference and diffraction. It uses holograms to get the intensity and the phase of object [109].

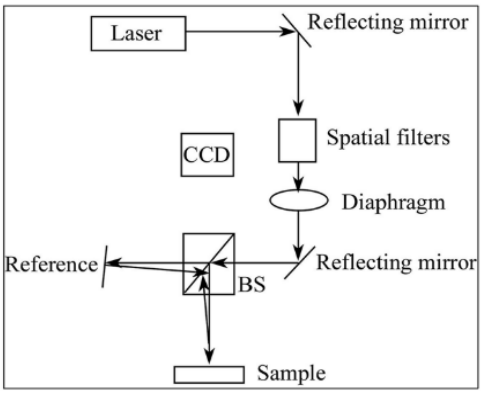

Figure 50. *Digital hologram recording setup based on Michelson interference. Image from* [109].

Even though on one hand optical methods are a more complex technology, on the other hand they have some inherent advantages [110]:

- The information content is high because processing an image allows to get spatial information without scanning;
- Measurements are fast and non-contact;
- Their non-contact nature leaves no scratches on the sample.

However, optical methods are more sensitive to variables like optical constants and surface features [100]. Moreover, almost none of these methods can be implemented for measurements in-line during production since they are methods that are designed for and work best in laboratory conditions.
Machine vision methods and vision-based methods in general are less sensible to disturbances and are apt to measure surface roughness, in fact they have attracted some research interest, as reported in literature [36], [110]–[117].

In this thesis we focused on the design and performed a feasibility study of a high-magnification backlit vision-based measurement system conceived to perform dimensional measurements at the microscale, in particular to measure surface roughness during in-line production. The system is thought to take images during turning and process them to determine surface roughness. Being image acquisition a very fast and non-contact process the system would open the possibility to have a short inspection time and a completely non-contact measurement, which would fit appropriately the requirements of ZDM, i.e. in-line quality control of 100% of production on moving/rotating parts. Such instruments are not commercially available and this is the main reason for focusing on this design.

3.3. Performance of a camera-based system: influencing factors

The work presented in this PhD thesis focused on the use of three different instruments:

- A laser-line triangulation system for gap and flush measurements;
- A telecentric profilometer for dimensional measurements;
- A backlit surface roughness measurement system.

While the optics and the functioning principles may differ, all three share a common feature, which is the use of solid state image detectors, either CCD (Charge-Coupled Device) sensors or CMOS sensors, which are used in the camera.
In this section we will discuss what are the factors that have an influence on the performance of a camera-based system.
In particular, three main aspects which influence the uncertainty and the spatial resolution of a system will be explained: the camera sensor, the modulation transfer function and effect of saturation.

3.3.1. Camera sensor

The camera sensor is the active part of a digital camera that converts light into an electrical signal, which is what is then processed and transformed into an image. A pixel (PIcture ELement) is the basic unit of a digital image and represents a single point of color.
The size of the sensor is usually expressed in inches and can vary between many different options, an overview is presented in Figure 51.

Figure 51. *Overview of different sensor sizes. Image from* [118].

The spatial resolution of a camera sensor depends on the number of pixels present on the area of the sensor. Hence the factors which determine the resolution limit of a camera are:

- Sensor size: the size of the sensor determines the amount of the pixels. The more pixels there are, the better the resolution and the sharper the image will appear;
- Pixel size: the smaller the pixel, the more pixels can fit on the sensor area. Moreover, smaller pixels imply a higher resolution power, consequently the details that can be detected are smaller.

However, a higher number of pixels does not necessarily mean that the image quality is better, as other factors such as lens quality, sensor size, and processing technology also play important roles. A way to quantify the influence of these factors on the output image, from the point of view of spatial resolution (lateral resolution) is the study of the modulation Transfer Function.

3.3.2. Modulation Transfer Function

The Modulation Transfer Function (MTF) is a measure of the quality of an optical system or a digital imaging system, that describes how well the system is able to reproduce fine details from an original image. In other words, it is a parameter which represents the sharpness of an imaging system. It is also known as the spatial frequency response of an imaging system to an input, therefore is directly related to the spatial resolution of the imaging system in the image plane (lateral resolution), giving an idea of how much of the detail present in the input image is lost in the output image.
Figure 52 represents an example of MTF of an ideal lens, limited only by diffraction.

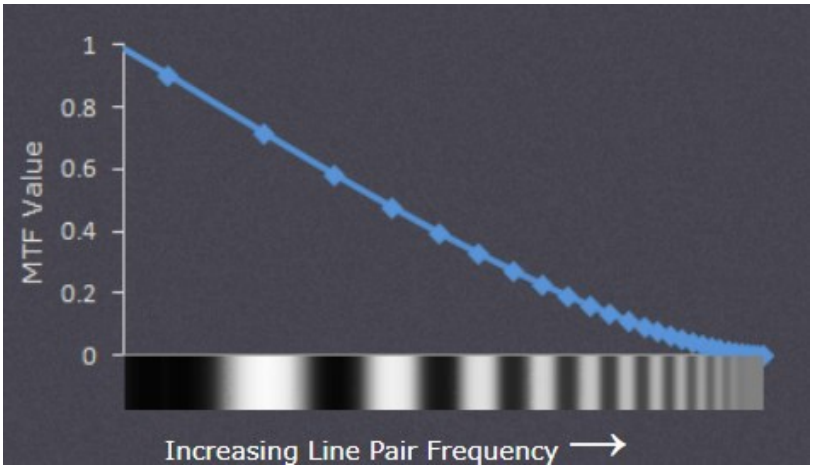

Figure 52. *The blue line represents the MTF curve of an ideal lens, limited only by diffraction. Image by* [119].

The amplitude of MTF can vary between 100% and 0%, with 1 indicating a perfect preservation of contrast, and values less than 1 show a progressive loss of contrast [120]. A high MTF value indicates that the system is able to reproduce fine details well, while a low MTF value indicates that the system is not able to preserve fine details in the output image. The reference parameter is represented by the MTF at 50%, which indicates the highest line frequency that can be replicated by a lens without allowing the MTF to go lower than 50%, in fact, this is the value related to perceived image sharpness.

Among the possible methods to evaluate the MTF we chose the Slanted Edge Method [121]: a step input is given to the imaging system through the image of a sharp slanted edge (see Figures 53 and 54 (Left)), the system's response is then the Edge Spread Function (ESF) which is then derived to obtain the Line Spread Function (LSF). Lastly the MTF is the Fourier Transform of the LSF [122]. To perform this analysis we used the Slanted Edge MTF Plugin of ImageJ open-source software package [122] because it is easily available since it is open-source and its known limitations (it does not perform well on noisy images) do not apply to our case.

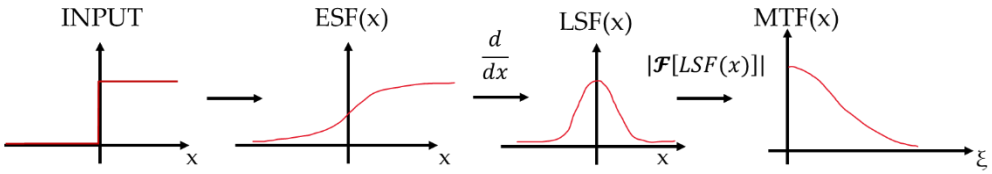

Figure 53. *The response of the system to the step input is the Edge Spread Function (ESF), then the spatial derivative of ESF data produces a Line Spread Function (LSF), which is then Fourier Transformed into the Modulation Transfer Function (MTF).*

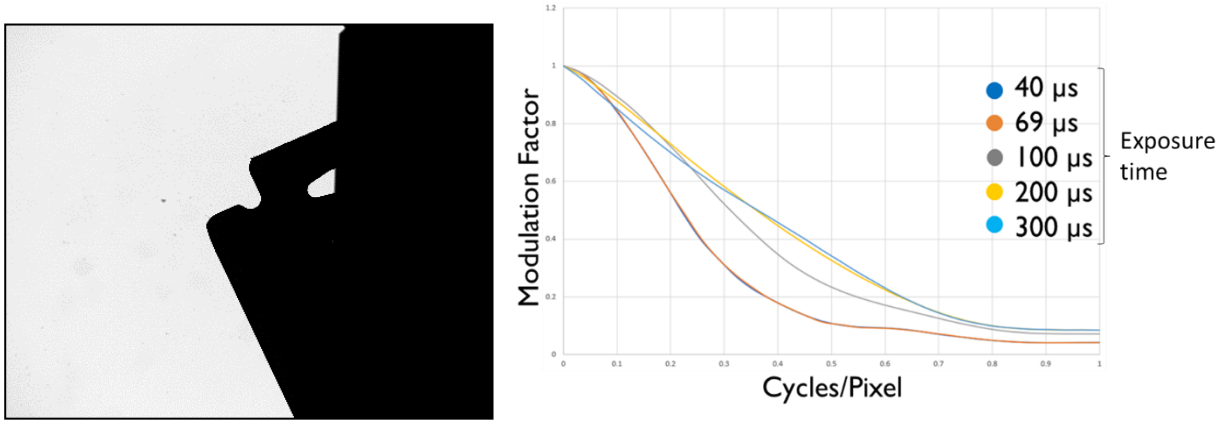

Figure 54. *(Left) Image of the sharp edge used as input; (Right) MTF of the imaging system at different exposure times.*

The study of the MTF was used twice in this work, both for the telecentric profilometer presented in Chapter 4 and for the surface roughness measurement system presented in Chapter 5. Based on the MTF, the right combination of exposure time and intensity of illumination was determined in order to obtain the highest contrast possible that would not cause saturation.

3.3.3. Effect of saturation

Pixels are light sensitive and store electrical charges proportional to the amount of light received, these charges are then transferred and used to produce a signal (Figure 55).

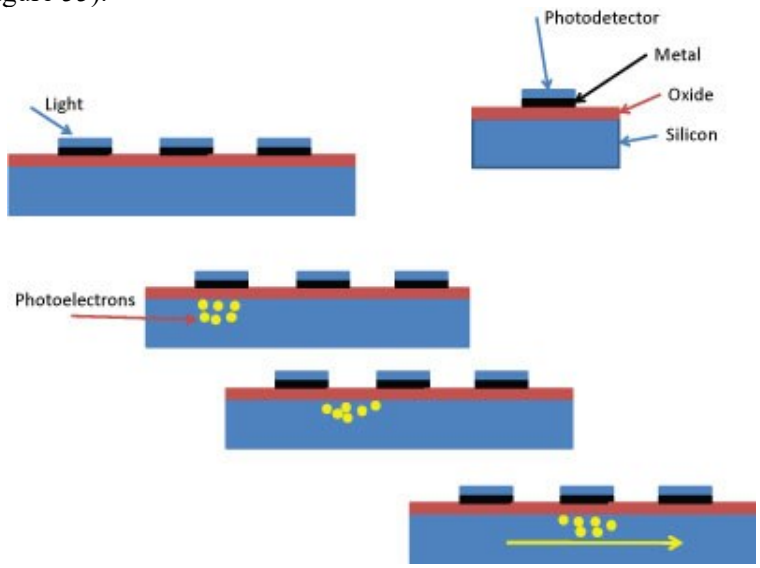

Figure 55. *MOS capacitors which are the basic elements of a CCD or a CMOS image sensor. Image from* [123].

The blooming effect in camera sensors occurs when photons from a bright source of light overload the light-sensitive pixels in an image sensor. It occurs when the pixels are saturated by over 100 per cent. This causes a change in the distributions of the electric charge on the camera sensor, charges spill over into adjacent pixels, producing a "bloom" of light that distorts the image [87].
Below is presented a sequence of images which explain the consequences of blooming, the first acquisition is obtained at optimal conditions, while the others are obtained at increasing values of exposure time. In the first frame the transition is the sharpest possible: only two pixels are required to pass from white to black, hence the edge of the sample corresponds to the transition point. In the second and third frames two things happen: the transition line is moved towards the black side and the white pixels “bloom” into the black ones creating a “transition zone” made of several pixels. In this case is impossible to locate with precision the edge of the sample, moreover the shift of the transition line towards the black side will cause thinning of the silhouette of the sample.

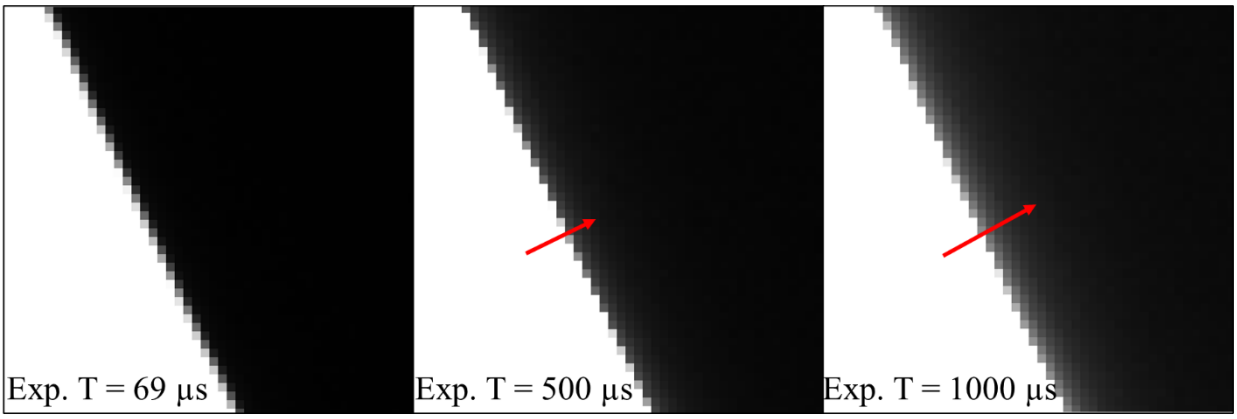

Figure 56. *Images of the same slanted edge obtained at increasing values of exposure time: the blooming effect causes the charge of the white pixels to spill into to the adjacent black pixels.*

In the case of dimensional measurements, this effect would result in completely wrong results

In Chapter 4 we will present the design and metrological characterization of the telecentric profilometer used in this work for measuring lengths and diameters of cylindrical parts.

Chapter 4.

OASIS: Custom-made telecentric optical profilometer

In this part of the work, we present a two-axis telecentric optical profilometer system, labelled OASIS, that was developed based on the technical requirements suggested by Zannini s.p.a., a local turning factory of high-precision mechanical parts. An uncertainty analysis was performed on measurements collected both with OASIS and other instruments commonly used in the company to check the compliance of parts produced to the technical drawings.
It should be highlighted here that the optical components (camera, lens and lighting system) used in the OASIS device were off-the-shelf components already available at Zannini and Z4tec s.r.l., a tech provider for Zannini, and they were not specifically selected for its development. Indeed, this breaks the rules for designing machine-vision based measurement systems, that ask to start from the target resolution needed to assess the target dimensions of a part according to target tolerances. For example, a wider telecentric lens could allow to measure a larger range of samples of different dimensions; a camera with a given sensor size but a higher number of pixels could provide a better resolution; on the other hand, a camera with a given pixel number and a larger sensor size would result in a drop in resolution.
Nevertheless, it is an interesting exercise that gives the possibility to discuss about common issues that should be faced when designing these devices, and how the whole assembly can affect their metrological performances.

4.1. Device description

The OASIS device is a measurement instrument based on telecentric optical profilometry and is targeted to in-production dimensional quality control of turned parts.
The main objectives were:

- High measurement resolution;
- Short inspection time;
- Possibility to simultaneously measure several dimensions on different sides of the part;
- Suitability for automated charge/discharge of turned parts.

In this section the design of the instrument and the specific problems related to the alignment of its different components are described.

4.1.1. Design

The OASIS device is a telecentric profilometer composed of a standard telecentric optical assembly:

- a 5 Mpixel camera: Teledyne Dalsa Genie Nano G3-GM11-M2420, with a resolution of 2448 x 2048 and a 2/3" sensor;
- a bi-telecentric lens (OptoEngineering, TC23036) with a 61 mm diameter and a working distance of 102.5 mm;
- a telecentric illuminator (OptoEngineering, LTCLHP036-G) with a wavelength of 520 nm (green), and a working distance of and 70-140 mm.

To perform dimensional measurements in two directions simultaneously (horizontally and vertically), OASIS is composed of a cross-shaped structure that holds two telecentric profilometers, as shown in Figure 57.
The part is placed on a glass tray so that both telecentric profilometers can work simultaneously. The layout allows for manual positioning of the part or automated positioning by a robot arm. For the sake of brevity, only the metrological performance of the horizontal telecentric profilometer is discussed in this thesis. Nevertheless, the general approach stands for the vertical direction too.

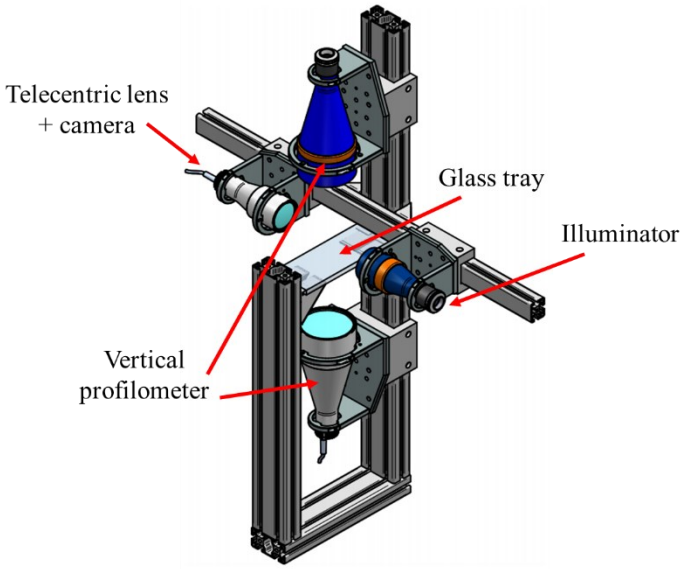

Figure 57. *Cross-shaped structure of OASIS. The piece to inspect is placed on the glass, between the two pairs of telecentric profilometers (one horizontal and one vertical).*

4.1.2. Critical problems

Optical profilometry is a typical example of measurement approaches in which optical issues and mechanical issues have to be faced jointly. Indeed, there are a few common problems that one should consider when dealing with optical profilometers: in this section we will explain the influence of spatial resolution and

the importance of guaranteeing alignment between the different components that are part of the instrument.

Spatial resolution

The study of the MTF was used twice in this work, both for the telecentric profilometer presented in this chapter and for the surface roughness measurement system presented in Chapter 5. Below, the setup used for the telecentric profilometer is used as an example (Figure 58).

To capture the image of the sharp edge needed for this analysis (see Chapter 3.3 for more details), a razor blade was placed in between the camera lens and the telecentric illuminator and it was tilted in order to obtain the slanted edge, the image obtained is shown in Figure 59 (Left). The use of a razor blade guarantees a very sharp and clean edge.

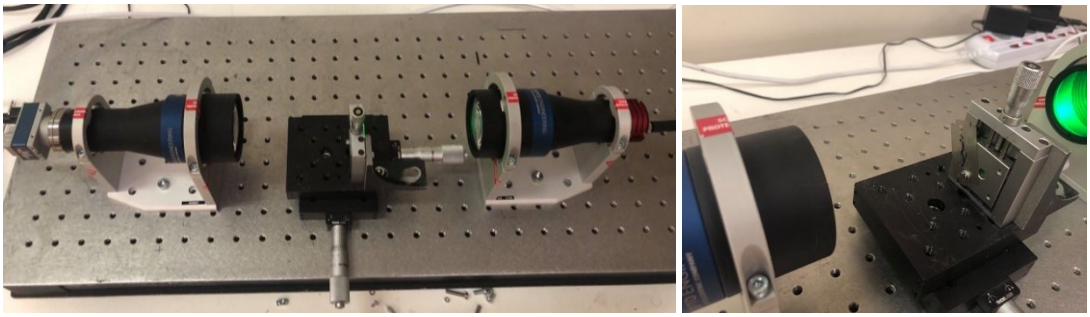

Figure 58. *Lab setup to measure MTF: (Left) a razor blade is positioned between the optics and the illuminator; (Right) close-up of the setup.*

Based on the MTF, the right combination of exposure time and intensity of illumination was determined in order to obtain the highest contrast that would not cause saturation. In fact, saturation increases with the increase of the exposure time and the performance of the vision system decreases accordingly. This is demonstrated in Figure 59 (Right), where the MTF of the vision system was obtained at different exposure times.

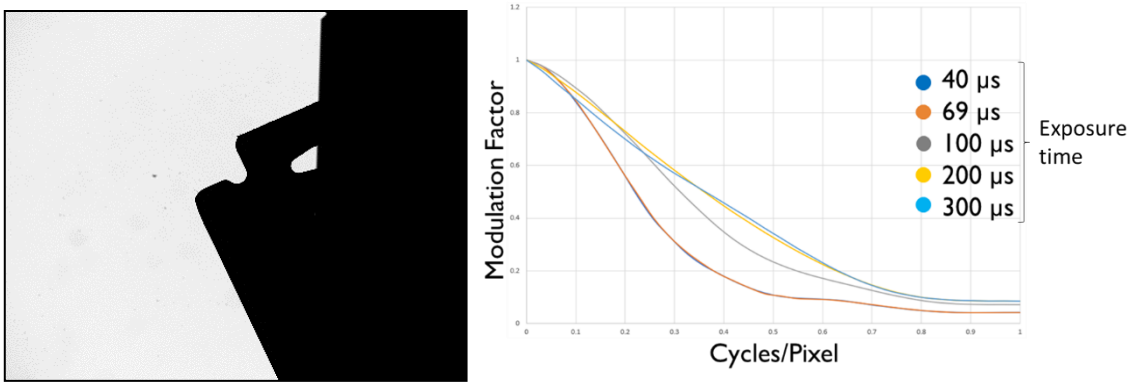

Figure 59. *(Left) Image of the sharp edge used as input; (Right) MTF of the imaging system at different exposure times.*

We could choose exposure times within a determined and finite set of values; available exposure times were: 40 µs, 69 µs, 80 µs, 100 µs, 150 µs, 200 µs and so on. This preliminary analysis was used to narrow down the range of exposure times. Then, the analysis was repeated once again at exposure times of 40 µs, 69 µs and 80 µs. The selected value between 40 and 69 µs was 69 µs, and it was chosen based on the better signal to noise ratio, since the difference in MTF was negligible. The spatial resolution of the imaging system is calculated starting from the MTF value at 50% and finding the corresponding cycles/pixel value (Figure 60).
Another factor that influenced the decision was the image saturation, in fact, the exposure time selected was the one that provided, together with the intensity of illumination, the highest contrast that would not cause saturation, see Figure 61. The saturation of the image causes two main problems: loss of information and blooming. In fact, the higher the intensity of illumination, the more the gaussian distribution of the pixel intensities moves towards the 255 limit of the 0-255 intensity range, until it is completely out of range.

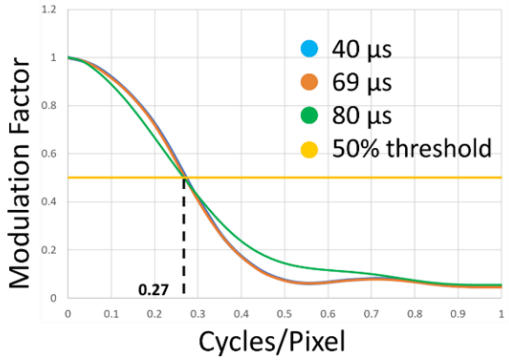

Figure 60. *Graph of the MTFs calculated at different exposure times, in yellow is reported 50% of the interval.*

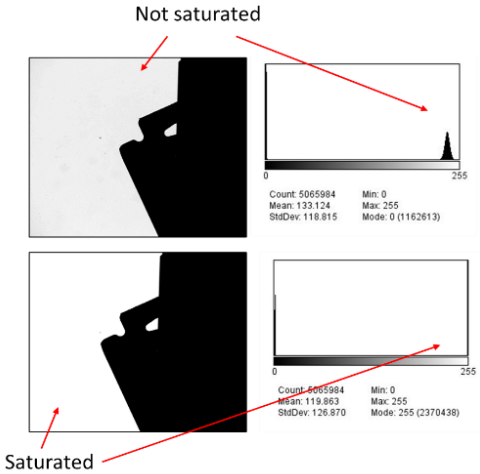

Figure 61. *Influence of the illumination intensity on the razor blade image: the higher the intensity, the higher the saturation. The image intensity histogram, which is limited in the 0-255 range, has to contain the gaussian distribution of the pixel intensities.*

This effect is directly correlated with blooming, in fact if the source of light is too bright, the distribution of the electric charge on the camera sensor changes distorting the image. It results in narrower silhouettes, which in the case of dimensional measurements would cause the user to get completely wrong results [87]. See Section 3.3.3.
To obtain the spatial resolution of the image system, we performed the evaluation starting from the 0.27 cycles/pixel value obtained for the MTF at 50%, see Figure 60. The value is then inverted (Eq. 4.1) and halved (Eq. 4.2) to calculate the resolution in pixels. Through the calibration, the corresponding conversion factor (0.014 mm/pixel) between pixels and millimeters was found, by using a target with known dimensions and finding the relative size in pixels. Then the conversion factor is used to convert the resolution in pixels into the resolution in millimeters (Eq. 4.3).

$$\frac{1}{0.27} = 3.65\ pixel/cycles \tag{4.1}$$

$$\frac{3.65}{2} = 1.82\ pixel \tag{4.2}$$

$$1.82\ pixel * 0.014\ \frac{mm}{pixel} = 0.0255\ mm = 25.5\ \mu m \tag{4.3}$$

The resulting value of 25.5 µm is the spatial resolution of the vision system.

Alignment of the telecentric profilometers

Alignment between the lens and the illuminator and the alignment between the telecentric system and the glass tray holding the piece are key aspects to consider to ensure accurate measurements, see Figure 62.
First, to be able to align the lens and the illuminator, it is of utmost importance that they are mounted on the same rectilinear profile, then the alignment was perfected with a pinhole: the illuminator was covered by a mask with a pin hole at the center to obtain a line of light; the lens was covered with a mirror and the position of the telecentric profilometer was adjusted until the reflection of the line of light overlapped with the line itself (Figure 63). The rectilinear profile will guarantee a high inertia and an isostatic structure, which will allow to avoid bending deformation of the structure, while thermal deformations will not cause the structure to change its shape.

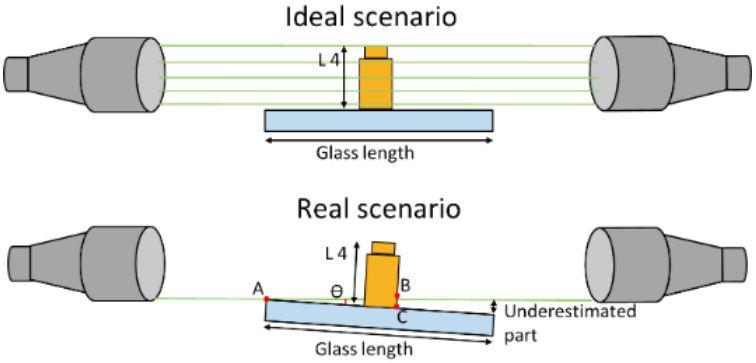

***Figure 62**. Ideal (top) and real (bottom) configurations of the vision system.*

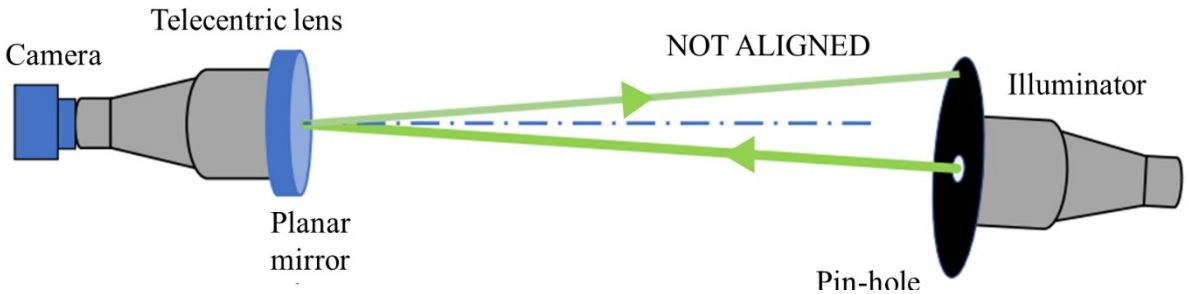

Figure 63. *Alignment process with pin-hole: the outgoing light ray is reflected on the surface of the mirror and the system is readjusted until the reflected ray is superimposed with the outgoing one.*

Alignment of the glass tray

The glass tray should be designed in a way that makes it possible to regulate the tilting of the tray with respect to the optical axes of the telecentric illuminator and lens. In fact, an eventual misalignment of the tray would compromise the orthogonal projection of the piece thus causing a wrong estimate of the length of the part inspected (Figure 62).

The portfolio of a high-precision machining company might include parts of different dimension: the glass tray needs to be designed to provide mechanical support to these different parts (hence being sufficiently large in size).

However, an over-dimensioning might affect the behavior of the vision system: if the tray is too large, its edge will be close to the camera and might appear out of focus, see Figure 64 (Top). This happens because its edge is at a shorter distance than the working distance of the lens (102.5 mm, in the OASIS setup). This makes it hard, if not impossible for a software to precisely identify the edge of the tray, since it is surrounded by a gray halo.

When sliding the glass to the right, so as to have the lens-facing edge closer to the focus point of the lens, the gray halo is still present, but the transition air\glass is definitely sharper (Figure 64 (Bottom)). The remaining halo is due to the glass not being perfectly parallel with respect to the telecentric system: the rear edge of the glass is being seen by the camera as well, and of course it is out of focus due to the working range of the objective.

Nonetheless, the achieved level of focus proved to be enough to perform measurements.

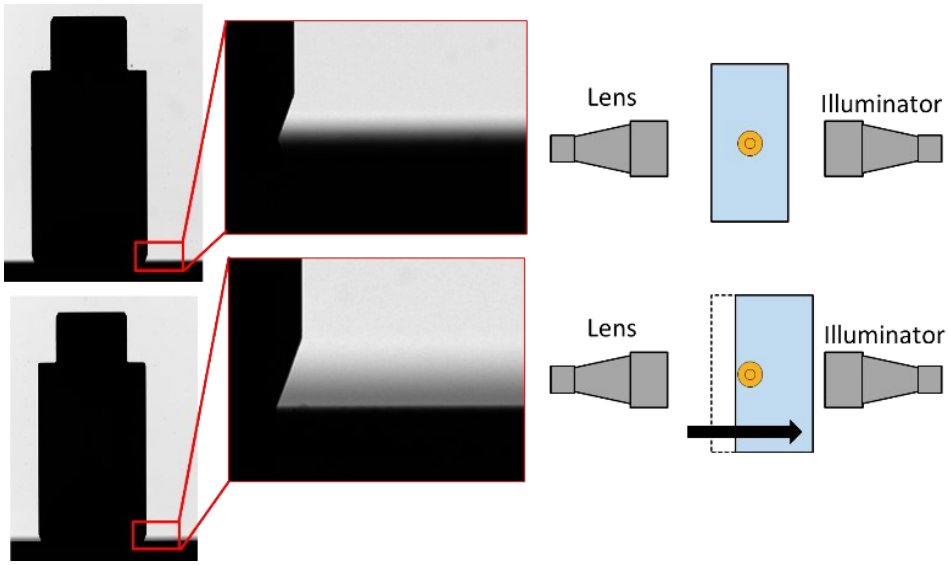

Figure 64. *Focus of the glass edge: (Top) when the glass is centered between the two lenses the edge is out of focus; (Bottom) displays the increase of definition of the edge when the glass has been slid to the right.*

Alignment of prismatic pieces

When dealing with prismatic pieces, it is of vital importance to consider also the alignment of the piece with respect to the optical axis of the telecentric profilometer. If the piece is not perfectly aligned, the shadow that is being projected on the lens is not the actual profile, but the length of the profile plus the projection of its side ($L+Psin(\theta)$), as shown in Figure 65. This is an effect that is not visible when measuring cylindrical pieces.

Even a small misalignment can cause quite a big impact on the measurement result, as can be seen in Figure 66 (in the case reported it was estimated an angle of $\theta = 0.25°$). In fact, the difference that is seen in Figure 66 is solely due to the misalignment, since all of the optical settings were kept constant and the glass tray position was not readjusted.

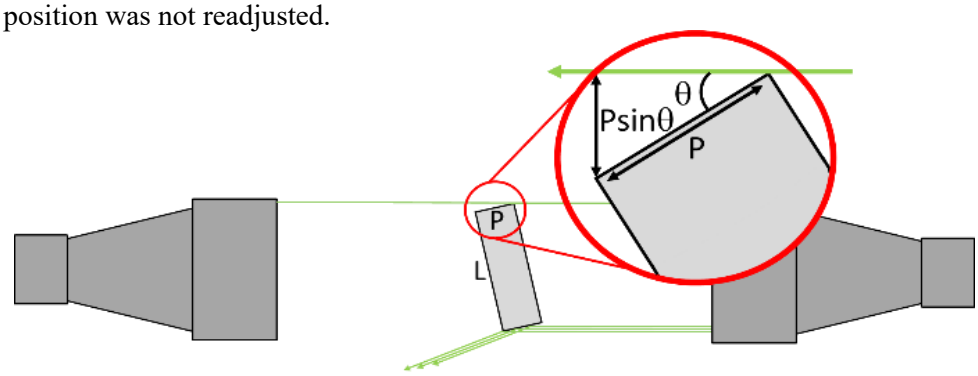

Figure 65. *Prismatic piece: effect of misalignment. L is the length of the profile, P is the length of its side and Θ is the angle of misalignment.*

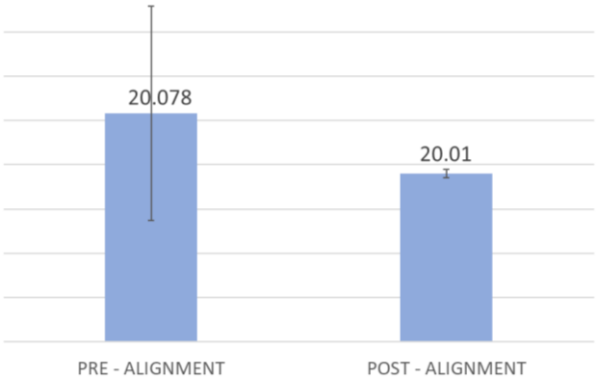

Figure 66. *Measurement mean of a 20.000 mm gauge block obtained with the OASIS in two different setups: with a manual alignment of the block and with a more precise alignment. The angle of misalignment is estimated to be 0.25°.*

4.2. Measurement campaign and uncertainty analysis

This section will describe the comparison analysis performed on measurement collected both with the OASIS and other on-the-market devices commonly used in production line.

4.2.1. Determination of the reference measurement instruments

When considering the performance of measurement instruments one can make a comparison either with a reference instrument or with a reference measurand, as discussed in Chapter 3.1. In most cases the true value of a measurand is unknowable, according to the International Vocabulary of Metrology [124]. Gauge blocks and pins, which have a certified dimension, can be used as reference measurands.
In our study we used a gauge block and a gauge pin, in order to have a reference measurand for both lengths (between parallel facets) and diameters respectively (see Figure 67), and we measured each one with different dimensional measurement devices present at Zannini s.p.a. production line and with the OASIS.

Figure 67. *Gauge block of 20 mm (Left) and pin of 12 mm (Right) used as reference measurands.*

The gauges used have the dimensions described in Table 1, as specified in the master's certificate by the Accredited Calibration Laboratory.

Table 1. Measurements of reference gauges

Gauge	Measurement [mm]	Uncertainty 95%[µm]
Block	19.9999	± 0.15
Pin	11.9928	± 0.41

This comparison of measurement performed on reference measurands, allowed to observe measurement uncertainty, discussed in detail in Section 4.2.3.; in particular, in this section it is shown how different instruments present different bias. And based on this bias, it is also possible to identify which instrument to consider as reference for that specific measurement.
The instruments used to measure the pieces are reported in Table 2.

Table 2. Summary of instruments

Instr. ID	Type of functioning	Declared uncertainty [µm]
1	Telecentric profilometer (A)	± 3
2	Telecentric profilometer (B)	± (2+L[mm]/200) ± (1+D[mm]/200)
3	Coordinate Measuring Machine (CMM)	± (1.7+3L[mm]/1000)
4	Snap gauge	± 0.3% of measurement
5	Micrometer (for diameters) Dial gauge (for lengths)	± 1
6	Telecentric profilometer (OASIS)	± 25.5

The uncertainty reported in column three is the one declared on the instruments' datasheet: it is evident that each producer uses a different way to declare it. It is worth mentioning that instrument 6, designed in the context of this PhD thesis, has a significantly larger uncertainty. The analysis reported below will be used to redesign it.
The results of the analysis are shown in the figures below, in particular the mean values of the gauge block and of the pin gauge measurements are represented in Figures 68 and 69 respectively. The boxes are the middle 50% of the data and the circles are the mean measurements. The whiskers are the ranges for the top and bottom 25% of the data, excluding outliers.

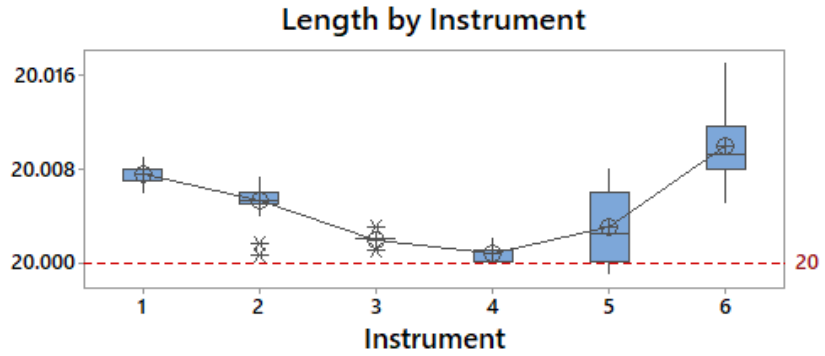

Figure 68. *Mean measurements of a 20.000 mm gauge block.*

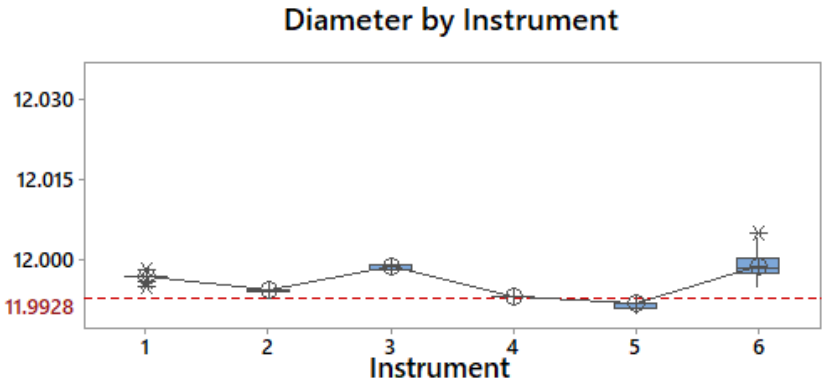

Figure 69. *Mean measurement of a 11.9928 mm pin gauge.*

Based on the results of the analysis we were able to determine which instruments to consider as reference to perform a comparison analysis, for length and diameter measurements respectively:

a) Length: both instrument 3 (CMM) and 4 (snap gauge) can be used as reference since their mean results are closest to the nominal value (CMM = 20.002 mm; snap gauge = 20.001 mm). It is necessary to keep in mind that in this study we selected the CMM as reference because the snap gauge only has a limited range of measurement (0-25 mm), which did not allow to measure all the dimensions considered in this experiment (Length 2 - see Table 3). Also, its mechanical structure does not allow to measure hollow pieces, like the one present in this study. Moreover, the CMM is more suitable for lengths since it bases its measurements on multiple points taken on the same plane. Instrument 5, being a manual instrument, is influenced, even if in minimal part, by the operator, hence it has a larger dispersion.

b) Diameter: instrument 4 (snap gauge) is the selected reference instrument since its mean results are the closest to the nominal value. It is more suitable because it uses parallel faces to measure a diameter, i.e., the contact surface is only a point, and there is no operator influence.

Figure 70. *Snap gauge used for the measurement campaign.*

4.2.2. Measurement campaign

The experimental campaign for assessing the performance of OASIS was also carried out at Zannini s.p.a. production line. Two different sets of ten pieces, were measured with different dimensional measurement devices. For the sake of brevity, the data discussed here refer only to one set of rectified turned parts; moreover, the focus is on just the diameters and lengths addressed in Figure 71 and Table 3.

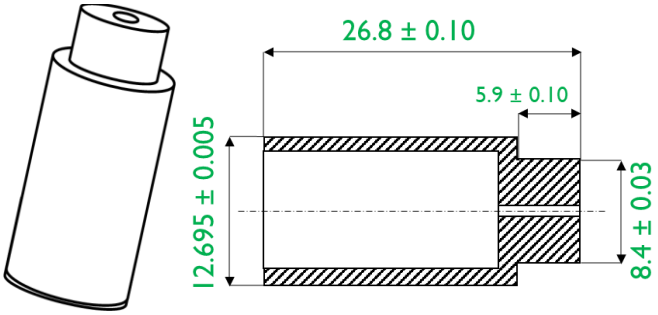

Figure 71. *Rectified turned piece and relative measurements.*

Table 3. Measurement values

Measurement type	Value [mm] ± tolerance[mm]
Diameter 1	12.695 ± 0.005
Diameter 2	8.4 ± 0.03
Length 1	5.9 ± 0.10
Length 2	26.8 ± 0.10

These dimensions have been selected given the wide range of dimensional tolerances (microns to one tenth of millimeter) involved and because they are lengths between parallel facets and diameters, therefore representative of the dimensions typically to be measured in a turned part.
The population of parts is made of 10 samples, randomly taken from the actual production.
Two different measurement campaigns were carried out:

a) Repeated measurements (10 times) on one sample (sample 1) by all the different instruments.
b) Repeated measurements (3 times) on all 10 parts by each instrument.

To simulate real working condition in production line, even if measurements were performed on the same sample, there was always a repositioning of the sample on each instrument between a measurement and the next.

4.2.3. Uncertainty

The two measurement campaigns were carried out respectively to:

a) estimate the metrological performance of each instrument: trueness and repeatability (i.e. bias and precision).
b) evaluate the combination of the variability due to the instruments (reproducibility) and the variability due to the pieces, and their relative weight on the results.

For each measurement campaign the mean value and two times the standard deviation were calculated. The means and deviations were calculated with Excel and a Gage R&R ANOVA test was performed with Minitab 17 on the data related to the different instruments.
The mean values were compared to the results obtained with the reference instrument, which was identified by measuring certified gauge pieces, different for diameters and lengths, as explained in Section 4.2.1. The analysis showed that the reference instruments, for diameters and lengths respectively, are instrument 4 and 3.

4.3. Results and conclusions

The results of the uncertainty analysis are presented in the figures below.
In Figures 72 and 73 are reported the means of the 10 repeated measurements on sample 1 obtained by each instrument. They show the nominal values of the piece, which are 12.695 mm for Diameter 1 and 26.8 mm for Length 2. The tolerance intervals for each measurement are represented by the gray area and are respectively ± 0.005 mm for Diameter 1 and ± 0.10 mm for Length 2. The blue dots are the mean values estimated on 10 measurements each, while the error bar represents two times the standard deviation of each set of measurements. Lastly, the reference measurement, obtained with the reference instrument, is shown in red.
The information we can infer from these data regards two main aspects: the influence of random errors (precision, related to the repeatability of the instrument) and

systematic errors (bias, related to the trueness).

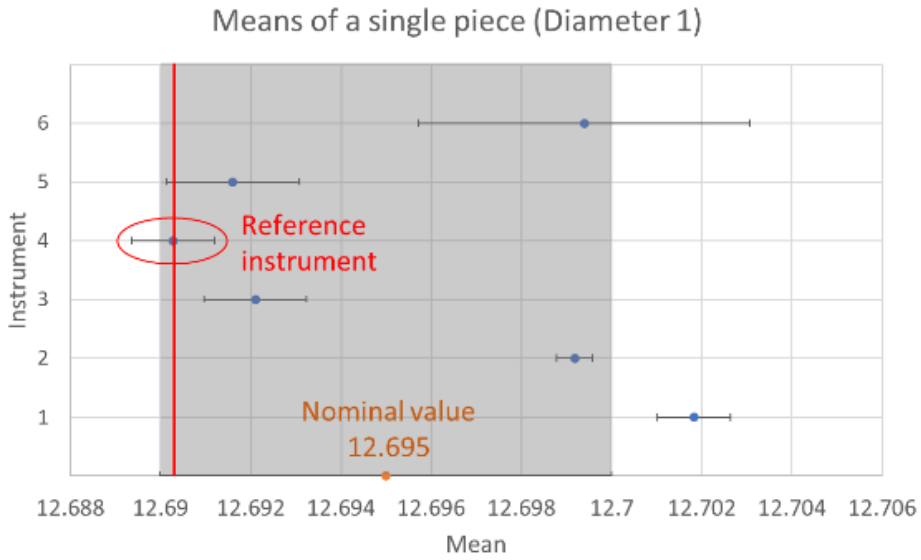

Figure 72. *Repeated measurements (10 times) of a single piece with each instrument; in blue is reported the mean and the error bar is two times the standard deviation. In orange is the nominal dimension and the gray area is the tolerance interval for Diameter 1.*

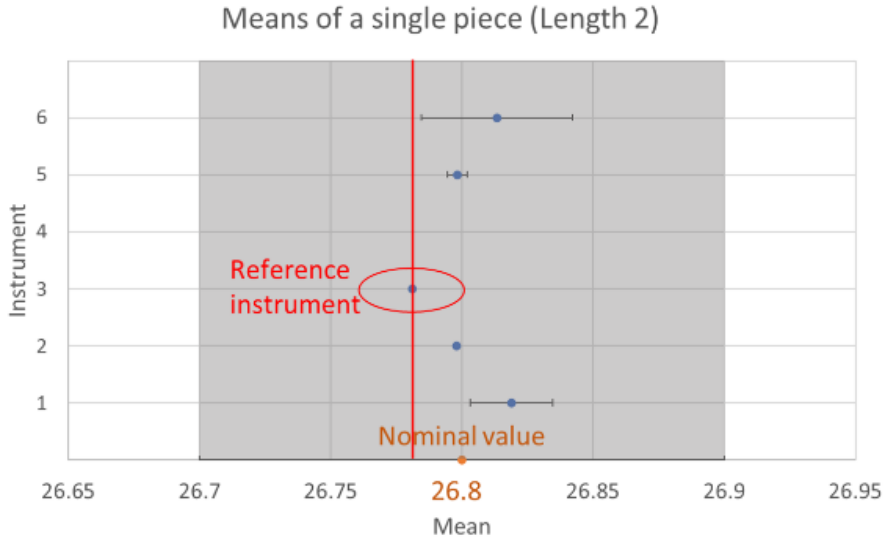

Figure 73. *Repeated measurements (10 times) of a single piece with each instrument; in blue is reported the mean and the error bar is two times the standard deviation. In orange is the nominal dimension and the gray area is the tolerance interval for Length 2.*

Figure 74 represents the mean measurements obtained from the 10 pieces taken from the production line, in this case, the tolerance interval is indicated by the orange area.

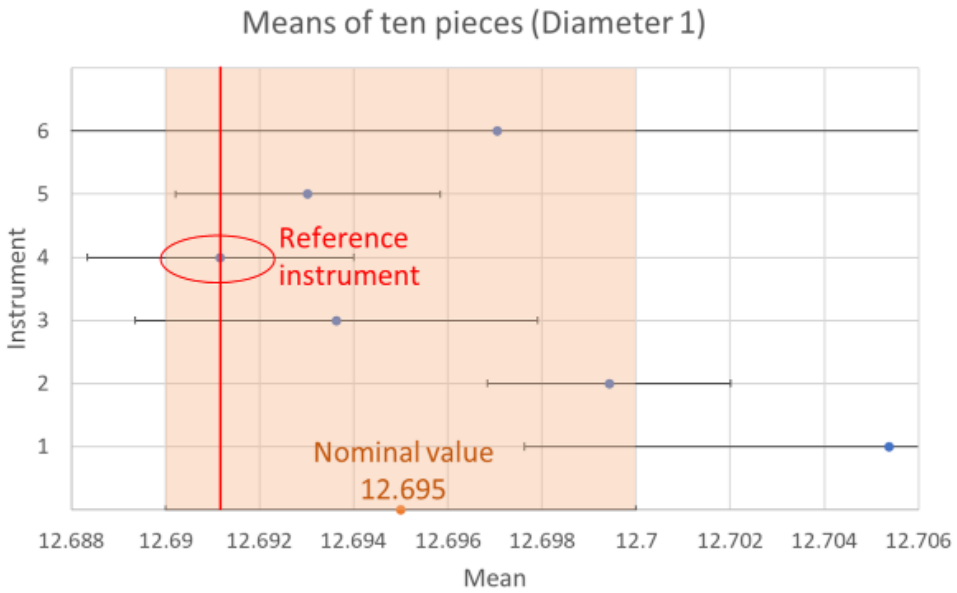

Figure 74. *Repeated measurements of ten pieces measured with each instrument; in blue is reported the mean and the error bar is two times the standard deviation. In orange is the nominal value and the orange area is the tolerance interval for Diameter 1.*

The Gage R&R analysis reported in Figures 75 through 78 was performed on the measurements obtained from the 10 pieces taken from the production line. The observations that we can make from this set of data concern the combined variability of the instruments and the pieces.

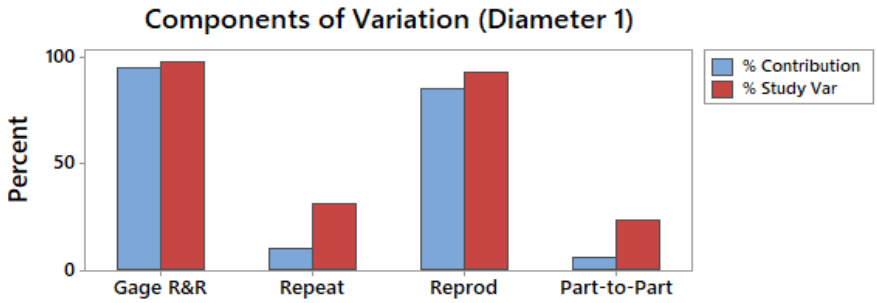

Figure 75. *Components of variation obtained from the Gage R&R analysis for Diameter 1.*

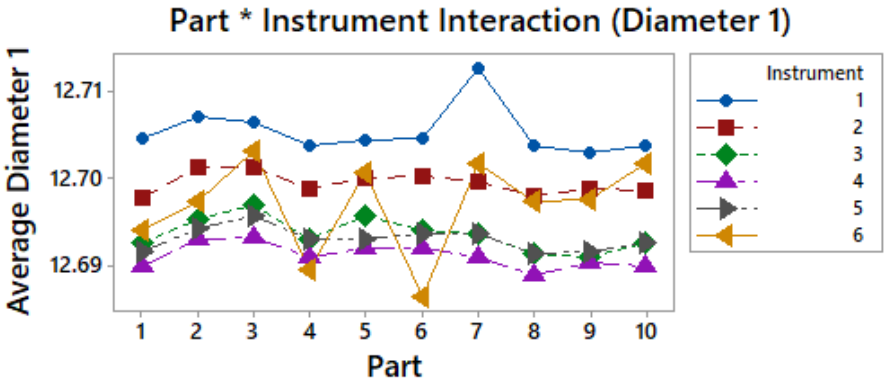

Figure 76. *Average measurements of Diameter 1 divided by part and by instrument.*

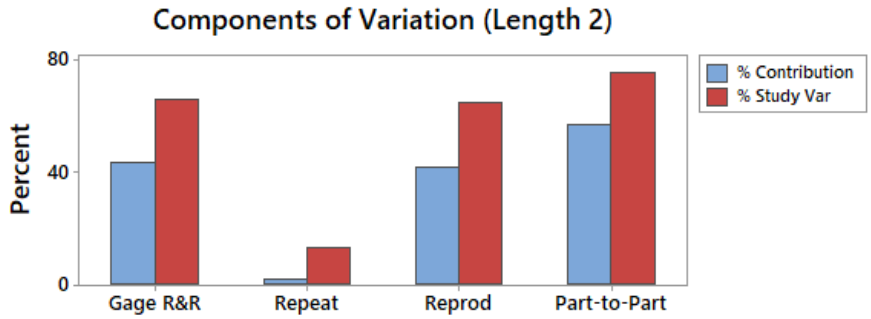

Figure *77. Components of variation obtained from the Gage R&R analysis for Length 2.*

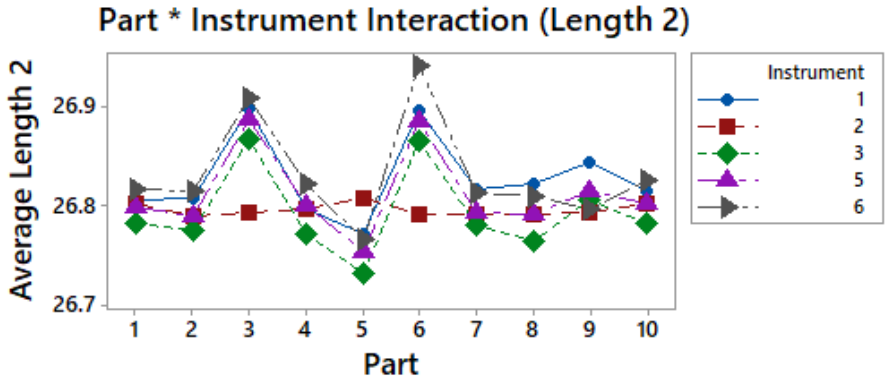

Figure 78. *Average measurements of Length 2 divided by part and by instrument.*

4.3.1. Results for diameter 1

In Figure 72, the piece inspected shows a mean measurement lower than the nominal value, according to the reference instrument; nonetheless, it still falls inside the tolerance interval, thus making it compliant with the specifications.
When comparing the means obtained with each instrument, the difference between each mean and the reference one indicates the bias error of the instrument, i.e. a systematic error component which characterizes the trueness of the instrument itself.

This error component can and must be corrected every time an instrument is used to measure a new piece. This must be done at the beginning of the production of each batch, by comparing measurements with the dimension of a "master" piece chosen from the batch itself. This correction should be done on pieces which have the same characteristics of the batch because the bias error between the instruments varies if considering measurements of certified gauge pieces and pieces taken from the production line. These differences are to be expected and are caused by the fact that real produced pieces have imperfections and a different surface roughness compared to gauge pieces. Moreover, the shape of the piece and its positioning during measurement also influence the results.
The dimensions of the master piece are determined using the instruments deemed as reference, through the analysis performed on gauge pieces, reported in Section 4.2.1.
The value of the standard deviation, referred to each instrument, represents the random uncertainty component of the measurement and it can never be completely zeroed but only reduced. For it to be acceptable, the value needs to be less or equal to 1/4 of the tolerance interval.
Based on the results reported in Figure 72, the standard deviations of the instruments are all reasonably small, except for OASIS (instrument 6) which makes it not suitable for measurements within such a small tolerance interval.
In Figure 74, the bias between the instruments and the reference instrument has the same pattern of the one present in Figure 72, thus highlighting the fact that the variance between the 10 samples only affects the standard deviation and that the differences between the mean measurements are due mainly to the different biases of the instruments.
This hypothesis is confirmed by the Gage R&R, reported in Figures 75 and 76. In particular, Figure 75 shows that the main contribution to the total variance is given by the total Gage R&R, which is the sum of the variance due to the repeatability (instrument's precision) and the one due to the reproducibility (differences between instruments). Within the total Gage R&R the main component is the reproducibility, as expected.
The part-to-part variation is relatively small thus confirming the good process capability. In Figure 76, the same concepts are presented in a different format: the bias between instruments is clearly present and instruments 1 and 6 show also a larger dispersion.

4.3.2. Results for length 2

For the length measurement we performed the same analysis sequence, which is reported in Figures 73, 77 and 78.
In Figure 73, the standard deviation of the OASIS (instrument 6) is smaller than the one it has when measuring diameters: therefore, the instrument appears more fit to measure length. However, it still presents an expanded uncertainty which does not match the requirements for conformance acceptance. This shows how much the results are dependent on the specific piece and type of measurement performed, i.e. in this case a length measurement.

In Figure 77, the main component of variance is represented by the part-to-part variation, since the tolerance interval (± 0.10 mm) is much larger than the one for Diameter 1 (± 0.005 mm). Concerning the contribution of the instrument, the Gage R&R, again is dominated by the differences between the instruments (reproducibility). Lastly, in Figure 78, we can see the presence of bias and the influence of a standard deviation which is closer to the conformance acceptance, i.e. the instruments (included number 6) follow the same trend.

4.3.3. Conclusions

As the overall performances of the OASIS are concerned, it should be remembered that its optical components (camera, lens, illuminator) are off-the-shelf components already available at the premises of Zannini and Z4tec, and they were not selected for the purpose. Better results in terms of uncertainty and bias could be obtained by selecting these components in order to improve the resolution of the optical system. For example, a camera with a better spatial resolution could be obtained using a camera with a sensor with a higher number of pixels. A wider telecentric lens could allow to measure a larger range of samples of different dimensions.
In conclusion, in this chapter we presented the typical problems that one should consider when dealing with optical profilometers and we stressed the importance of the influence of the alignment on the measurement results.
Moreover, when performing a comparison analysis, it was evident how it is always necessary to correct bias: this was achieved by comparing measurements with a "master" piece of the production line, whose dimensions were determined using a reference instrument. On the other hand, the choice of the reference instrument needs to be based on measurement of certified reference pieces.

In Chapter 5 we will discuss another backlighting vision system which in this case was used for dimensional measurements at the microscale, i.e. for surface roughness measurements.

Chapter 5.

Surface roughness measurement system

In this chapter the design and a feasibility study of a high-magnification backlit vision-based measurement system is presented. The instrument is conceived to perform dimensional measurements at the microscale, in particular to measure surface roughness during in-line production. The system is designed to take images during turning and process them to determine surface roughness. Since image acquisition is a very fast and non-contact process, the system would enable the possibility of shortening inspection time and completely non-contact measurement, which would appropriately fit the requirements of ZDM, i.e., in-line quality control of 100% of production on moving/rotating parts.
In order to carry out the development of the system we divided the research into two steps: the first is the design and analysis of performance in lab conditions. Once the performance is assessed and optimized, the system will be integrated in a production line lathe machine for validation in operating conditions.
This PhD project focused on the first phase of the research.
In Section 5.1 the design of the instrument is presented and the measurement algorithm is described. Optimization of the system parameters is reported and in Section 5.2 it is explained how the measurement campaign was planned, how the test samples were prepared and which instruments were used to perform a comparison. Section 5.3 reports the results of the study which are discussed with the focus on critical problems we found related to the location of measurement and the resolution of the stylus.

5.1. Device description

A scheme of how the measurement system works is presented in Figure 79: a turned sample (a cylinder) is placed in front of a camera, its axis is orthogonal to the camera axis, the camera axis is aligned tangent to the cylinder, and it is backlit by a collimated source of light. This optical configuration is typical of telecentric vision or backlit vision and it provides the image of the edge of the sample.

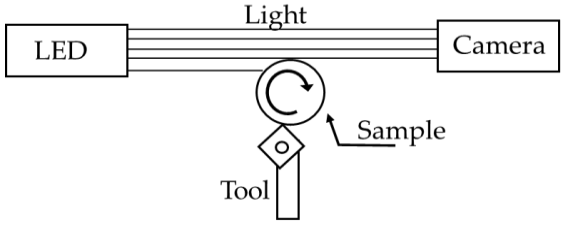

Figure 79. *Simplified scheme of the conceived backlit vision-based measurement instrument where a cylindric bar is turned between a camera and a light source and surface roughness is measured in-line during production.*

If magnification is sufficiently large, the acquired image allows resolution of surface roughness which appears as a black wavy profile over a white background. During image processing, the image is analyzed, the profile is extracted and the average surface roughness is measured as the average of the distances of the peaks and valleys from the mean line.

5.1.1. Design

The instrument was designed by selecting the components of the imaging part and of the illumination part in order to achieve the desired performances in terms of Field of View (FoV) and spatial resolution suitable to measure surface roughness in a range of approximately 2–15 µm. The addition of a tunable lens allows electronic control of the focus. All components were selected from commercially available parts taking into account cost–performance ratio in order to be suitable for future industrialization.
The measurement system setup consists of two main parts, the imaging setup and the backlighting system (see Figure 2 (Left)). The imaging part is made of:

- An objective composed of two parts:
    a. An electrically tunable lens (ETL) EL-10-30 C (Optotune);
    b. A dynamic focus VZM lens (Edmund Optics) with a magnification range of 0.65×–4.6×;
- A 5 Mpix camera with a "2/3" sensor (Lucid Vision Labs Triton, TRI051S-MC).

The ETL was useful to optimize the focus without having to readjust the reciprocal position of the sample and the vision system each time. This component makes it a smart system that can be controlled with a feedforward type of control. The ETL is made of two elastic polymer membranes which are filled with an optical fluid, and the deflection of the lens is proportional to the pressure in the fluid. To exert pressure on the fluid, there is an electromagnetic actuator, hence by applying current to the actuator it is possible to change the focal distance of the lens in a matter of milliseconds, see Figure 80.

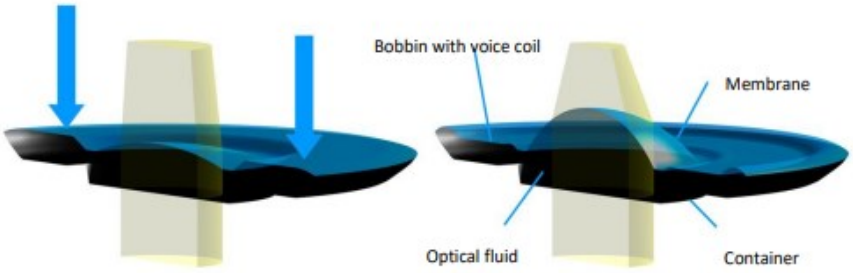

Figure 80. *Working principle of the EL-10-30 series. Image from datasheet.*

The wide magnification range of this design grants a very small FoV. In our configuration we obtained an approximate FoV of 1.5 mm by 1.8 mm using 4.6×

magnification power. The variation in focus given by the ETL also created a slightly variable FoV of the system, ranging from 1.4 mm by 1.6 mm to 1.5 mm by 1.8 mm. This FoV is imaged onto the 5 Mpix 2/3" sensor, thus allowing for the necessary spatial resolution; pixel dimensions projected over the object plane resulting between 0.6 µm/pixel and 0.7 µm/pixel at the maximum magnification of 4.6×. The depth of field of the imaging objective results are 84–90 mm at the maximum magnification of 4.6×.
As for the backlighting of the vision measurement system, it is made up of two parts:

- A white 3W LED;
- A lens with focal length of 150 mm.

This created the parallel collimated illumination needed for this application to have a sharp edge instead of the blurred shadow that would arise if uncollimated light were used. The illumination intensity is uniform across the image, resulting in a flat-top profile. In fact, over an 8-bit image intensity scale (0–255), the average illumination is in the range 150–200 with a dispersion lower than three estimated as standard deviation.
In Figure 81 (Left) a schematic of the instrument is represented, while Figure 81 (Right) is an image of the actual measurement setup.

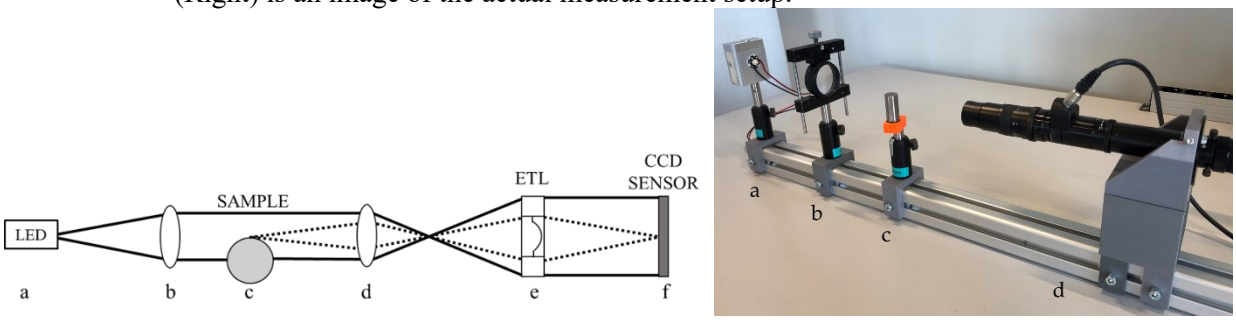

Figure 81. *Measurement system setup. (Left) is a schematic of the instrument composed as follows: (a) LED light, (b) lens, (c) test sample, (d) dynamic focus lens, (e) electrically tunable lens (ETL), (f) "2/3" CCD camera sensor. The black lines represent the light rays from the LED to the sensor, while the dashed lines are from an image point on the focus plane to the sensor. (Right) is an image of the actual measurement setup: (a) LED light, (b) lens, (c) test sample, (d) objective.*

Even if the industrialization of this idea is out of the scope of this PhD, such a conceptual scheme allows the realization of an optical instrument that could be designed for an in-line application in a lathe. The parallel light projector should be placed on one side of the turning piece, while the imaging objective and the camera should be on the other side. To remove image blur induced by motion, light should be pulsed and camera acquisition shuttered at proper aperture time. This would be useful if an in-process roughness measurement is desired. As a second option, the system could be placed by the lathe, and turned parts could be picked up by a robotic arm and placed in the measurement system. This would allow a measurement by-the-process. In both cases, this would be fully in line with the scope of having measurements on 100% of parts produced, as required by ZDM.

Measurement algorithm

The target images are a sharp close-up view of the edge of the sample, where the wavy shadows created by the machining process are clearly visible, see Figure 82. In the figure are depicted two different samples with different surface roughness. The image on the left is of a sample with low surface roughness (R_a = 2.4 µm), while the one on the right has much higher surface roughness (R_a = 15.1 µm). At the edge of the image, a light scattering effect is visible. This will be discussed in later on.

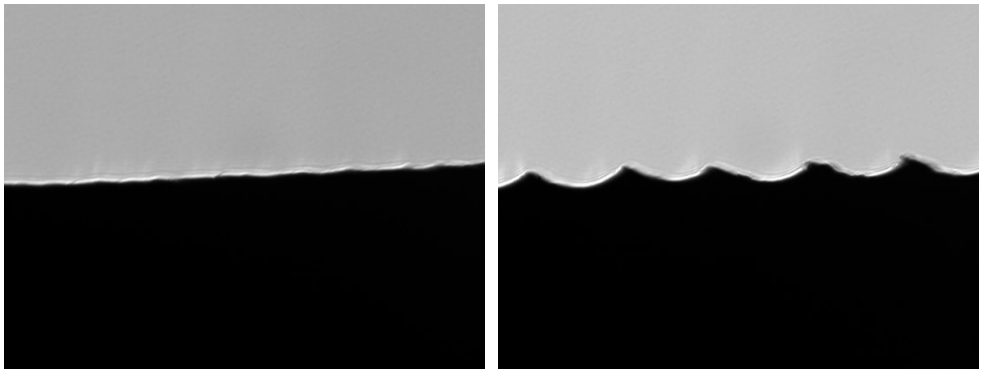

Figure 82. *Acquired images of the edge of sample 5 (Left) of R_a = 2.4 µm and sample 7 (Right) of R_a = 15.1 µm. Full image size is 2448 × 2048 pixels corresponding to 1.4 × 1.7 mm.*

The measurement algorithm is based on four steps (see also Figure 83):

- An edge-preserving filter (i.e., median filter) is used to remove noise from the 8-bit grey-level image;
- The image is scanned from grey to black with a Sobel algorithm to detect the edge of the sample [125]. It detects edges in both directions and it finds edges where gradient is maximum. To this end, the edge function in Matlab was used;
- To determine the mean line and to detrend the mean surface, the edge of the piece is linearly fitted by using a least square fit model of the type y = ax + b;
- The average surface roughness, R_a, is calculated as the arithmetic mean of the absolute ordinate values within a sampling length [93]:

$$R_a = \frac{1}{n}\sum_{i=1}^{n}|Z_i| \tag{5.1}$$

where n is the number of data points (i.e., the sampling length) and Z_i is the ordinate value of the i^{th} point from the mean line (see Figure 83, step 4).

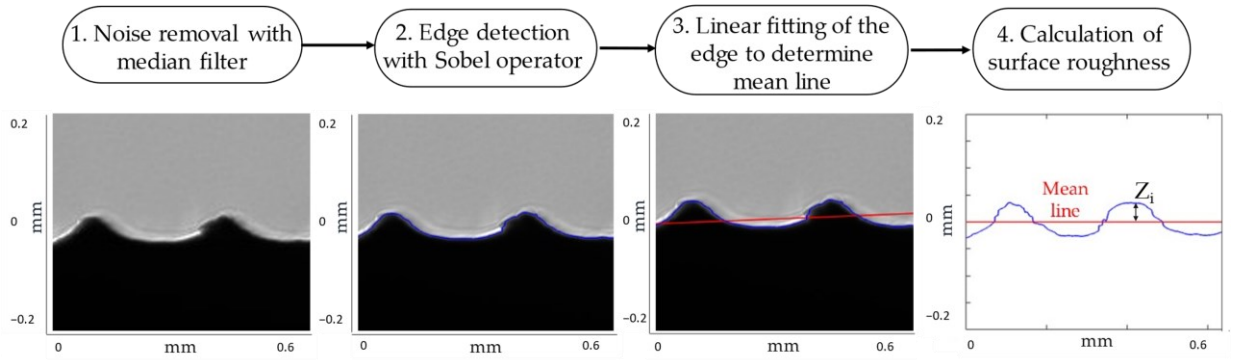

Figure 83. *Steps of the measurement algorithm: (1) Filtering of the image; (2) The blue profile line is determined through the Sobel edge detection method; (3) The red line is the mean line obtained with the linear fit of the edge; (4) R_a is measured as the average of the distances Z_i between each i^{th} point of the profile and the mean line.*

5.1.2. Optimization of system parameters

This section will discuss the steps performed to optimize the vision system:

- The calibration of the camera;
- The analysis of the spatial resolution through MTF;
- Thresholding algorithm.

Calibration

In order to calibrate the vision system, a high resolution microscope checker calibration target (Edmund Optics, #37-540) with 50 µm by 50 µm squares was used. The variability of the FoV is an effect of the combination of all the optics. Its change depends on the ETL used. In fact, the conversion factor between mm and pixel would change every time the current applied to the ETL changed. To solve this problem, a calibration function correlating ETL current and conversion factor was experimentally built, based on the knowledge that the relationship between the two is linear. This would also indirectly tie the ETL current and the FoV.
Figure 84 shows the results of the calibration and proves the linear correlation between ETL current and FoV.
Six images of a calibration target were collected at different but known current values of the ETL, placing the target in focus by moving it manually and not changing the current. The conversion factor was extracted for each image by correlating the number of pixels to the known dimensions of the squares. This way we obtained six pairs of values on which we reconstructed a linear function. Once we had a function correlating the conversion factor to the input current of the ETL, for each measurement we recalculated the conversion factor based on the ETL current of that specific case. This kind of feedforward approach makes the instrument adapt to the measurement conditions in a smart way.
The current interval needed to place into focus the samples during measurements was between 78.4 mA and 165.6 mA, hence the relative computed range of conversion factors resulted to be between 0.6 µm/pixel and 0.7 µm/pixel in both the

x and y directions of the camera sensor, with a standard deviation of 5.7 × 10−5 µm/pixel.

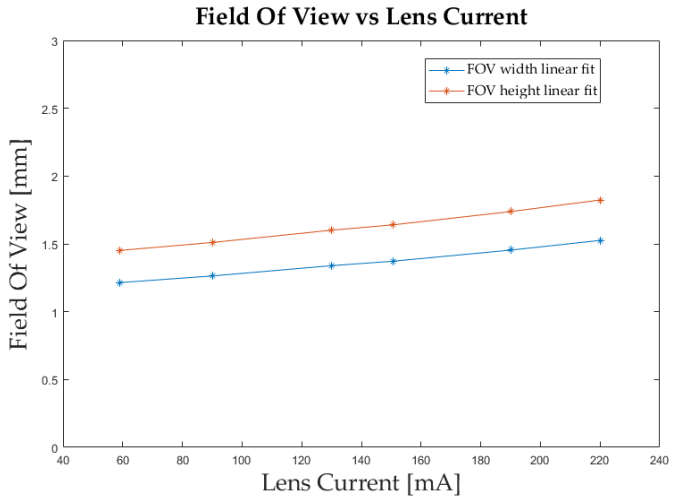

Figure 84. *Linear correlation between the field of view (FoV) and the ETL current obtained through six calibration images.*

Modulation Transfer Function

The modulation transfer function (MTF) is a parameter which represents the sharpness of an imaging system, making it possible to evaluate the imaging conditions and to assess the performance of the optical system. It is also known as the spatial frequency response of an imaging system to an input, therefore is directly related to spatial resolution of the imaging system.

Similarly to what was already described in Chapter 4, to evaluate the MTF, the image of a razor blade was used, see Figure 85 (Left). Based on the MTF, the right combination of exposure time and intensity of illumination was determined in order to obtain the highest contrast that would not cause saturation. This would cause blooming, hence a change in charge distribution on the camera sensor. This affects profile shape and position which should be avoided when performing geometric measurements. The exposure time thus selected was the one that would increase the band width the most and the obtained preservation of contrast was of 0.058 cycles/pixels.

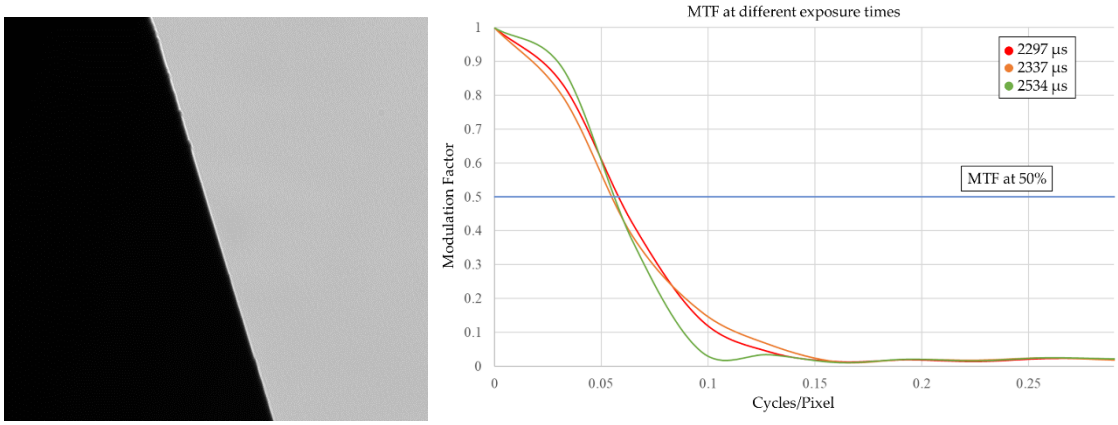

Figure 85. *(Left) Image of the sharp edge used as input; (Right) MTF of the imaging system at different exposure times (the blue line is the MTF at 50%).*

Threshold

If we look at the edge of the sample, it is evident that there is light scattering caused by the collimated impinging light interacting with the surface that in turn produces diffraction fringes. The phenomenon appears as fringes parallel to the edge. In diffraction, fringe spacing depends on wavelength λ; therefore, fringes will be sharp only with monochromatic illumination. In Figure 86, it is presented an intensity profile orthogonal to the surface (Figure 86 (Left)); we see a transition from black to the first peak of the diffraction fringe followed by other smaller oscillations (Figure 86 (Right)). If we had used a monochromatic light source the diffraction fringes would be clearly distinct and sharp, while if we had used a wide-spectrum light source they would appear as a fuzzy blur due to the superposition of fringes with different geometry. In our case, the LED source is neither monochromatic nor a continuous spectrum; its spectrum has a peak in the 450–460 nm range, but it also covers the range of 480–700 nm, hence we are in between the blurry fringes and the distinct fringes.

Overall, the edge is not sharp. Nonetheless, the threshold-based edge detection algorithm is able to accurately detect the edge of the sample. The value associated with the threshold is the cut-off value between black and white pixels in a binary representation of the image intensity. In Figure 87 the effect of different thresholds is represented. It can be seen that the shape of the profile is maintained and only shifted either towards the black side or towards the grey side. In fact, even if the transition from black to grey is not sharp, a difference in threshold would only cause a shift in the detected profile as schematized in Figure 86 (Right): the intersection between the threshold and the transition profile from black to grey is only offset towards the right.

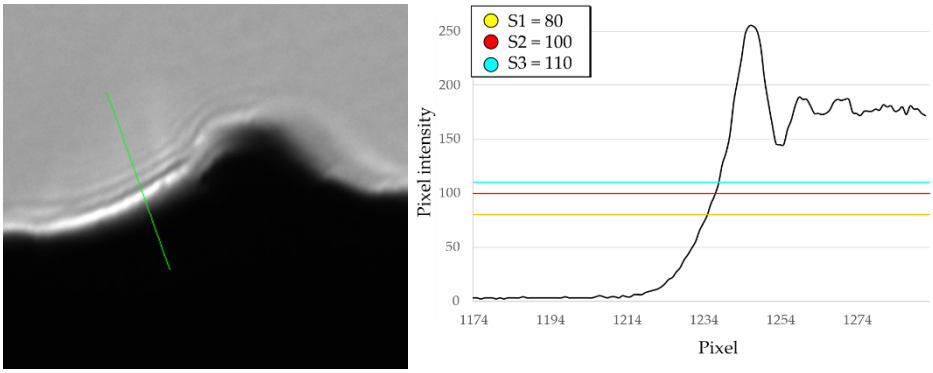

Figure 86. *(Left) The green line is an intensity profile orthogonal to the surface that intercepts the diffraction fringes. Image size is 350 × 350 pixels, corresponding to 0.2 × 0.2 mm; (Right) Pixel intensity correlated to the green line: we see a transition from black to the first peak of the diffraction fringe followed by other smaller oscillations. Threshold values represent the cut-off values between black and white pixels in a binary representation of the image intensities: when the value changes the intensity transition is shifted either towards the black or towards the white.*

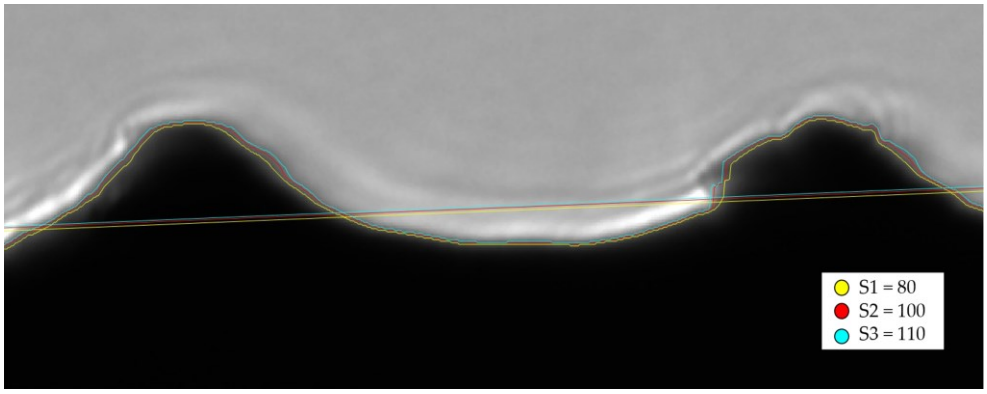

Figure 87. *Comparison of different thresholds on the same close-up of the edge: the shape of the profile is maintained and only shifted, therefore R_a is not affected. The three thresholds are described in the legend. Image size is 700 × 380 pixels, corresponding to 0.5 × 0.3 mm.*

The position between the mean lines changes only by 1 pixel. This difference is also coherent with the offset of the profile lines which also differ by 1–2 pixels. If a change in threshold causes a shift in the profile, the estimate of R_a does not vary, since R_a is a quantity that describes the shape of the profile, not its actual position. The R_a values corresponding to the three thresholds (S1, S2, S3) are, respectively: R_a = 16.1 µm, R_a = 16.6 µm and R_a = 16.9 µm.

Another issue which usually affects the performance of optical instruments is measurement noise depending on random fluctuations of illumination and image sensor response [126], [127]. This noise typically affects a measurement method based on intensity. However, the method proposed here overcomes these limitations thanks to the thresholding used for binarization of the images. Indeed, in a backlit vision system the object will appear as a dark shadow over a bright field and the

geometry being measured is the edge between the two areas. This edge is identified by a threshold which is not affected by intensity fluctuations if the contrast is high enough and the edge sharp enough as discussed above.
It would be different if we were trying to measure an actual dimension, like a length, as already discussed in Chapter 4. When performing dimensional measurements, a change in the position of the profile, for example caused by saturation, results in a wrong estimate of the dimension.

5.2. Measurement campaign and uncertainty analysis

To evaluate the uncertainty of the designed measurement system, we measured the same set of samples with different instruments, both contact-based and non-contact-based. The samples had different surface roughness to test the sensitivity of the measurement systems and their performance at different values of roughness. The sample set was made by manual turning of a steel rod and this process is described in Section 5.2.1, while the instruments used for the comparison and the uncertainty analysis are described respectively in Sections 5.2.2 and 5.2.3.

5.2.1. Sample preparation

To test the metrological performance of the designed backlit vision system we manufactured a set of samples of different average surface roughness (R_a) through the machining of a C45 steel rod on a manual lathe. The rod was cut in pieces of same length and diameter of 12 mm, then the samples were turned on the same machine varying one of the process parameters and keeping the others constant.
In Figure 88 some of the variables involved in the turning process are shown:

- V_t = cutting speed of the workpiece (m/min);
- p = depth of cut (mm);
- f = feed rate (mm/rev).

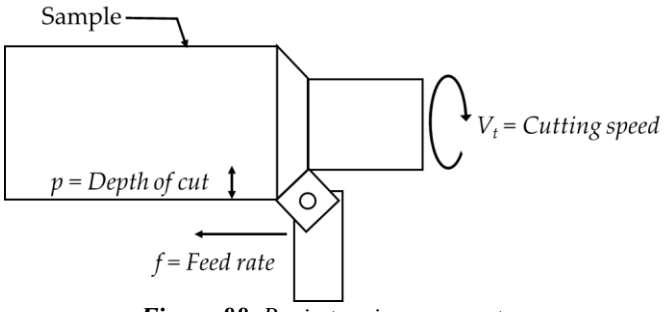

Figure 88. *Basic turning parameters.*

Figure 89 shows the manual lathe, available at the workshop of the Department of Industrial Engineering and Mathematical Sciences of Università Politecnica delle Marche.

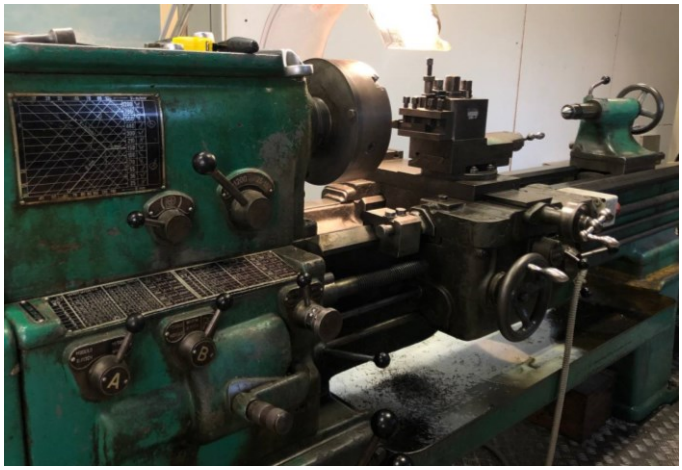

Figure 89. *Manual lathe used for the making of the sample set.*

The variables that were kept constant were the cutting speed at 440 m/min and the depth of cut at 1 mm, while the feed rate was varied from 0.05 mm/rev to 0.6 mm/rev. This method enabled us to obtain a wide range of samples with different surface roughness, from 2.4 µm to 15.1 µm. In technical drawings of mechanical parts, R_a values are usually specified as upper limits; less often they are indicated as an interval between upper and lower limit. Typical R_a roughness achieved in turning processes is between 1.6 and 12.5 µm, therefore our experiment covers most of this range including R_a = 3.2 µm (standard commercial machine finish), which is default roughness unless otherwise specified. The range of values used was selected based on literature regarding surface roughness measurements [110], [115]–[117], [128] and also because this range is of interest in common turning processes. Moreover, it covers a range wide enough to assess the performance of the instruments.
Table 4 shows the minimum and maximum roughness values measured with a stylus-based instrument with a tip radius of 2 µm and a tip angle of 60°; this was considered the reference instrument. In the last column, the range was computed as the maximum value minus the minimum value. The average values of R_a were calculated on five different measurements obtained from different locations on each sample.

Table 4. Surface roughness range measured with a stylus profilometer.

Sample	Avg R_a (µm)	Min R_a (µm)	Max R_a (µm)	Range (µm)
1	14.4	13.7	14.7	1
2	6.2	5.7	6.7	1
3	4.7	4.4	4.9	0.5
4	3.1	2.9	3.3	0.4
5	2.4	2.3	2.6	0.3
6	3.3	2.6	3.8	1.2
7	15.1	14.3	15.5	1.2
8	14.3	13.9	15.2	1.3
9	14.6	13.9	15.3	1.4

In Figure 90, pictures of three of the analyzed samples are shown, which are representative of the surface roughness range: sample 5, sample 2 and sample 7, respectively at R_a 2.4 µm, 6.2 µm and 15.1 µm. The typical helicoidal grooves generated by the cutting tool on the rotating surface of the cylinder can be clearly observed. These grooves are parallel to each other, providing a rough surface with a quasi-periodic morphology. Observing the surface from a side, along a tangent direction, the series of valleys and peaks shown in Figure 3 will clearly appear to the observer, provided it has a sufficient spatial resolution.

(a) (b) (c)

Figure 90. *Surface roughness of sample 5 (a), sample 2 (b) and sample 7 (c).*

5.2.2. Comparison analysis

The comparison analysis was conducted with the use of both contact and non-contact state-of-the-art measurement systems as follows (more information about the instruments can be found at the manufacturer's website):

- a Surface Roughness Tester (Mitutoyo, S-3000), with a 2µm, 60° angle tip, referred to as SRT 1;
- a Surface Roughness Tester (Mitutoyo, SJ-210), with a 2µm, 60° angle tip, referred to as SRT 2;
- a confocal laser scanning microscope (Keyence, VK-X1000).

SRT 1 is equipped with a vibration isolating base and it can be set to perform automated measurements thanks to the ability to control all axes and rotary table. SRT 2 is a portable measuring instrument, for the experiments described in this thesis, it was mounted on a hand-operated bracket.
Each sample was measured with the three instruments and the results obtained were compared to the backlit vision instrument designed in this work. The measurements, even if different in nature, were performed in a way to obtain similar results:

- For the backlit vision system, to obtain one average surface roughness value, each sample was rotated 10 times and measured on different edges and the single value was calculated as the resulting average. This process was repeated five times, see Figure 91 (Left);
- For the surface roughness testers, the samples were measured and subsequently rotated five times in order to collect measurements of different edges. The evaluation length (ℓn) on which the measurements were based was 15 mm, see Figure 91 (Right);

- For the confocal microscope, the images collected were post-processed with its software (MultiFileAnalyzer) and the measurements were performed with a setting that would mimic the stylus-based instruments, on a ℓn = 15 mm as well.

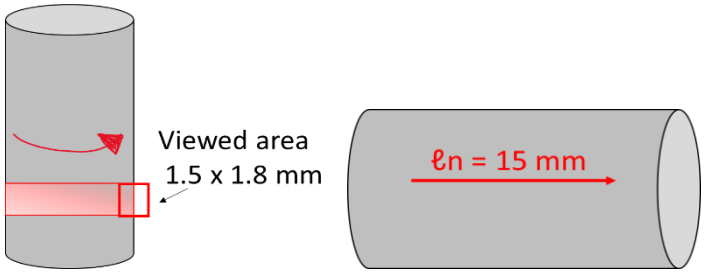

Figure 91. *Measurement procedure followed: (Left) Procedure for the backlit vision system; (Right) Procedure for the other instruments.*

At first, to simulate a procedure typical of real work environments, the measurements were performed on five different locations, not predetermined but evenly distributed on the surface. Later, we will see how these measurement conditions will influence the uncertainty associated with the measurement.
Details about the instruments' resolution are reported in Table 5. It is important to mention that the resolution value relative to the backlit vision instrument is the pixel resolution, which is the corresponding pixel size in microns.

Table 5. Summary of instruments.

Instr. ID	Type of Functioning	Resolution [µm]
1	Surface roughness tester 1 (SRT 1)	0.001 (for an 80 µm Z-range)
2	Surface roughness tester 2 (SRT 2)	0.002 (for a 25 µm Z-range)
3	Confocal microscope (CM)	±1.0 + L/100 (L = measuring length)
4	Backlit vision instrument (BV)	0.6–0.7 (µm/pixel) (pixel resolution range)

5.2.3. Uncertainty analysis

The performance of the backlit vision measurement system proposed in this study was compared to the other measurement instruments which are both contact and non-contact based. We based the performance comparison on the results obtained with the stylus-based instrument SRT 1, hence this was the reference instrument.
The ISO GUIDE 98-3 [39] is the main reference for the estimate of uncertainty, even if for industrial applications its complexity is being debated and simpler approaches are being proposed [129]. We carried out a Type A analysis of uncertainty and according to the ISO GUIDE 98-3 [39], given the limited number of samples available, we used the range as an estimate of the scatter of data instead of the

standard deviation. The range is the difference between the highest and the lowest result.

5.3. Results and conclusions

The results of the comparison analysis are presented in Figure 92. The samples are plotted in order of increasing roughness and the error bars represent two times the ranges associated with the measurements.

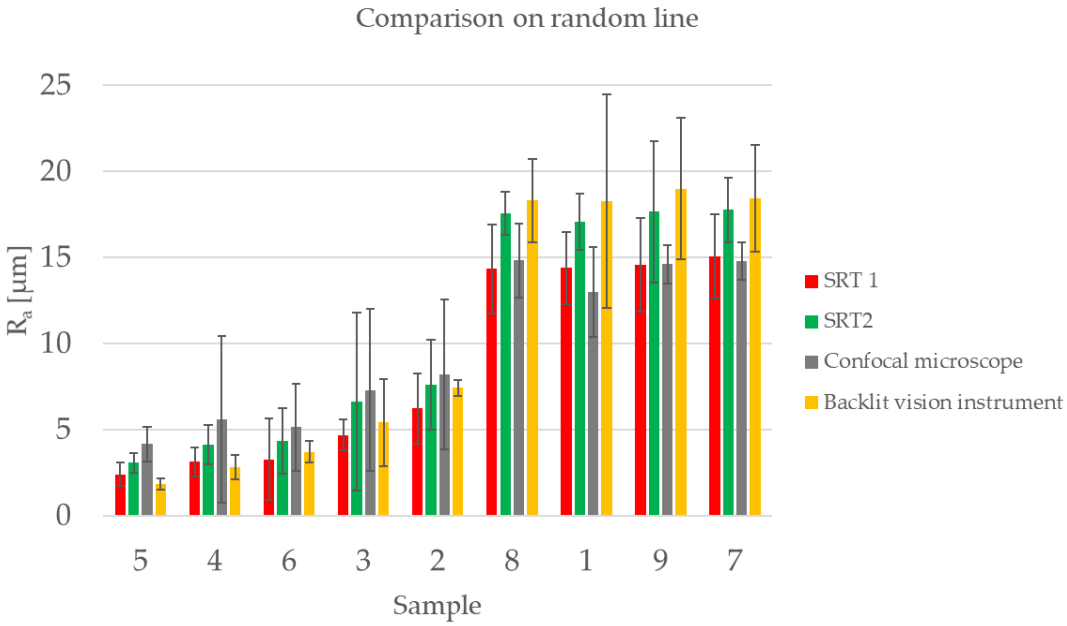

Figure 92. *Overview of the results obtained by comparing the instruments on measurements performed on a random line on the surface. The samples are plotted in an increasing order of surface roughness of the reference instruments SRT 1. The error bar represents two times the range of the repeated measurements for each sample and each instrument.*

By looking at the overview of the results in Figure 92, two things can be noticed:

1. Two different behaviors can be seen based on the surface roughness: Samples 2 through 5 have a low surface roughness (between 2 µm and 6 µm), while Samples 1, 7, 8 and 9 have a higher surface roughness of around 14.5 µm;
2. Regarding the uncertainty associated with each measurement (the uncertainty range), depicted in Figure 12, it can be said that in general the uncertainty is larger when measuring larger values of R_a.

If we consider data reported in Figure 92 and limit the comparison to the backlit vision system and SRT 2, we can observe that results are compatible, i.e., the error bars are partially superimposed.

5.3.1. Critical problems related to the uncertainty

When analyzing the data we pinpointed two reasons for the difference in uncertainty of measurement which we are going to discuss in this section:

- The location of the measurement on the surface of the turned part;
- The evaluation length on which the roughness measurement is based.

Location of measurement

Surface roughness is always calculated as an average value over a relatively short length (see Equation (1)), making the value intrinsically variable over the surface. In particular in turned pieces, the machining process itself creates an instability and a variability of the surface finish. Hence, if the measurements are not performed in the same location with all the instruments taking part in the experiment, the resulting values will have a higher variability due to both the variability of the surface itself and to the variability between the instruments. Using these values to compare the performance of different instruments may be questionable. Indeed, we miss a true reference, capable of providing a known input common to all instruments. To address this hypothesis, we performed a test: we used the backlit vision instrument to again measure one sample, but in this case the measurements were performed always in the same location. The results of the test are reported in Figure 93.

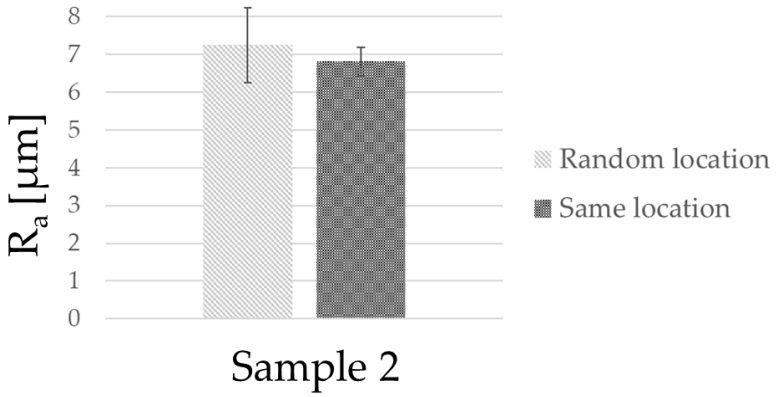

Figure 93. *Comparison of results obtained by measuring surface roughness on different edges of the same sample with the VB instrument. The histogram on the left represents measurements performed in random locations, while the histogram on the right represents measurements taken on the same location. The error bars represent the range of the measurements*

Performing measurements in the same location allowed us to demonstrate that when performing measurements in the same location there is a noticeable decrease in the range associated with the results. The mean values are compatible, while the range associated with the random locations is significantly larger (1.0 µm) than the one associated with the same location (0.4 µm), which signifies that the variability in the part contributes significantly to disperse repeated measurements.

Evaluation length

The second reason for a difference in measurement uncertainty is the length on which the mean is evaluated (ℓn, evaluation length). In fact, it should increase with the increase of surface roughness.

For the contact instruments and for the confocal microscope, the evaluation length considered was ℓn = 15 mm. On the other hand, since the FoV of the designed backlit vision instrument is about 1.5 mm by 1.5 mm, this could be one of the reasons for its higher associated uncertainty. Each single measurement is calculated on the average of ten values measured on ten 1.5 mm by 1.5 mm images, which would equal the evaluation length considered for the other instruments. This has proven to be sufficient to obtain values which are in line with the other instruments, but it could also be one of the reasons its associated uncertainty is higher, especially on samples with higher R_a.

To confirm the influence of the evaluation length, a second test was performed: a few samples were measured again with the confocal microscope but this time the surface roughness was based on five segments of ℓn = 1.5 mm. Then, these measurements were compared with the ones obtained on ℓn = 15 mm.

The results of the test are shown in Figure 94, and they highlight how the change in evaluation length has a clear impact on the range of the measurements. Dispersion decreases if evaluation length increases, as expected for the measurement of statistical quantities, such as R_a.

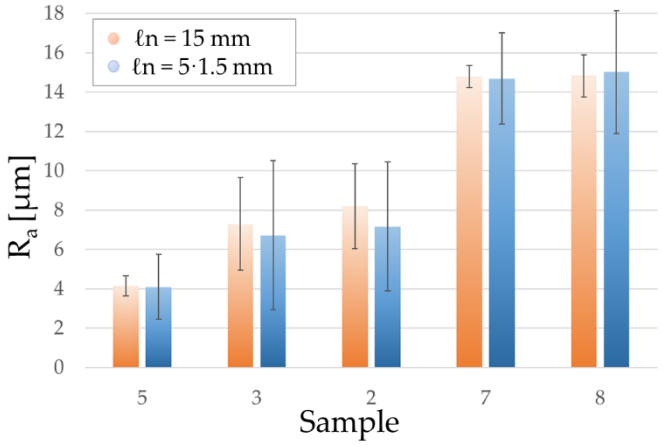

Figure 94. *Comparison of results obtained by measuring surface roughness on different evaluation lengths (ℓn). The orange bars are the ranges associated with measurements taken on ℓn = 15 mm, while the blue bars are associated with five distinct measurements taken on ℓn = 1.5 mm.*

5.3.2. Critical problems related to higher R_as

The difference in behavior that can be noticed between lower and higher R_as could be caused by the difference in measuring techniques: the working principles of the instruments are different as might be the processing algorithms.

The most probable hypothesis concerns the size of the diamond tip of the stylus, which represents a limit to the instrument's resolution. In fact, generally the error

increases with the increase of the tip size or the increasing of the peak-to-valley height [130].
To discuss this hypothesis we developed a simple 2D geometrical model in which we simulate a roughness measurement performed with a stylus having a tip with radius 2 µm and a tip angle of 60°; in our experiments, both surface roughness testers had a tip with these characteristics. The physical dimension of the stylus tip prevents the probe from perfectly following the shape of the surface, especially when there is a sharp peak in roughness. The state of art in industrial application of styluses shows that a 2 µm tip is the lower limit to the probe tip radius [131]; in fact even recent literature studies the effect of stylus tip radius in Ra. Our simple model is descriptive of best case scenarios in terms of tip radius in industrial applications.
In Figure 95 there are three step functions that represent the theoretical profile of three surfaces. We choose a step profile, because step response functions are generally useful to determine the performance of a measurement system. The model was meant to represent the concept of a sharp peak even if in real machined surfaces steps do not exist; the findings derived from it are descriptive of the situation that we observed at highest R_as. In particular, we simulate three steps having three increasing values of roughness: a 7 µm step, a 14 µm step and a 28 µm step. The corresponding R_a theoretical values are exactly half of the step values, since the average surface roughness is measured as the distance of each point from a mean line (see Equation (1)), and they are reported in Table 6, column one.

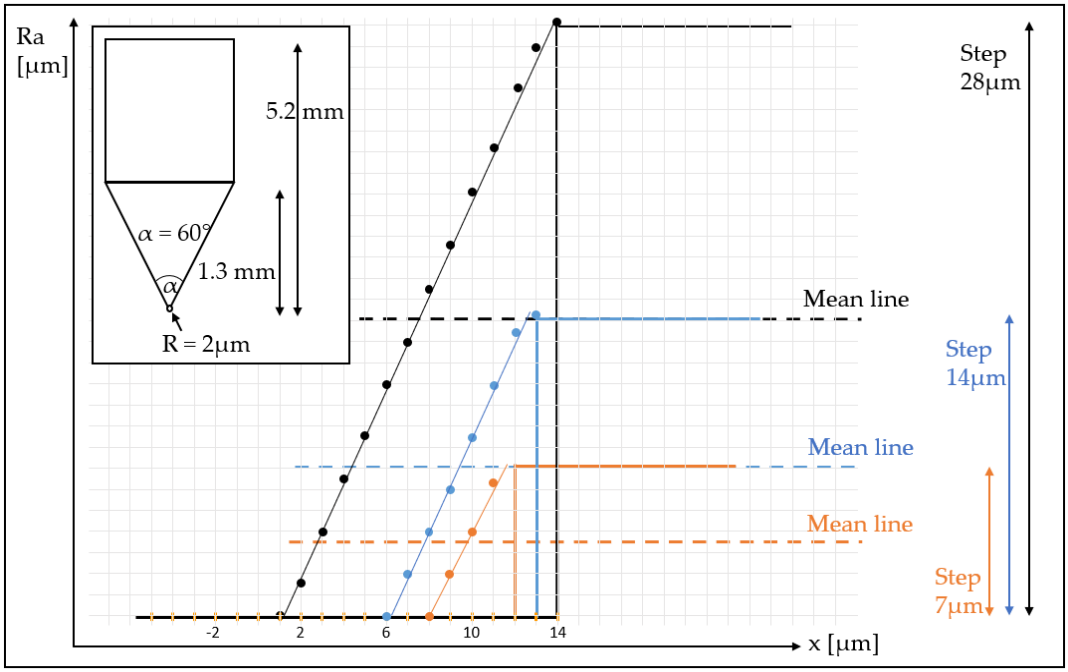

Figure 95. *Simulation of a roughness measurement performed with a stylus' three step functions of increasing amplitude. In the top left corner, there are the dimensions of the stylus tip: the tip radius is 2 µm and the tip angle is 60°.*

Table 6. Surface roughness of step function.

Reference Step (µm)	R_a Measured by Stylus (µm)	Difference ΔR_a (µm)
$R_a = 3.5$	$R_a = 3.2$	$R_a = -0.3$
$R_a = 7$	$R_a = 5.9$	$R_a = -1.1$
$R_a = 14$	$R_a = 11.3$	$R_a = -2.7$

The lines presented in the figure represent the simulation of the trajectory a stylus tip of the given dimensions (tip radius and angle) would follow when measuring a step profile: the shape of the tip prevents the stylus from reaching the bottom of the step transition, hence, a much softer trajectory is followed instead [132]. This is schematized in Figure 96. We traced the trajectory and used the corresponding values to calculate the surface roughness that the stylus would measure. The results are reported in Table 6, column two. When the step gets larger, the stylus underestimates R_a. In particular, if we look at ΔR_a we can notice how the difference increases with the increase of the surface roughness. Hence, this simple geometrical model shows how the stylus method tends to underestimate the real roughness value, especially in presence of sharp peaks which occur in case of large values of roughness.

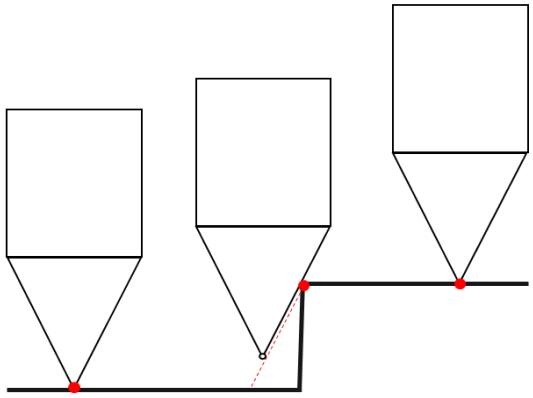

Figure 96. *Effects of a finite stylus shape: the tip prevents the stylus from reaching the bottom of the step transition, the red trajectory is followed instead.*

This is a possible explanation of why the vision-based system that we have designed shows a different behavior, with respect to the reference instrument SRT1, when measuring higher R_as as compared to the lower R_as. While in the lower ranges of R_a the two instruments are definitely consistent and in alignment, when moving to the large values of R_a, the offset between the two increases and the stylus underestimates the roughness, which instead is correctly measured by the vision system. In fact, the backlit vision instrument is not limited by any kind of physical resolution if not only by the resolution of the optical system. Being a contactless sensor, no limitation arises from the physical contact of the probe to the target surface.

5.3.3. Second set of measurements

In Figure 97 the results of a new set of measurements are reported. In this case they were performed in the same location with the same evaluation length. It can be noticed that the uncertainty associated with the measurements performed by all of the instruments is much lower and that the error bars are partially superimposed.

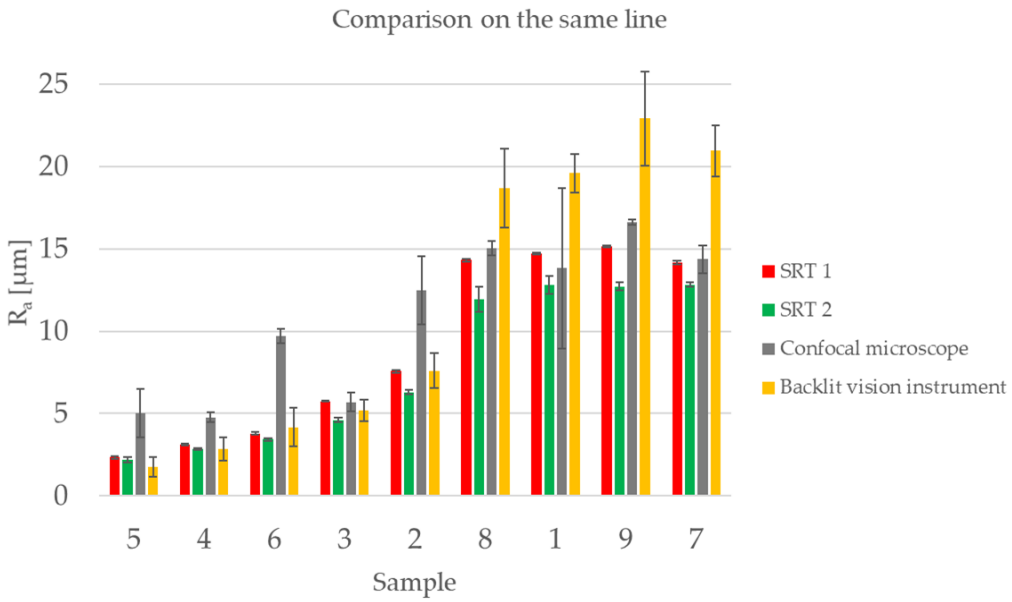

Figure 97. *Overview of the results obtained by comparing the instruments on measurements performed on the same line on the surface. The samples are plotted in an increasing order of surface roughness of the reference instruments SRT 1. The error bar represents two times the range of the measurements.*

The results show a general scatter of the data across all the different instruments and between the lower and higher R_as, making it difficult to state with certainty which instrument performs better compared to the reference one. Results show both bias and random scatter for all four instruments, so that none of them can be considered as a reference instrument from a metrological point of view.
Regarding the backlit vision system, the measurements of the samples with lower surface roughness are compatible with the results obtained with the surface roughness testers. While the measurements of the samples with higher surface roughness had a higher offset with respect to the surface roughness testers. The reason for this is the resolution limit of the stylus as explained in the model in Section 5.3.2.

5.3.4. Conclusions

In this chapter we presented a backlit vision-based non-contact system to measure the surface roughness of a range of samples in a contactless mode with the purpose of in-line measurements.
We presented the design of the system, with attention towards:

- High magnification, fit to resolve R_a in the range of 2–15 μm;
- An electronic control of focus through a tunable lens;
- White light for collimated backlighting.

After being assembled the system has been tested on typical cylindrical samples produced by turning a C45 steel rod on a manual lathe to obtain samples with R_a in the range of interest.
The optimal imaging conditions were found by combining the use of the MTF and an ETL, which allows sharpening of the focus by controlling the current of the lens without repositioning the sample.
The measurements were based on the images of the samples acquired, then the average surface roughness R_a was calculated thanks to the edge detection algorithm developed.
To evaluate the measurement uncertainty of the developed instrument, its performance was compared to the ones of other state-of-the-art roughness measurement systems. The measurement uncertainty was assessed by calculating the mean and uncertainty range associated with the measurement results, and the performance of each instrument has been compared to the chosen reference instrument, i.e., the stylus-based instrument SRT 1.
The conclusions derived from this comparison are as follows:

- The comparison of the results of the backlit system depends on the values of surface roughness considered;
- The measurements performed by the backlit vision system have a larger bias compared to the ones obtained by the stylus when measuring larger values of roughness, also because the stylus underestimates the R_a;
- The results are compatible with the ones of the stylus at lower values of roughness. In fact, the error bands are superimposed by at least 58% based on the cases analyzed. The value was computed as percentage of overlap between the two uncertainty ranges with reference to the smaller one.

In conclusion:

- The proposed instrument gives results which are comparable to the other state-of-the-art instruments when measuring lower surface roughness (2.4–6.2 μm), which are within the range normally achieved in turning, where the standard commercial machine finish is R_a = 3.2 μm. This is important because it provides an innovative

non-contact instrument for a potential application for ZDM quality control in many industrial turning processes;

- At higher values of surface roughness (14.3–15.1 μm) the offset with the reference instrument increases. Such high values are less frequent and less relevant for standard turning processes, however we tried to provide an explanation for this problem.

To provide an explanation of the problems encountered at the higher R_a values, a simple geometrical model was developed, simulating a stylus measuring roughness through a surface having a step profile. The model confirms that large amplitude of the step determines the stylus to underestimate its R_a. This observation shows a potential advantage of the backlit vision system: being non-contact, the measurement does not suffer any limitation due to the shape of the probe, while the stylus does.
Further studies will involve a more in-depth analysis of the influence of the location of the measurement and a study of the importance of the processing algorithms implemented by the different instruments.
We like to highlight that the developed backlit vision system for roughness measurement offers a setup that performs fast non-contact measurements, and in perspective, it opens the possibility of being implemented in the production line, allowing the inspection of 100% of production as required in ZDM.

In Chapter 6 a laser-line triangulation system for gap and flush measurements will be presented and the performed R&R analysis of variance will be discussed.

Chapter 6.

G3F: Gap & Flush measurement system

This PhD thesis aims to describe how the uncertainty of a gap & flush measurement performed by an operator using a hand-held non-contact laser scanner (from here on: G3F) is affected by working conditions which are different from ideal ones.

The laser-line triangulation sensor used in this work was developed by Minnetti et al. in 2020 [80] in the framework of the GO0D MAN—aGent Oriented Zero Defect Multi-stage mANufacturing project. The scope of the project was to develop a device with the following characteristics: portability, sensing capabilities, wireless connectivity to a network, computational power, a human-machine interface and the possibility to implement smart behaviors. All of which were integrated in a smartphone. This device was patented in 2019 [81].

6.1. Device description

The G3F is a device that measures gap and flush in car body assembly; it integrates in a smart phone cover (see Figure 98): an InfraRed distance sensor, a laser-line projector and a camera creating a triangulation system. Data acquisition and additional sensor devices are performed by a Raspberry Pi. A laser beam is projected orthogonally both at the surface and at the gap between two adjacent car parts and a picture of the projection is taken, then, based on the laser profile, gap and flush are measured.

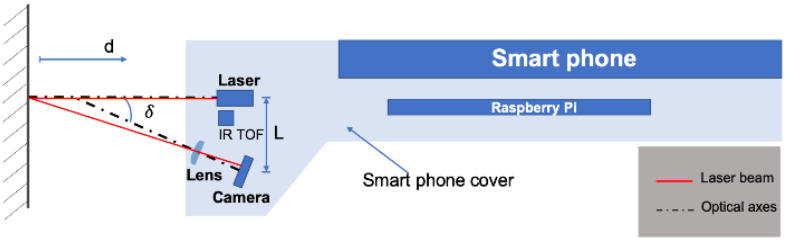

***Figure 98**. Scheme of the laser-line triangulation system of the G3F, where d is the distance from the target, δ is the fixed angle between the laser beam and the optical axis of the camera and L is the fixed distance between the laser and the camera.*

6.1.1. System characteristics

The working principle of the device is shown in Figure 99 (Left): the laser line, with a fan angle $\alpha = 60°$, is projected parallel to the smart phone display, on the car body surfaces S1 and S2. The line is observed by a camera embedded in the external cover, whose optical axis is angled $\theta = 45°$ with respect to the axis of the laser: this way the height differences of the object are visible as displacement on the camera

sensor. The laser profile z(x) is then extracted from the image and gap and flush values are calculated through processing algorithms. The reader can find more details at [80].

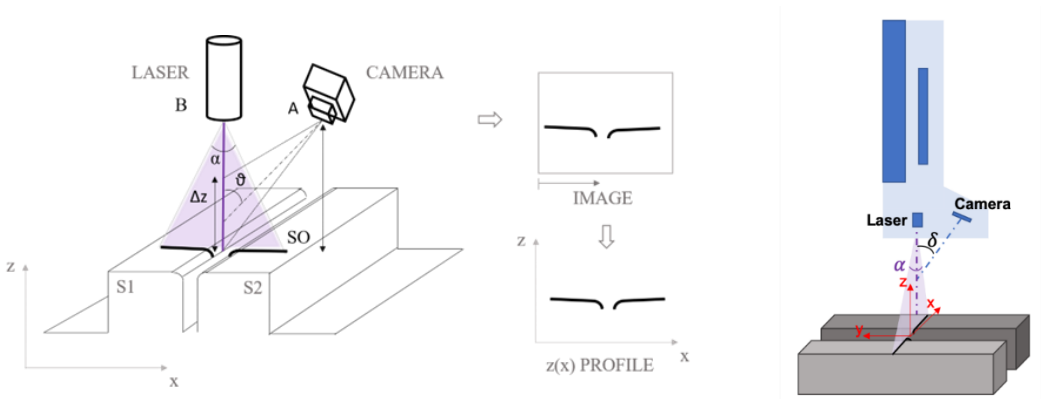

***Figure 99**. (Left) Working principle of the laser-line triangulation system* [80]*; (Right) Implementation of the triangulation system in a phone case.*

The cover was obtained by additive manufacturing of PLA (polylactide) and it holds the smartphone and the laser triangulation system (see Figure 99 (Right)). In the front there is a rubber seal which prevents scratches and the hood that holds the triangulation optics also acts as a barrier from ambient light, see Figure 100.

***Figure 100.** Phone case integrating the laser-line triangulation system* [80].

In a laser-line triangulation system, the characteristics of the surface are a pivotal element. In fact, the surface can act as a mirror, reflecting light in a directional way, or it can diffuse light in the surrounding space. The behavior of the surface depends mostly on the average surface roughness (R_a). In particular, when the ratio between R_a and the wavelength of incident light (λ) increases, it improves the light-diffusive behavior of the surface. Therefore, since R_a is a parameter that depends on the car body surface, to have an optically rougher surface it was necessary to use light with a short wavelength. The best candidate was a violet laser since it has a wavelength of $\lambda = 405$ nm.

6.1.2. Measurement algorithm

The camera, an 8-bit RGB camera highly sensitive to violet light, is driven by the Raspberry Pi: it can detect the surface color and adapt light exposure with respect to the surface optical characteristics as well as the external illumination. The acquired images are sent to the smart phone through a type-C USB link, then the processing of images acquired is performed exploiting the computation resources of the smart phone. The image reproduces the projected laser line, whose light intensity profile is then processed, with a Gaussian Kernel based ridge detection algorithm [133], to extract the line profile, from which gap and flush can be calculated: the data points at the edges are clustered and different procedures are carried out to extract gap and flush values (Figure 101). First the facing edges of the clusters are detected and two lines, tangent to the edges, are drawn; then the distance between the lines, which corresponds to the gap value, is calculated. To determine the flush value, one of the two clusters is chosen as reference and a straight line, fitting the reference cluster, is drawn. Then, the distance between the line and the other cluster is calculated as the flush value.

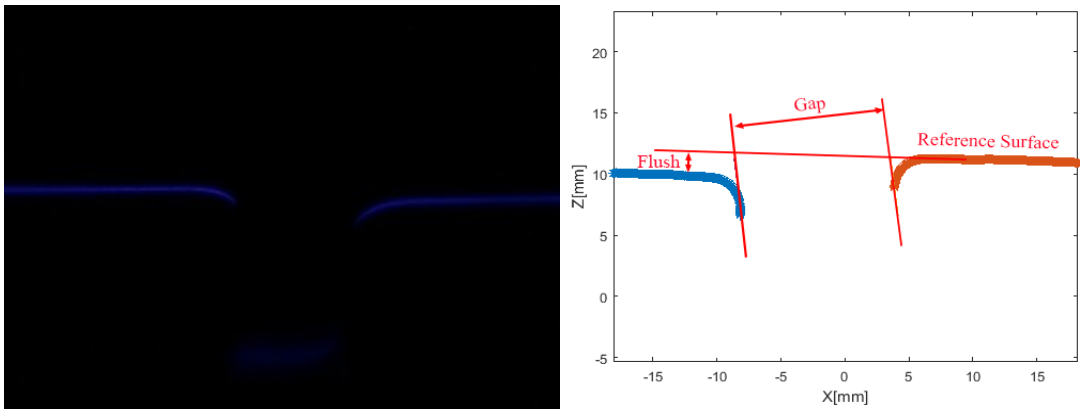

Figure 101. *(Left) Typical laser line projected; (Right): Definition of gap and flush* [80].

6.1.3. Critical variables

In order to obtain a precise measurement of gap and flush, there are four critical variables to take into consideration (Figure 102):

- d: the distance between the device and the surface;
- φ: the yaw angle;
- θ: the pitch angle;
- ψ: the roll angle.

These four variables influence respectively:

a) The working distance of the device;
b) The gap measurement. In fact, if the angle φ is greater than 0 the resulting gap will be overestimated;

c) The light distribution. If the device is not orthogonal to the surface, the presence of a flush, especially if the two car parts create a curved surface, can result in shadowing. Therefore, the profile might not be extracted correctly since it is not completely illuminated;
d) The amount of light received by the camera sensor with respect to the optical properties of the surface (scattering).

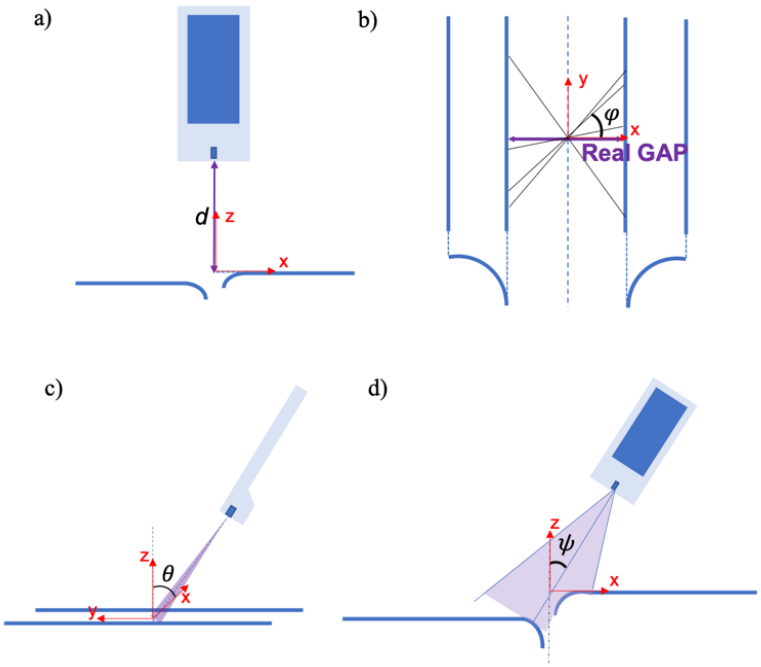

***Figure 102**. The four critical variables taken into consideration: a) the distance between the device and the surface, b) the yaw angle, c) the pitch angle and d) the roll angle.*

6.2. Measurement uncertainty analysis

Given the hand-held nature of the tool, uncertainty of the whole measurement process includes the uncertainty caused by the operator (Figure 103). The tool has some embedded features to guide the operator in the measurement and compensate for potential human errors. For instance, it requires the operator to select beforehand the car body part to analyze, and if the image detected does not match the selected area, the measurement does not take place. This avoids the assignation of gap and flush values to the wrong areas. Moreover, it allows to optimize measurement conditions (e.g. exposure time, contrast, etc.) based on the area selected, creating a lower uncertainty on the measurement result.
It is needless to say that, even with the embedded features of the device, the operator remains a big source of uncertainty. Indeed, the measuring tool strongly relies on the positioning ability of the operator.

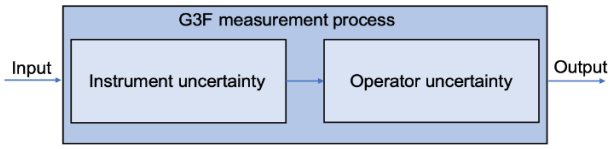

Figure 103. *Schematic of the uncertainty of the G3F measurement process.*

The uncertainty associated to the instrument and to the measurement chain is assessed with a Type A performance analysis: different investigation points are identified on the body of a Toyota Auris and, in order to evaluate reproducibility, a series of measurements is taken by different human operators which are instructed to keep the G3F as perpendicular as possible to the surface of the car and as centered as possible with respect to the center of the gap. Of course, the critical variables d, φ, θ and ψ are considered as a whole. Then, the obtained data are analyzed by the Gage R&R analysis of Minitab 17.

6.2.1. Test set-up

The analysis was performed on data collected from a Toyota Auris and the chosen parts to measure were representative of different surfaces. In particular, measurements were taken on 3 different locations addressing metal-metal surfaces: two on the front and back side door of the car (front-to-back front side door; back to frame back-side door) and on the fuel cap (see Figure 104). The car is painted in white.
Each measuring point was inspected at least 20 times by each one of the 3 different operators:

- Operator 1: male, right-handed, 185 cm tall, 58 years old;
- Operator 2: female, right-handed, 164 cm tall, 53 years old;
- Operator 3: female, right-handed, 166 cm tall, 17 years old.

Measurements took place on the car parked outside in the shade, on days with similar lighting conditions (this because no access was allowed to the laboratories during the COVID-19 quarantine period). The operators were shown were to measure and no training was provided, other than a brief explanation on the basic functions of the instrument.

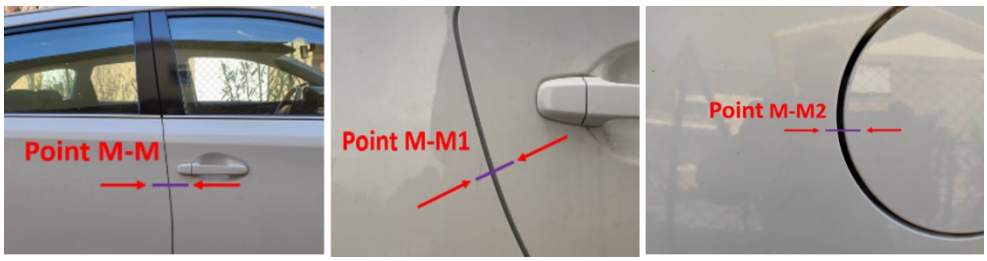

Figure 104. *Pictures of the 3 different metal-metal surfaces: point M-M on the front side door of the car; point M-M1 on the back side door of the car; point M-M2 on the fuel cap.*

6.2.2. Data analysis

The data collected were analyzed through Gage R&R crossed study. The analysis was performed exploiting Minitab 17.
A Gage R&R crossed study is used when each operator measures each part multiple times and it helps investigate [134]:

- repeatability, i.e. how much variability in the measurement system is caused by the measurement device;
- reproducibility, i.e. how much variability in the measurement system is caused by differences between operators;
- whether the measurement system variability is small compared with the process variability and if it is capable of distinguishing between different parts.

Measurement data were categorized depending on the operator and on the measuring point. Results provided by the analysis are reported in Figures 105 through 108.
Each Gage analysis includes six graphs:

- Components of variation: it displays the estimated variation components for each source;
- S Chart: it is a control chart of the standard deviations over the operators, for each part measured. It is used to see operator consistency;
- Xbar Chart: it represents the sample mean for each part, over the operators. The central line is the total mean of all the parts, and it is used to test the measurement system variation;
- Measurement by part: it shows the measurements (boxes) and the means (circles), divided by parts;
- Measurement by operator: it is analogous to the above-mentioned graph, but the measurements are divided based on the operators;
- Part*operator interaction: it is similar to the Xbar chart, but it overlaps in one graph the contributions from each operator. It is useful to see if the operators introduce a bias.

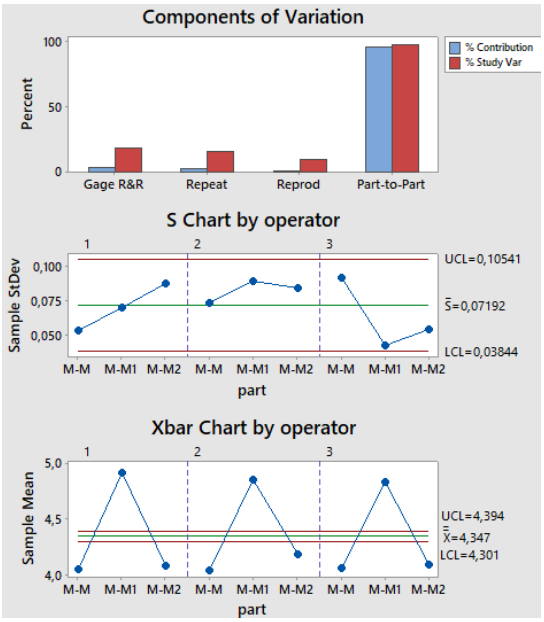

Figure 105. *Gage R&R analysis of gap measurement results: Components of variation [%], S Chart [mm] and Xbar Chart [mm].*

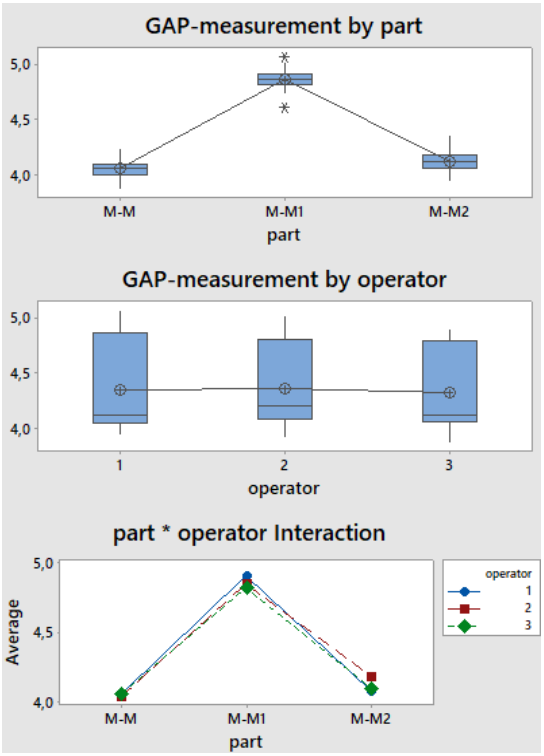

Figure 106. *Gage R&R analysis of gap measurement results: Measurement by part [mm], Measurement by operator [mm] and Part*operator interaction [mm].*

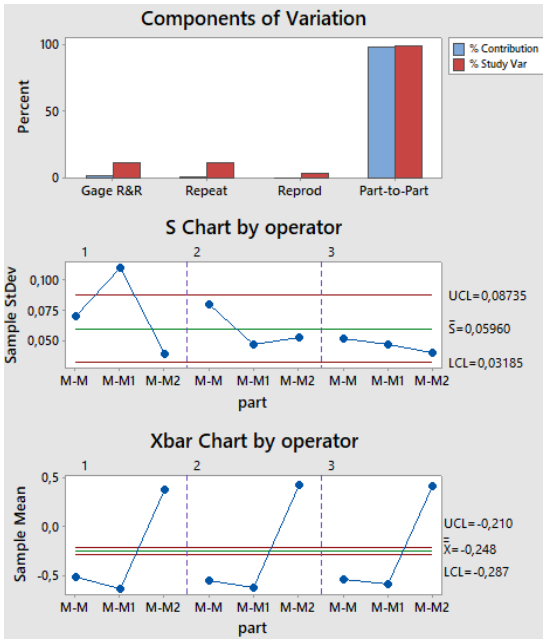

Figure 107. *Gage R&R analysis of flush measurement results: Components of variation [%], S Chart [mm] and Xbar Chart [mm].*

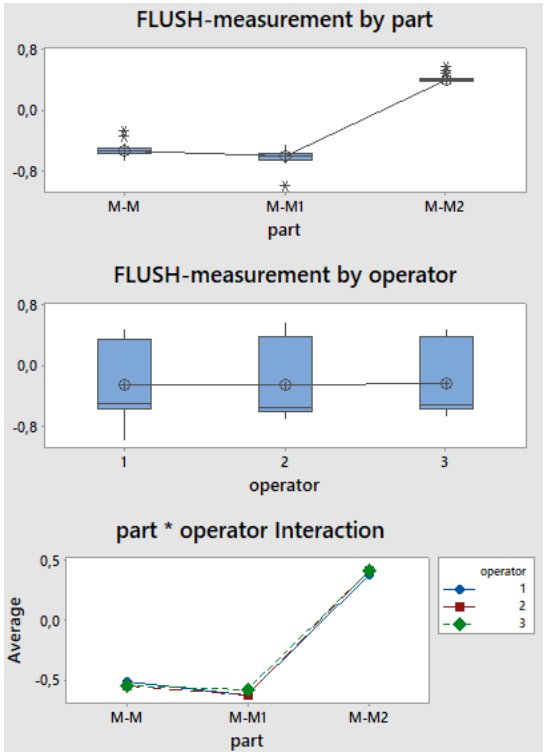

Figure 108. *Gage R&R analysis of flush measurement results: Measurement by part [mm], Measurement by operator [mm] and Part*operator interaction [mm].*

The results of the statistical analysis showed that the whole measurement chain has an expanded uncertainty of ±0.15 mm for the gap measurement and of ±0.13 mm for the flush measurement, which are acceptable for the purpose of in-line measurement. In fact, the requirement values for in-line gap and flush measurements are respectively 0.5 mm for the gap and 0.1 mm for the flush. Moreover, it should be kept in mind that operators often only use their fingers to manually assess the presence of a flush.

Operator consistency has been proven based on the S charts and Xbar charts of gap and flush, even if there are some differences between the operators, in fact not all parts have the same means and standard deviations. If we analyze the components of variation, of course the largest is the part-to-part variation; this is obvious, because three different parts were measured. Variation is estimated in terms of standard deviation; it is therefore an estimate of uncertainty, which allows to compute expanded uncertainty using a coverage factor of two. When considering the Gage R&R variation, we observe that for the gap, the repeatability of the measurement chain accounts for 0.07 mm; while the reproducibility accounts for 0.04 mm over a total Gage R&R of 0.09 mm. Being these figures standard deviations, the corresponding expanded uncertainty is equal to ±0.17 mm (95% confidence level). Therefore, the R&R analysis provides an estimate of expanded uncertainty for the gap of the same order of the direct type A analysis.

Analogously, for the flush, the repeatability and reproducibility are respectively 0.06 mm and 0.02 mm, over a total Gage R&R of 0.07 mm. These correspond to an expanded uncertainty of ±0.13 mm (95% confidence level). This is in full agreement with the type A analysis (see Tables 7 and 8).

Table 7. GAP Gage R&R results indicating the standard deviation for each source.

Source	Standard Deviation
Total Gage R&R	0.09
- Repeatability	0.07
- Reproducibility	0.04
--Operator	0
--Operator*part	0.04
Part-To-Part	0.45
Total Variation	**0.46**

Table 8. FLUSH Gage R&R results indicating the standard deviation for each source.

Source	Standard Deviation
Total Gage R&R	0.07
- Repeatability	0.06
- Reproducibility	0.02
--Operator	0
--Operator*part	0.02
Part-To-Part	0.57
Total Variation	**0.57**

6.3. Results and conclusions

In this study, a first attempt to characterize the uncertainty associated to the gap&flush measurement chain involving a hand-held non-contact laser scanner (G3F) and human operators for the car assembly lines is described. The human operator is an active part of the measurement chain, hence it is of extreme importance to provide evidence of the variability of data when the measurement is performed manually. Indeed, parameters like device pose with respect to target, highly influence the measurement accuracy. To fulfill this task, the performances of the device in "in-line simulated" conditions, where the critical parameters are considered as a whole, are analyzed.

The measurements were repeated 20 times on 3 different targets, by a series of operators in order to evaluate intra-operator reproducibility, as well as inter-operator reproducibility. This data set has been processed by a statistical type A analysis and by a crossed Gage R&R study with Minitab 17.

Both methods lead to the same results and allowed an estimate of expanded uncertainty for gap and flush, measured in conditions which simulate a real application. The expanded uncertainty for gap is ±0.17 mm, while for the flush is ±0.13 mm.

The results showed that the measurement system has an acceptable uncertainty and that, even if there are some differences between the operators, their consistency was proven. The components of variation were analyzed and, regarding the Gage R&R variation, repeatability was the largest component.

Further work will be focused on understanding why some difference between operators can be observed, as well as on finding ways to reduce it.

Overall, there are tasks that still require the use of human operators because of its dexterity, judgement and ability to adapt; nevertheless human operators are inevitably prone to error, for this reason it is important to provide a measurement device able to guide the operator during measurement execution, to reduce the final error and to enhance valuable human characteristics, like expertise and dexterity.

Chapter 7.

Conclusions

Quality control is a process that takes place to make sure that the quality of the product is maintained. Ideally, the variables at fault of having caused the defective products should be identified and corrected. This approach is the basis on which the evolving trend of Zero Defect Manufacturing (ZDM) is based. In fact, the goal of ZDM is to obtain a sustainable, efficient and effective production eliminating production scraps, not only through detecting and correcting defective products but also thanks to defect prediction and prevention. These corrective decisions are based on the data collected throughout the production, it is obvious that the quality of data depends entirely on the uncertainty of measurement, which in turn affects the reliability of the diagnosis made on measured data.

Right now, in manufacturing industries, measurements performed at the production level involve two main approaches: measurements are carried out either by human operators or by means of an automated process. When operators are involved, there is an added contribution to the uncertainty of the measurement other than the uncertainty of the instrument itself, and this is the uncertainty due to the operator.

In this sense, technology can be used to improve the knowledge and capabilities of operators. If this is the case, questions like ergonomics, human dexterousness, operator training but also human-machine interface design need to be taken into consideration and analyzed. When operators are involved, in general, measurements are not possible on 100% of production.

Automated quality control is able to reduce human mistakes in the workflow, in fact, replacing manual proof reading can eliminate inefficiencies and improve performance, speeding up the time-to-market. Automated quality control can achieve 100% quality control. Other advantages also include safety and a lower operating cost. Hence production line quality control usually integrates both aspects, taking advantage of automatization to relieve operators of alienating and repetitive tasks and overcoming sample-based quality control.

The contents of this PhD thesis were published in four separate occasions at both international conferences and on an international journal and can be found at [135]-[138].

Objective 1:
Design and development of vision-based dimensional measurement systems for quality control which could be integrated in-line.

For the first objective of this work, we designed and developed two measurement instruments, a telecentric profilometer and backlit vision-based surface roughness measurement system, targeted for different scale measurements. The telecentric

profilometer was used to perform dimensional measurements in the range of millimeters, while the surface roughness measurement system was used to analyze the surface roughness of turned samples, i.e., measurements in the range of micrometers.
The telecentric profilometer developed proved to be suitable for automated charge/discharge of parts and the short inspection time needed to collect measurements was compatible with in-line measurements for quality control.
It provided some challenges in guaranteeing alignment of the different components and the problems related to misalignment were described.
The backlit vision-based system for surface roughness was designed to be implemented in line, but it was tested only at a laboratory level. Nonetheless, the proposed instrument, thanks to the combined use of the modulation transfer function and an electrically tunable lens was able to perform smart behaviors such as finding the optimal imaging conditions and sharpening the focus without needing to reposition the sample. These characteristics will play an important role in the in-line implementation of the instrument.

Objective 2:
Uncertainty analysis of the measurement systems

For the second objective of this work, each chapter contained a section discussing the analysis of measurement uncertainty. The methods used to do this were chosen following the Guide to the expression of Uncertainty in Measurement (GUM) in ISO IEC GUIDE 98-3, and were a Type A statistical uncertainty analysis and a Gage R&R analysis.

The performance of the telecentric profilometer was evaluated with both methods, especially with a Gage R&R. This study was used to estimate the metrological performance of each instrument, in terms of trueness and repeatability; and the combination of variability due to the instruments (reproducibility) and to the samples. Overall, the telecentric profilometer proved to be more fit to measure lengths as opposed to diameters. Even if the measurement uncertainty was not within the requirements, a change in optical components, for example a higher resolution camera, could solve this problem. Better results in terms of uncertainty and bias could be obtained in future work by selecting these components in order to improve the resolution of the optical system.
The backlit vision-based system for surface roughness measurements was analyzed in comparison with other instruments with a Type A analysis due to the limited amount of samples. Evaluation length and the location of measurement proved to be criticalities in the measurements, nonetheless the performance of the designed instrument gives results comparable to the reference instrument when measuring in the range of surface roughness normally achieved in turning (R_a = 3.2 μm).
Further work will involve a more in-depth analysis of the influence of the location

of the measurement and a study of the importance of the processing algorithms implemented by the different instruments.
The dataset produced with the laser-line triangulation system to measure gap and flush, was processed with a Type A statistical analysis and the critical variables were analyzed as whole with a crossed Gage R&R study.
The results showed that the measurement system has an acceptable uncertainty and that, even if there are some differences between the operators, their consistency was proven. Additional work will be focused on understanding the reason of the difference between operators, as well as on finding ways to reduce it.

In conclusion, in this work we focused on two main industrial processes, assembly of adjacent parts and the turning of metal parts, and we narrowed the measurements down to two main categories:

- For the assembly of adjacent parts, we focused on gap and flush measurements,
- For the turning of metal parts, we focused on the most important geometrical characteristics of cylindrical products, which are lengths, diameters and average surface roughness.

The work presented in this PhD thesis focused on three different instruments and we were interested in their measurement uncertainty:

- A laser-line triangulation system for gap and flush measurements, and we evaluated its measurement uncertainty, particularly the influence of the operator on the total variance.
- A telecentric profilometer designed for dimensional measurements, whose performance we compared to other existing instruments.
- A backlit measurement system designed for average surface roughness measurements, we compared this new non-contact instrument to other contact-based existing instruments.

References

[1] D. Powell, M. C. Magnanini, M. Colledani, and O. Myklebust, "Advancing zero defect manufacturing: A state-of-the-art perspective and future research directions," *Comput. Ind.*, vol. 136, p. 103596, 2022, doi: https://doi.org/10.1016/j.compind.2021.103596.

[2] "https://www.investopedia.com/terms/q/quality-control.asp (Accessed on 03/02/23)." .

[3] A. Sinha, E. Bernardes, R. Calderon, and T. Wuest, *Digital Supply Networks: Transform Your Supply Chain and Gain Competitive Advantage with Disruptive Technology and Reimagined Processes.* New York, NY, USA: McGraw-Hill, 2020.

[4] J. Shi, "Stream of Variations Analysis," in *Encyclopedia of Systems and Control*, J. Baillieul and T. Samad, Eds. London, UK: Springer London, 2014, pp. 1–6.

[5] "https://research-and-innovation.ec.europa.eu/funding/funding-opportunities/funding-programmes-and-open-calls/horizon-europe_en (Accessed on 03/02/23)." .

[6] "https://digitalfactoryalliance.eu/wp-content/uploads/2021/07/2021_06_4ZDMClusterOverview_JuananArrieta.pdf (Accessed on 03/02/23)." .

[7] C. Cristalli *et al.*, "Integration of Process and Quality Control using Multi-Agent Technology," in *2013 IEEE International Symposium on Industrial Electronics, Taipei, Taiwan, 28-31 May 2013*, doi: https://doi.org/10.1109/ISIE.2013.6563737.

[8] M. Arsuaga Berrueta, J. Ortiz, R. Lobato, A. Fernandez Valdivielso, and L. N. Lopez De Lacalle, "Instrumentation and control methodology for zero defect manufacturing in boring operations," *23rd DAAAM Int. Symp. Intell. Manuf. Autom. 2012*, vol. 1, no. 1, pp. 385–388, 2012, doi: 10.2507/23rd.daaam.proceedings.089.

[9] K. S. Wang, "Towards zero-defect manufacturing (ZDM)-a data mining approach," *Adv. Manuf.*, vol. 1, no. 1, pp. 62–74, 2013, doi: 10.1007/s40436-013-0010-9.

[10] M. A. Montironi, P. Castellini, L. Stroppa, and N. Paone, "Adaptive autonomous positioning of a robot vision system: Application to quality control on production lines," *Robot. Comput. Integr. Manuf.*, vol. 30, no. 5, pp. 489–498, 2014, doi: 10.1016/j.rcim.2014.03.004.

[11] L. Stroppa, P. Castellini, and N. Paone, "Self-Optimizing Robot Vision for Online Quality Control," *Exp. Tech.*, p. n/a-n/a, 2015, doi: 10.1111/ext.12152.

[12] J. Queiroz and P. Leitão, "Agent-Based Data Analysis Towards the Dynamic Adaptation of Industrial Automation Processes.," in *Camarinha-Matos, L.M., Falcão, A.J., Vafaei, N., Najdi, S. (eds) Technological Innovation for Cyber-Physical Systems.*, Springer, Cham., 2016.

[13] P. Chiariotti, M. Fitti, P. Castellini, S. Zitti, M. Zannini, and N. Paone, "Smart

Quality Control Station for Non-Contact Measurement of Cylindrical Parts Based on a Confocal Chromatic Sensor," *IEEE Instrum. Meas. Mag.*, vol. 21, no. 6, pp. 22–28, 2018, doi: 10.1109/MIM.2018.8573589.

[14] C. Caccamo, R. Eleftheriadis, M. C. Magnanini, D. Powell, and O. Myklebust, "A Hybrid Architecture for the Deployment of a Data Quality Management (DQM) System for Zero-Defect Manufacturing in Industry 4.0," *IFIP Adv. Inf. Commun. Technol.*, vol. 632 IFIP, pp. 71–77, 2021, doi: 10.1007/978-3-030-85906-0_8.

[15] F. Eger *et al.*, "Part Variation Modeling to Avoid Scrap Parts in Multi-stage Production Systems," *Procedia CIRP*, vol. 107, pp. 851–856, 2022, doi: 10.1016/j.procir.2022.05.074.

[16] S. Campbell, S. Cáceres, G. Pagalday, R. Poler, and R. Jardim-Gonçalves, "A European Manufacturing Platform for Zero-Defects," *CEUR Workshop Proc.*, vol. 2900, pp. 0–2, 2020.

[17] "https://portal.effra.eu/projects (Accessed on 03/02/23)." .

[18] "https://zdmanufuture.org/projects/ (Accessed on 03/02/23)." .

[19] P. Castellini *et al.*, "Towards the Integration of Process and Quality Control using Multi-agent Technology," in *IECON 2011 - 37th Annual Conference of the IEEE Industrial Electronics Society, Melbourne, VIC, Australia, 07-10 November 2011*, pp. 374–379, doi: https://doi.org/10.1109/IECON.2011.6119347.

[20] D. Trentesaux and S. Karnouskos, "Engineering ethical behaviors in autonomous industrial cyber-physical human systems," *Cogn. Technol. Work*, vol. 24, no. 1, pp. 113–126, 2022, doi: 10.1007/s10111-020-00657-6.

[21] C. Cimini, F. Pirola, R. Pinto, and S. Cavalieri, "A human-in-the-loop manufacturing control architecture for the next generation of production systems," *J. Manuf. Syst.*, vol. 54, no. July 2019, pp. 258–271, 2020, doi: 10.1016/j.jmsy.2020.01.002.

[22] D. Romero *et al.*, "Towards an Operator 4.0 Typology: A Human-Centric Perspective on the Fourth Industrial Revolution Technologies," *CIE 2016 46th Int. Conf. Comput. Ind. Eng.*, no. October, pp. 0–11, 2016.

[23] M. P. Pacaux-Lemoine, M. Sallak, R. Sacile, F. Flemisch, and P. Leitão, "Introduction to the special section humans and industry 4.0," *Cogn. Technol. Work*, vol. 24, no. 1, pp. 1–5, 2022, doi: 10.1007/s10111-022-00696-1.

[24] J. Müller, "Enabling Technologies for Industry 5.0: Results of a workshop with Europe's technology leaders," *Eur. Comm.*, no. September, p. 19, 2020, doi: 10.2777/082634.

[25] "https://blog.globalvision.co/quality/why-automated-quality-control-is-the-key-to-getting-products-to-market-faster/#:~:text=Automated%20quality%20control%20is%20a,market%20faster%20without%20compromising%20quality. (Accessed on 03/02/23)." .

[26] "https://www.qad.com/blog/2022/01/manufacturing-automation-what-does-it-mean-for-manufacturers (Accessed on 03/02/23)." .

[27] "https://www.houstexonline.com/news/guide-to-automated-manufacturing-systems/#:~:text=What%20Are%20Automated%20Manufacturing%20Systems,managed%20by%20these%20control%20systems. (Accessed on

03/02/23).” .
[28] “https://www.expo21xx.com/news/micro-epsilon-surfacecontrol-3d-3510-snapshot-sensor/ (Accessed on 03/02/23).” .
[29] “https://www.micro-epsilon.co.uk/applications/branch/Kunststoff/Inline-Farbmessung-Kunststoff-Spritzgussteilen/ (Accessed on 03/02/23).” .
[30] “https://www.nirox.it/wp-content/uploads/2019/01/nirox-metal-INSPECTION-OF-SURFACE-DEFECTS.pdf (Accessed on 03/02/23).” .
[31] “https://z4tec.com/landing/ (Accessed on 03/02/23).” .
[32] “https://www.creaform3d.com/en/metrology-solutions/technology-integration-services (Accessed on 03/02/23).” .
[33] “https://kreon3d.com/scanning-arm/ace-skyline/ (Accessed on 03/02/23).” .
[34] “https://www.zeiss.com/metrology/solutions/car-body/inline.html (Accessed on 03/02/23).” .
[35] “https://www.muelaner.com/dimensional-measurement/#:~:text=Dimensional%20measurement%20is%20how%20we,for%20interchangeability%20and%20global%20trade (Accessed on 03/02/23).” .
[36] A. C. Reddy, “Evaluation of Surface Roughness Using Image Processing Technique,” *Int. Conf. Syst. Cybern. Informatics*, pp. 571–573, 2004.
[37] O. J. Zurita-Hurtado, V. C. Di Graci-Tiralongo, and M. C. Capace-Aguirre, “Effect of surface hardness and roughness produced by turning on the torsion mechanical properties of annealed AISI 1020 steel,” *Rev. Fac. Ing.*, no. 84, pp. 55–59, 2017, doi: https://doi.org/10.17533/udea.redin.n84a07.
[38] T. T. Tran and C. K. Ha, “Non-contact Gap and Flush Measurement Using Monocular Structured Multi-line Light Vision for Vehicle Assembly,” *Int. J. Control. Autom. Syst.*, vol. 16, no. 5, pp. 2432–2445, 2018, doi: 10.1007/s12555-017-0535-y.
[39] “ISO/IEC GUIDE 98-3; Uncertainty of measurement — Part 3 : Guide to the expression of uncertainty in measurement. ISO (International Organization for Standardiztion); Geneva, Switzerland,” 2012.
[40] “ISO 5725- 1: 2004 Accuracy (trueness and precision) of measurement methods and results - Part 1: General principles and definitions.” .
[41] “ISO 5725 - 2: 2019 Accuracy (trueness and precision) of measurement methods and results - Part 2: Basic method for the determination of repeatability and reproducibility of a standard measurement method.” .
[42] “ISO 3435 - 2: 2006 Statistics - Vocabulary and symbols. Part 2: Applied statistics.” .
[43] “ISO 14253-1; Geometrical product specifications (GPS) - Inspection by measurement of workpieces and measuring equipment - Part 1: Decision rules for verifying conformity or nonconformity with specifications. ISO (Intern. Org. for St.); Geneva, Switzerland,” 2017.
[44] “ISO 14253-5: 2015 Geometrical product specifications (GPS) - Inspection by measurement of workpieces and measuring equipment - Part 5: Uncertainty in verification testing of indicating measuring instruments.” .
[45] “JCGM 106: 2012 Evaluation of Measurement Data: The Role of Measurement Uncertainty in Conformity Assessment,” 2012.

[46] Joint Committee for Guides in Metrology (JCGM), “International Vocabulary of Metrology – Basic and General Concepts and Associated Terms (VIM) 3rd Edition,” *English*, no. Vim, pp. 1–127, 2006.
[47] S. Shirmohammadi, L. Mari, and D. Petri, “On the Commonly-Used Incorrect Visual Representation of Accuracy and Precision,” *IEEE Instrum. Meas. Mag.*, vol. 24, no. 1, pp. 45–49, 2021, doi: 10.1109/MIM.2021.9345597.
[48] “https://www.bipm.org/en (Accessed on 06/02/23).” .
[49] “https://sixsigmastudyguide.com/repeatability-and-reproducibility-rr/ (Accessed on 03/02/23).” .
[50] S. Crowder, C. Delker, E. Forrest, and N. Martin, *Introduction to Statistics in Metrology*. Springer, 2020.
[51] S. B. Vardeman and J. M. Jobe, *Statistical Methods for Quality Assurance: Basics, Measurement, Control, Capability, and Improvement*, Second edi., vol. 51, no. 2. Springer, 2016.
[52] D. Flack and J. Hannaford, “Measurement Good Practice Guide No.80: Fundamental Good Practice in Dimensional Metrology,” *Natl. Phys. Lab.*, no. 80, 2005.
[53] M. Meirbek, H. Meifa, and T. Zhemin, “Current issues in uncertainty of dimensional tolerance metrology and the future development in the domain of tolerancing,” *IOP Conf. Ser. Mater. Sci. Eng.*, vol. 715, p. 012084, 2020, doi: https://doi.org/10.1088/1757-899X/715/1/012084.
[54] “https://project-management.info/cost-of-quality-coq/ (Accessed on 13/02/23).”
[55] “https://www.electricaldeck.com/2021/04/classification-of-measuring-instruments.html (Accessed on 03/02/23).” .
[56] “https://www.utensileriaonline.it/strumenti-di-misura-c-28/calibri-ventesimali-c-28_181/calibri-analogici-c-28_181_180/calibro-a-corsoio-rupac-con-asta-tonda-misura-fino-a-200-mm-p-15910.php (Accessed on 06/02/23).” .
[57] “https://www.fervi.com/eng/measure/measuring-tools/screw-pitch-gauge/feeler-gauge-set-pr-12623.htm (Accessed on 07/02/23).” .
[58] “https://www.foxcar.it/prodotto/spessimetro-per-carrozzeria/ (Accessed on 03/02/23).” .
[59] “https://spareto.com/products/ks-tools-feeler-gauge-set-gap-size/150-1570 (Accessed on 03/02/23).” .
[60] “www. stemmer-imaging .com/en/knowledge-base/laser-triangulation/ (Accessed on 03/02/23).” .
[61] S. Kumar, P. K. Tiwari, and S. B. Chaudhury, “An Optical Triangulation Method for Non-Contact Profile Measurement,” *Proc. IEEE Int. Conf. Ind. Technol.*, pp. 2878–2883, 2006, doi: 10.1109/ICIT.2006.372653.
[62] S. Li, X. Jia, M. Chen, and Y. Yang, “Error analysis and correction for color in laser triangulation measurement,” *Optik (Stuttg).*, vol. 168, pp. 165–173, 2018, doi: 10.1016/j.ijleo.2018.04.057.
[63] “https://www.movimed.com/knowledgebase/what-is-laser-triangulation/ (Accessed on 03/02/23).” .

[64] M. Zaiß, J. Demmerle, J. N. Oergele, and G. Lanza, “New Concepts for Quality Assurance of Lightweight Material,” *Procedia CIRP*, vol. 66, pp. 259–264, 2017, doi: 10.1016/j.procir.2017.03.224.
[65] D. Kosmopoulos and T. Varvarigou, “Automated Inspection of Gaps on the Automobile Production Line through Stereo Vision and Specular Reflection,” *Comput. Ind.*, vol. 46, no. 1, pp. 49–63, 2001, doi: 10.1016/S0166-3615(01)00113-0.
[66] D. F. Garcia, M. Garcia, F. Obeso, and V. Fernandez, “Flatness Measurement System Based on a NonLinear Optical TriangulationTechnique,” *IEEE Trans. Instrum. Meas.*, vol. 51, no. 2, pp. 188–195, 2002, doi: 10.1109/19.997810.
[67] P. Castellini, A. Bruni, and N. Paone, “Design of an Optical Scanner for Real Time on-line Measurement of Wood-Panel Profiles,” *Int. Soc. Opt. Eng.*, 2007, doi: 10.1117/12.725042.
[68] L. H. Pham, D. N. N. Tran, J. Y. Byun, C. H. Rhie, and J. W. Jeon, “A Smartphone-Based Laser Measuring System for Gap and Flush Assessment in Car Body,” *IEEE Trans. Ind. Electron.*, vol. 68, no. 7, pp. 6297–6307, 2021, doi: 10.1109/TIE.2020.2992971.
[69] R. Slossberg, A. Wetzler, and R. Kimmel, “Freehand Laser Scanning Using Mobile Phone,” pp. 88.1-88.10, 2015, doi: https://dx.doi.org/10.5244/C.29.88.
[70] T. Pribanić, T. Petković, M. Đonlić, V. Angladon, and S. Gasparini, “3D Structured Light Scanner on the Smartphone,” in *13th International Conference on Image Analysis and Recognition, ICIAR 2016, Póvoa de Varzim, Portugal, 13-15 July 2016*, doi: http://dx.doi.org/10.1007/978-3-319-41501-7_50.
[71] G. F. Barbosa, G. F. Peres, and J. L. G. Hermosilla, “R&R (repeatability and reproducibility) gage study applied on gaps’ measurements of aircraft assemblies made by a laser technology device,” *Prod. Eng.*, vol. 8, no. 4, pp. 477–489, 2014, doi: 10.1007/s11740-014-0553-z.
[72] J. Kholkhujaev, G. Maculotti, G. Genta, M. Galetto, and J. Inoyatkhodjaev, “Non-Contact Articulated Robot-Integrated Gap and Flushness Measurement System for Automobile Assembly,” *IEEE Access*, vol. 10, no. August, pp. 86528–86541, 2022, doi: https://doi.org/10.1109/ACCESS.2022.3199066.
[73] “https://www.micro-epsilon.com/displacement-position-sensors/laser-sensor/ (Accessed on 03/02/23).” .
[74] “https://kreon3d.com/3d-scanners/ (Accessed on 03/02/23).” .
[75] “https://lmi3d.com/family/line-profile-sensors/ (Accessed on 03/02/23).” .
[76] “https://www.stemmer-imaging.com/it-it/products/series/lmi-gocator-3000/ (Accessed on 03/02/23).” .
[77] “https://www.qfp-service.it/en/products/gap-and-flush-measurement-systems/gapgun-pro-2/ (Accessed on 03/02/23).” .
[78] “https://www.wenglor.com/en/2D3D-Sensors/2D3D-Profile-Sensors/2D3D-Profile-Sensor/p/MLSL123 (Accessed on 07/02/23).” .
[79] “https://www.keyence.com/ss/products/measure/library/type/laser_2d.jsp (Accessed on 13/02/23).” .

[80] E. Minnetti *et al.*, “A Smartphone Integrated Hand-Held Gap and Flush Measurement System for in Line Quality Control of Car Body Assembly,” *Sensors (Switzerland)*, vol. 20, no. 11, pp. 1–17, 2020, doi: 10.3390/s20113300.
[81] N. Paone, P. Castellini, P. Chiariotti, and E. Minnetti, “System For Measuring Gap and Flush,” PCT/IB2019/051662, 2019.
[82] “https://www.reviewbox.it/micrometri/ (Accessed on 03/02/23).” .
[83] “https://www.pineappleracing.com/dialindicatorwithmagneticbase.aspx (Accessed on 03/02/23).” .
[84] “https://www.wasyresearch.com/tactile-cmm-the-reference-of-dimensional-and-geometrical-measuring-machine-in-industry/(Accessed on 03/02/23).” .
[85] “https://usautocorp.com/product/edge-to-edge-backlights/ (Accessed on 03/02/23).” .
[86] “https://www.effilux.com/en/products/backlight (Accessed on 03/02/23).” .
[87] “https://www.vision-doctor.com/en/illumination-techniques/backlight-illumination.html (Accessed on 03/02/23).” .
[88] “https://www.opto-e.com/it/resources/tutorials/telecentric-lenses-tutorial (Accessed on 03/02/23).” .
[89] “https://www.deltavisione.com/en/products/automatic-sorting-machines/dv-rdsm-rotary-disc-sorting-machine (Accessed on 03/02/23).” .
[90] “https://www.vicivision.com/it/macchine-di-misura-ottica-aumento-produttivita-riduzione-scarti/serie-techno-macchine-ottiche/ (Accessed on 03/02/23).” .
[91] “https://www.marposs.com/eng/product/2d-optical-measuring-unit-for-shop-floor-and-laboratory (Accessed on 03/02/23).” .
[92] “https://www.keyence.co.uk/products/measure/micrometer/tm-3000/models/tm-065/ (Accessed on 06/02/23).” .
[93] “ISO 4287; Geometrical Product Specifications (GPS). Surface texture: Profile method - Terms, definitions and surface texture parameters. ISO (International Organization for Standardiztion); Geneva, Switzerland,” 1999.
[94] A. O. Pino, J. Pladellorens, and J. F. Colom, “Method of measure of roughness of paper based in the analysis of the texture of speckle pattern,” *Speckle 2010 Opt. Metrol.*, vol. 7387, p. 73871W, 2010, doi: 10.1117/12.869655.
[95] “ISO 4288: 1996 Geometrical Product Specifications (GPS). Surface texture: Profile method - Rules and procedures for the assessment of surface texture.” .
[96] “EN ISO 3274; Geometrical product specifications (GPS). Surface texture: Profile method - Nominal characteristics of contact (stylus) instruments. ISO (International Organization for Standardization); Geneva, Switzerland,” 1998.
[97] “https://www.keyence.eu/ss/products/microscope/roughness/equipment/line_01.jsp (Accessed on 03/02/23).” .
[98] D. Kubátová, M. Melichar, and J. Kutlwašer, “Impact of Stylus Size in Roughness Measurement,” *Ann. DAAAM Proc. Int. DAAAM Symp.*, pp. 457–

466, 2017, doi: https://doi.org/10.2507/28th.daaam.proceedings.064.
[99] J. S. Villarrubia, “Algorithms for Scanned Probe Microscope Image Simulation, Surface Reconstruction, and Tip Estimation,” *J. Res. Natl. Inst. Stand. Technol.*, vol. 102, no. 4, pp. 425–454, 1997, doi: https://doi.org/10.6028/jres.102.030.
[100] T. V. Vorburger, H. G. Rhee, T. B. Renegar, J. F. Song, and A. Zheng, “Comparison of optical and stylus methods for measurement of surface texture,” *Int. J. Adv. Manuf. Technol.*, vol. 33, no. 1–2, pp. 110–118, 2007, doi: https://doi.org/10.1007/s00170-007-0953-8.
[101] D. Francis, R. P. Tatam, and R. M. Groves, “Shearography technology and applications: A review,” *Meas. Sci. Technol.*, vol. 21, no. 10, 2010, doi: https://doi.org/10.1088/0957-0233/21/10/102001.
[102] F. Meli, “Roughness measurements according to existing standards with a metrology AFM profiler,” in *3rd Euspen conference, Eindhoven, The Netherlands, May 2002*, pp. 533–536.
[103] Y. Gong, J. Xu, and R. C. Buchanan, “Surface roughness: A review of its measurement at micro-/nano-scale,” *Phys. Sci. Rev.*, vol. 3, no. 1, pp. 1–10, 2018, doi: https://doi.org/10.1515/psr-2017-0057.
[104] “https://www.nanoandmore.com/what-is-atomic-force-microscopy (Accessed on 03/02/23).” .
[105] C. Babu Rao and R. A. J. Baldev, “Study of engineering surfaces using laser-scattering techniques,” *Sadhana*, vol. 28, no. 3–4, pp. 739–761, 2003, doi: https://doi.org/10.1007/bf02706457.
[106] C. Lukianowicz and T. Karpinski, “Scatterometry Of Machined Surfaces,” in *XVI IMEKO World Congress, Vienna, Austria, 25-28 September 2000*, pp. 1–5.
[107] W. Kapłonek and K. Nadolny, “Laser methods based on an analysis of scattered light for automated, in-process inspection of machined surfaces: A review,” *Optik,* vol. 126, no. 20, pp. 2764–2770, 2015, doi: https://doi.org/10.1016/j.ijleo.2015.07.009.
[108] A. M. Hamed and M. Saudy, “Computation of surface roughness using optical correlation,” *Pramana*, vol. 68, no. 5, pp. 831–842, 2007, doi: https://doi.org/10.1007/s12043-007-0081-x.
[109] W. jing Zhou, K. qin Peng, and Y. J. Yu, “Surface roughness measurement and analysis of mechanical parts based on digital holography,” *Adv. Manuf.*, vol. 4, no. 3, pp. 217–224, 2016, doi: https://doi.org/10.1007/s40436-016-0146-5.
[110] H. H. Shahabi and M. M. Ratnam, “Noncontact roughness measurement of turned parts using machine vision,” *Int. J. Adv. Manuf. Technol.*, vol. 46, no. 1–4, pp. 275–284, 2010, doi: https://doi.org/10.1007/s00170-009-2101-0.
[111] S. B. Jayabarathi and M. M. Ratnam, “Comparison of Correlation between 3D Surface Roughness and Laser Speckle Pattern for Experimental Setup Using He-Ne as Laser Source and Laser Pointer as Laser Source,” *Sensors*, vol. 22, no. 16, p. 6003, 2022, doi: https://doi.org/10.3390/s22166003.
[112] B. M. Kumar and M. M. Ratnam, “Study on Effect of Tool Nose Radius Wear on Hybrid Roughness Parameters during Turning Using Vision-Based

Approach," *IOP Conf. Ser. Mater. Sci. Eng.*, vol. 530, no. 1, p. 012009, 2019, doi: https://doi.org/10.1088/1757-899X/530/1/012009.
[113] H. H. Shahabi and M. M. Ratnam, "Simulation and measurement of surface roughness via grey scale image of tool in finish turning," *Precis. Eng.*, vol. 43, pp. 146–153, 2016, doi: https://doi.org/10.1016/j.precisioneng.2015.07.004.
[114] A. M. Atieh, N. A. Rawashdeh, and A. N. AlHazaa, "Evaluation of Surface Roughness by Image Processing of a Shot-Peened, TIG-Welded Aluminum 6061-T6 Alloy: An Experimental Case Study," *Materials,* vol. 11, no. 5, p. 771, 2018, doi: https://doi.org/10.3390/ma11050771.
[115] B. Y. Lee, S. F. Yu, and H. Juan, "The model of surface roughness inspection by vision system in turning," *Mechatronics*, vol. 14, no. 1, pp. 129–141, 2004, doi: https://doi.org/10.1016/S0957-4158(02)00096-X.
[116] B. M. Kumar and M. M. Ratnam, "Machine vision method for non-contact measurement of surface roughness of a rotating workpiece," *Sens. Rev.*, vol. 35, no. 1, pp. 10–19, 2015, doi: https://doi.org/10.1108/SR-01-2014-609.
[117] O. W. Taha and O. F. Abdulateef, "Surface roughness prediction in turning process by applying computer vision method," *IIUM Eng. J.*, vol. 22, no. 2, pp. 249–260, 2021, doi: https://doi.org/10.31436/iiumej.v22i2.1507.
[118] "https://www.impronte.com/le-dimensioni-dei-sensori/ (Accessed on 08/02/23)." .
[119] "www.cambridgeincolour.com (Accessed on 03/02/23)." .
[120] G. D. Boreman, "Chapter 1 - MTF in Optical Systems," in *Modulation Transfer Function in Optical and Electro-Optical Systems*, Washington, DC, USA: SPIE—The International Society for Optical Engineering, 2001, pp. 1–30.
[121] G. D. Boreman, "Chapter 4 - MTF Measurement Methods," in *Modulation Transfer Function in Optical and Electro-Optical Systems*, Washington, DC, USA: SPIE—The International Society for Optical Engineering, 2001, pp. 69–84.
[122] C. Mitja, "Slanted Edge MTF. Availabe online: https://imagej.nih.gov/ij/plugins/se-mtf/index.html (Accessed on 29/01/2023)." .
[123] "https://twistedphysics.typepad.com/cocktail_party_physics/2009/10/images-of-supernovae-and-supermodels.html (Accessed on 08/02/23)." .
[124] "International Vocabulary of Metrology-Basic and General Concepts and Associated Terms," *Joint Committee for Guides in Metrology*, 2012. https://jcgm.bipm.org/vim/en/2.11.html.
[125] J. R. Parker, *Algorithms for Image Processing and Computer Vision*, 2nd edi. Indianapolis, 1997.
[126] P. de Groot and J. DiSciacca, "Definition and evaluation of topography measurement noise in optical instruments," *Opt. Eng.*, vol. 59, no. 06, p. 064110, 2020, doi: https://doi.org/10.1117/1.oe.59.6.064110.
[127] R. Leach, H. Haitjema, R. Su, and A. Thompson, "Metrological characteristics for the calibration of surface topography measuring

instruments: A review," *Meas. Sci. Technol.*, vol. 32, no. 3, p. 032001, 2020, doi: https://doi.org/10.1088/1361-6501/abb54f.
[128] V. P. Astakhov, "Surface integrity - Definition and Importance in Functional Performance," in *Surface Integrity in Machining*, London, UK: Springer London, 2010, pp. 1–35.
[129] G. B. Rossi, F. Crenna, and A. Palazzo, "A Proposal for a More User-Oriented GUM," *IEEE Trans. Instrum. Meas.*, vol. 68, no. 5, pp. 1343–1352, 2019, doi: https://doi.org/10.1109/TIM.2019.2899183.
[130] J. Song *et al.*, "Stylus Tip-Size Effect on the Calibration of Periodic Roughness Specimens with Rectangular Profiles," in *ICSM3 Conference, Annecy, France, 21-23 March 2012*, no. 54, pp. 530–533.
[131] W. dos Santos Motta Neto, J. E. S. Leal, L. J. Arantes, and R. V. Arencibia, "The effect of stylus tip radius on Ra, Rq, Rp, Rv, and Rt parameters in turned and milled samples," *Int. J. Adv. Manuf. Technol.*, vol. 99, no. 5–8, pp. 1979–1992, 2018, doi: https://doi.org/10.1007/s00170-018-2630-5.
[132] R. K. Leach, *The Measurement of Surface Texture using Stylus Instruments*, no. 2. Teddington, Middlesex, United Kingdom: National Physical Laboratory, 2001.
[133] C. Steger, "An unbiased detector of curvilinear structures," *IEEE Trans. Pattern Anal. Mach. Intell.*, vol. 20, no. 2, pp. 113–125, 1998, doi: 10.1109/34.659930.
[134] "https://support.minitab.com/en-us/minitab/19/help-and-how-to/quality-and-process-improvement/measurement-system-analysis/supporting-topics/gage-r-r-analyses/what-is-a-gage-r-r-study/. (Accessed on 11/02/23)." .
[135] A. Baleani, P. Castellini, P. Chiariotti, N. Paone, and L. Violini, "Analysis of reproducibility and repeatability of a hand-held laser scanner for gapflush measurement in car-assembly line," *2020 IEEE Int. Work. Metrol. Ind. 4.0 IoT, MetroInd 4.0 IoT 2020 - Proc.*, pp. 648–653, 2020, doi: 10.1109/MetroInd4.0IoT48571.2020.9138222.
[136] A. Baleani *et al.*, "Dimensional measurements in production line: a comparison between a custom-made telecentric optical profilometer and on-the-market measurement systems," in *2021 IEEE International Workshop on Metrology for Industry 4.0 and IoT (MetroInd4.0 & IoT) Rome, Italy, 7-9 June 2021*, pp. 693–698, doi:https://doi.org/10.1109/MetroInd4.0IoT51437.2021.9488428.A.
[137] Baleani, N. Paone, J. Gladines, and S. Vanlanduit, "Surface roughness measurements of turned parts through a vision-based measurement system: uncertainty analysis and performance comparison with state-of-the-art instruments," in *2022 IEEE International Workshop on Metrology*
[138] A. Baleani, N. Paone, J. Gladines and S. Vanlanduit, "Design and Metrological Analysis of a Backlit Vision System for Surface Roughness Measurements of Turned Parts" *Sensors*, vol. 23, no. 3, pp. 0–20, 2023, doi: 10.3390/s23031584.